Analysis of subsystems in wavelength-division-multiplexing networks

Liu, Fenghai

Publication date:
2001

Document Version
Publisher's PDF, also known as Version of record

ANALYSIS OF SUBSYSTEMS IN

WAVELENGTH-DIVISION-MULTIPLEXING NETWORKS

Fenghai Liu

The work presented in this thesis was carried out at the Research Center COM in partial fulfillment of the requirement for the Ph.D. degree from the Technical University of Denmark.

Supervisor : Prof. Dr. tech. Palle Jeppesen
Assistant Supervisor : Associate Research Prof. Rune J.S. Pedersen

Abstract

Wavelength division multiplexing (WDM) technology together with optical amplification has created a new era for optical communication. Transmission capacity is greatly increased by adding more and more wavelength channels into a single fiber, as well as by increasing the line rate of each channel. WDM not only can be used to increase transmission capacity, but also to introduce a new dimension to design and implement flexible, reliable, cost-effective optical networks.

Optical signals may pass through several nodes in the optical network without being terminated and converted into an electrical signal. The impairments from the subsystems in an optical network, such as interferometric crosstalk, filtering effect, dispersion in optical components, fiber dispersion and non-linearity, will accumulate and degrade the signal, hence limit the size of the network. Therefore, the study of these impairments and their influence in a cascade of subsystems is very important.

In this Ph.D. thesis, several important subsystems are investigated theoretically and experimentally.

Useful tools are developed to study the cascadability of subsystems. A crosstalk model is developed to estimate the influence of interferometric crosstalk; the model has been used in calculation of the possible size of wavelength routing networks using arrayed-waveguide-grating (AWG) routers, and in calculation of the number of wavelengths that can be handled in a new 2×2 multiwavelength cross-connect. A method to measure dispersion in optical components is proposed and used to characterize an optical add/drop multiplexer. A fiber re-circulating loop set-up is upgraded to support multiple channels. It has been used to experimentally investigate the cascadability of AWG routers, 10Gb/s wavelength converters based on cross gain modulation in semiconductor optical amplifiers (SOAs), and dispersion managed fiber sections.

New subsystems are also proposed in the thesis: a modular 2×2 multiwavelength cross-connect using wavelength switching blocks, a wavelength converter based on cross phase modulation in a semiconductor modulator, a wavelength selectable light source using DFB fiber lasers and a single shared pump, an interferometric crosstalk suppressor using a saturated SOA, and a simple chirped return-to-zero transmitter.

The thesis consists of a summary and 20 accompanying papers related to the investigation. Some detailed theoretical derivations not included in the papers are added in the Appendices.

Resumé

Kombinationen af teknikker til optisk bølgelængde-multipleksning og optisk forstærkning har skabt en ny æra for optisk kommunikation, hvor en meget stor forøgelse af den samlede transmissionskapacitet er opnået ved at benytte stadig flere bølgelængdekanaler i hver fiber og samtidig øge den enkelte bølgelængdekanals datahastighed. Optisk bølgelængde-multipleksning muliggør dog ikke alene en forøgelse af transmissionskapaciteten, men tilføjer også en ny dimension i design og virkeliggørelse af fleksible og pålidelige optiske netværk med stor ydeevne per investeret krone.

Optiske signaler vil kunne udbrede sig gennem adskillige knudepunkter i et optisk netværk uden at blive termineret og omsat til elektriske signaler. Forringelser - eksempelvis interferometrisk krydstale, filtreringseffekter, dispersion i optiske komponenter samt dispersion og ulinearitet i fibre - fra det optiske netværks delsystemer vil således akkumuleres og forringe kvaliteten af det optiske signal, hvilket i sidste ende sætter en grænse for netværkets størrelse. Derfor er studiet af disse forringelser og deres indflydelse i en kaskadekobling af delsystemer meget vigtig.

I nærværende Ph.d.-afhandling undersøges adskillige vigtige delsystemer teoretisk og eksperimentelt.

Nyttige værktøjer er blevet udviklet til studier af forholdene, når et optisk signal udbreder sig gennem en kaskadekobling af delsystemer. En krydstalemodel er blevet udviklet til vurdering af indflydelsen af interferometrisk krydstale; modellen er blevet benyttet til beregning af den mulige størrelse af optiske netværk, der benytter arrayed-waveguide-grating (AWG) routere til at dirigere de forskellige bølgelængder rundt i netværket, samt til beregningen af det antal bølgelængder, der kan håndteres i en ny 2×2 multibølgelængde cross-connect. En metode til måling af dispersionen i optiske komponenter foreslås, og den er blevet brugt til karakterisering af en optisk add/drop multiplekser. En recirkulerende optisk fiberring er blevet opgraderet til at understøtte mere end en enkelt bølgelængde. Denne fiberring er blevet benyttet til eksperimentel undersøgelse af forholdene ved kaskadekobling af AWG routere, 10 Gbit/s bølgelængdekonvertere baseret på krydsforstærkningsmodulation i optiske halvlederforstærkere (SOA), og dispersionskomtrollerede fibersektioner.

Nye delsystemer foreslås også i denne afhandling: i) En modulær 2×2 multibølgelængde cross-connect baseret på 2×2 blokke, der hver især håndterer en enkelt bølgelængde, ii) en bølgelængdekonverter baseret på krydsfasemodulation i en halvledermodulator, iii) en lyskilde opbygget af DFB fiberlasere og en enkelt pumpe til frembringelse af lys med en bølgelængde, der kan vælges blandt et antal mulige bølgelængder, iv) et delsystem, der benytter en SOA drevet i mætning til undertrykkelse af interferometrisk krydstale, og v) en simpel sender til frembringelse af optiske signaler i chirped return-to-zero formatet.

Afhandlingen består af en sammenfatning og 20 tilhørende artikler, der i større detaljeringsgrad beskæftiger sig med de undersøgte emner. Udførlige teoretiske udledninger, der er udeladt i artiklerne, er tilføjet i appendiks.

摘　要

光波分复用和光放大技术使光纤通信进入一个新纪元。通信容量通过增加波长信道和提高信道速率而得以大大提升。不仅如此，光波分复还为设计实施灵活、可靠、成本效益好的光纤网络提供了新的一维空间。

在光纤网络中，光信号在转换成电信号之前可能经过多个光结点。光纤网络中的子系统引入的传输特性的缺陷会在信号传递过程中积累并使光信号恶化，比如相干串扰，滤波效应，光器件中的色散以及光纤色散和非线性效应等。这些效应的积累使光纤网络的覆盖范围受到限制。因此，研究这些效应及其在子系统级联中的影响是非常重要的。

本博士论文对光纤网络中一些重要的子系统进行了理论和实验研究。

论文中开发了用于研究子系统级联特性的有效工具：建立了评估相干串扰影响的理论模型。该模型被用于计算基于波导阵列光栅路由器的波长路由网络的规模，还被用于计算一种新型 2×2 多波长交差互联器处理波长的最大能力；提出了一种测量光器件色散的方法并成功地测量出光波上下话路复接器的色散特性；更新了已有的光纤环路试验装置，使其具有实验测试多波长子系统的能力。该装置被用于实验测量基于波导阵列光栅的波长路由器的级联特性，基于半导体光放大器交叉增益调制的每秒十千兆比特的波长变换器的级联特性，以及具有色散管理功能的光纤链路的级联特性。

论文中也提出一些新型子系统：由波长交换模块组成的模块化 2×2 多波长交差互联器，基于半导体调制器中交叉相位调制的波长变换器，使用光纤分布反馈激光器及共享泵谱源构成的可选波长光源，基于饱和半导体光放大器的相干串扰压缩装置，以及结构简单的啁啾归零码发射机。

该博士论文由二十篇博士工作期间在相关研究领域国际期刊和学术会议上发表的论文和一篇总结构成。未发表的有关理论推导的细节附在论文的附录中。

Acknowledgements

The author would like to take this opportunity to express his sincere thanks to the individuals and institutions who in various ways have contributed to this investigation.

First, the author would like to acknowledge his supervisors at the Research Center COM: Professor Palle Jeppesen and Rune J.S. Pedersen (now with Tellabs Denmark) for their support, guidance, encouragement and inspiration. Also thanks to the Danish Technical and Research Foundation for the financial supports.

The author would like to thank all co-authors for the good co-operation, fruitful discussions and exciting time in the laboratory. They are: Xueyan Zheng, Christian J. Rasmussen, Christophe Peucheret, Stig N. Knudsen, Jianjun Yu, Allan Kloch, David Wolfson, Henrik N. Poulsen, Anders T. Clausen, Alvaro Buxens, Yujun Qian, Poul Varming, Leif Oxenløwe, Tina Fjelde, Irine Munoz, Jim Fraser, John D. Bainbridge and Mike Cox. Many of his colleagues at COM and EMI, although not on the list of co-authors, are acknowledged for their kind help and everlasting friendship.

The author would like to give special thanks to Bo F. Jørgensen (now with Tellabs) for the patient instruction in the lab during the first few months of the author's stay, to Ralph B. Dean (Nortel Networks) for keeping posting excellent devices.

Lucent Technologies Denmark and Nortel Networks are acknowledged for providing optical fibers and optical components.

Last but not least, thanks to my family for their support throughout the project.

Fenghai Liu

Lyngby, Denmark

December 2000

Publication list

[I] F. Liu, C.J. Rasmussen, and R.J.S. Pedersen: “Experimental verification of a new model describing the influence of incomplete signal extinction ratio on the sensitivity degradation due to multiple interferometric crosstalk”, IEEE Photonics Technology Letters, Vol. 11(1), 1999, pp. 137-139.

[II] C.J. Rasmussen, F. Liu, R.J. S. Pedersen and B.F. Jørgensen: “Theoretical and experimental studies of the influence of the number of crosstalk signals on the penalty caused by incoherent optical crosstalk”, Proc. OFC'99, San Jose, USA, February 1999, paper TuR5, pp. 258-260.

[III] F. Liu, C.J. Rasmussen and R.J.S. Pedersen: “Influence of interferometric crosstalk in a cascade of 10 Gb/s wavelength routers and an improved Gaussian crosstalk model”, Tech. Dig. CLEO'98, San Fransisco, California, USA, May 1998, pp. 318-319.

[IV] F. Liu, R.J.S. Pedersen and P. Jeppesen: “Very low crosstalk wavelength router construction using arrayed-waveguide grating multi/demultiplexers”, Electronics Letters, Vol. 35(10), 1999, pp. 839-840.

[V] F. Liu, R.J.S. Pedersen, C. Peucheret, and P. Jeppesen: “Experimental verification of a very low crosstalk wavelength router using arrayed-waveguide grating”, Proc. IEEE/LEOS Summer Topicals meeting, San Diego, USA, 1999, pp. 33-34.

[VI] F. Liu, X. Zheng, H.N. Poulsen, D. Wolfson and P. Jeppesen: “Reduction of interferometric crosstalk induced penalty using a saturated semiconductor optical amplifier”, Proc. LEOS Annual Meeting 2000, Puerto Rico, November 2000, pp.273-274.

[VII] F. Liu, X. Zheng, R.J.S. Pedersen and P. Jeppesen: “Interferometric crosstalk suppression using polarization multiplexing technique and an SOA”, Tech. Dig. CLEO’2000, San Fransisco, California, USA, May 2000, pp.91-92.

[VIII] X. Zheng, F. Liu, D. Wolfson and A. Kloch: “Suppression of interferometric crosstalk and ASE noise using a polarization multiplexing technique and SOA”, IEEE Photonics Technology Letters, Vol.12 (8), 2000, pp.1091-1093.

[IX] X. Zheng, F. Liu, J. Yu, D. Wolfson, A. Kloch and T. Fjelde: “Simultaneous interferometric crosstalk suppression in WDM channels using polarization multiplexing technique and SOA”, Proc. ECOC’2000, Munich, September 2000, pp.169-170.

[X] X. Zheng, F. Liu, and A. Kloch: “Experimental investigation of the cascadability of across-gain modulation wavelength converter”, IEEE Photonics Technology Letters, Vol.12 (3), 2000, pp272-274.

[XI] X. Zheng and F. Liu: “Cascadability improvement of a cross-gain modulation wavelength converter using a grating based optical add/drop multiplexer”, Proc. OFC'2000, Baltimore, Maryland, USA, February 2000, paper TuF4.

[XII] F. Liu, X. Zheng, L. Oxenloewe, R.J.S. Pedersen, P. Jeppesen, J. Fraser, J.D. Bainbridge and M. Cox: "Wavelength conversion based on cross-phase modulation in a semiconductor Mach-Zehnder modulator", Proc. OFC'2001, Anaheim, California, USA, March 2001, paper WK4.

[XIII] F. Liu, R.J.S. Pedersen and P. Jeppesen: "Performance analysis of a novel multi-wavelength cross-connect based on optical add/drop multiplexers", Proc. ECOC'99, Nice, France, September 1999, vol. 1, pp. 422-423.

[XIV] F. Liu, R.J.S. Pedersen and P. Jeppesen: "Novel 2×2 multiwavelength optical cross-connects based on optical add/drop multiplexers", IEEE Photonics Technology Letters, Vol.12 (9), 2000, pp.1246-1248.

[XV] F. Liu, X. Zheng, R.J.S. Pedersen and P. Jeppesen: "Fully reconfigurable 2x2 optical cross-connect using tunable wavelength switching modules", Proc. OFC'2001, Anaheim California, USA, March 2001, paper TuW1.

[XVI] F. Liu, X. Zheng, R.J.S. Pedersen, P. Varming, A. Buxens, Y. Qian and P. Jeppesen: "Cost-effective wavelength selectable light source using DFB fiber laser array", Electronics Letters, Vol.36 (7), 2000, pp 620-621.

[XVII] C. Peucheret, I. Munoz, A. Buxens, F. Liu and S. N. Knudsen: "L-band transmission over 1000 km using standard and dispersion-compensating fibers in pre-compensation scheme optimized at 1550 nm", Electronics Letters, Vol. 35(20), 1999, pp. 1759-1761.

[XVIII] F. Liu, C. Peucheret, X. Zheng, R.J.S. Pedersen and P. Jeppesen: "A novel chirped return-to-zero transmitter and transmission experiments", Proc. ECOC'2000, Munich, Germany, September 2000, Vol.3, pp.113-114.

[XIX] F. Liu, X. Zheng, C. Peucheret, S.N. Knudsen, R.J.S. Pedersen and P. Jeppesen: "Chirped return-to-zero source used in 8×10Gb/s transmission over 2000km of standard singlemode fibre", Electronics Letters, Vol.36 (16), 2000. pp.1399-1400.

[XX] C. Peucheret, F. Liu and R. J. S. Pedersen: "Measurement of small dispersion values in optical components", Electronics Letters, Vol.35 (16), 1999, pp. 409-411.

[XXI] F. Liu, X. Zheng, R.J.S. Pedersen, P. Jeppesen, J. Fraser, J.D. Bainbridge and M. Cox: "Increasing line rate by combining ETDM and OTDM in a semiconductor Mach-Zehnder modulator", Proc. OFC'2001, Anaheim California, USA, March 2001, paper MJ4.

[XXII] X. Zheng, F. Liu, and P. Jeppesen: "Optimisation of optical receiver for 10 Gbit/s optical duobinary transmission system", Proc. OFC'2001, Anaheim California, USA, March 2001, paper WDD64.

[XXIII] J. Yu, X. Zheng, F. Liu, A. Buxens and P. Jeppesen: "Simultaneous realization wavelength conversion and signal regeneration using a non-linear optical loop mirror", Optics Communications, Vol. 175, 2000, pp. 173-177.

[XXIV] J. Yu, X. Zheng, F. Liu, C. Peucheret, A. T. Clausen, H. N. Poulsen and P. Jeppesen: "8×40 Gb/s 55-km WDM transmission over conventional fiber using a new RZ optical source", IEEE Photonics Technology Letters, Vol. 12(7), 2000, pp. 912-914.

[XXV] C. Rasmussen, F. Liu and P. Jeppesen: "Accurate formulas for the penalty caused by interferometric crosstalk, Proc. ECOC'2000, Munich, Germany, September 2000, pp149-150.

[XXVI] X. Zheng, F. Liu, A. Clausen and A. Buxens: "High Performance Wavelength Converter Based on Semiconductor Optical Amplifier and Mach-Zehnder Interferometer Optical add/drop Multiplexer", 10th Optical Amplifiers and Their Applications, OSA Technical Digest, Nara, Japan, June 1999, p132-134.

[XXVII] X. Zheng and F. Liu: "A novel dynamic wavelength cross-connect based on Mach-Zehnder Interferometer Optical add/drop multiplexer and optical space switch", Proc. CLEO Pacific Rim'99, Korea, 1999, pp.783-784.

[XXVIII] H.N. Poulsen, A.T. Clausen, A. Buxens, L. Oxenloewe, C. Peucheret, C. Rasmussen, F. Liu, J. Yu, A. Kloch, T. Fjelde, D. Wolfson, P. Jeppesen: "Ultra fast all-optical signal processing in semiconductor and fiber based devices", invited paper, Proc. ECOC'2000, Munich, Germany, September 2000, Vol. 3, pp.59-62.

Contents

Summary

1. Introduction

1.1 Background

Transmission capacity in optical fiber communication systems is greatly increased by the use of wavelength division multiplexing (WDM) technology and optical amplification. At present, the highest capacity in a single fiber is approaching 10 Tb/s in the laboratories [1, 2]. In order to satisfy the ever-increasing capacity demand from Internet, mobile and multimedia services, the transmission capacity will keep growing by exploration of new transmission windows in the fiber and the use of high spectrum utilization modulation formats [3, 4].

A three-layered structure was defined for optical transport networks by ITU-T [5] which are briefly described as follows:

- **Circuit layer:** The circuit layer manages end-to-end connections (circuits) established dynamically on the basis of short term provisioning, such as circuit switching, packet switching, cell relay, frame relay etc.; each circuit is related to a particular service: telephony, data transmission and so on;
- **Optical transmission media layer:** The transmission media layer provides point-to-point inter-connection between network nodes by fiber systems;
- **Path layer:** The path layer bridges these two layers, mainly with Digital Cross Connection (DXC) systems. In particular, different circuits, related to different services, are united to form a path (such as Plesiochronous Digital Hierarchy (PDH) path, Synchronous Digital Hierarchy (SDH) path, Asynchronous Transfer Mode (ATM) path, etc.) and routed through the network; network monitoring and restoration are also realized in this layer.

As the transport capacity increases dramatically, it is hard to satisfy the demand if the path layer is completely realized by DXC's, owing to the limitations of processing speed, power consumption, and cost. In order to cope with this evolution, it has been proposed to introduce an optical path layer underneath the electrical path layer in which both transmission and routing facilities would be available particularly on high bit-rate optical channels, in order to limit the size of the electronic switches [6]. WDM not only can be used to increase transmission capacity, but also to introduce a new dimension to design and implement flexible, reliable, cost-effective optical networks. Very high capacity data streams are routed through the optical path layer by means of optical cross connects (OXC) that operate directly in the optical domain and the OXC is interfaced with a DXC to allow demultiplexing and routing at lower hierarchical levels [7].

Two of the most important issues in optically cross-connected transport networks are: 1) optical channel monitoring and management; 2) cascadability of subsystems used in the optical path layer as well as in the transmission layer. The subsystem is here defined as a combination of components which can provide an independent function in the optical network, such as a wavelength router, an optical cross-connects, a wavelength converter. A

transmission link that includes transmission fiber, optical amplifier and dispersion compensator is also defined as a subsystem.

Optical signals may pass through several nodes in an optically cross-connected network without being terminated and converted into an electrical signal, so the impairments from the subsystems, such as crosstalk, ASE noise, filtering effect, non-linearity, chromatic dispersion and polarization mode dispersion, will accumulate and degrade the signal, hence limit the size of the network. Study of these impairments in subsystems is very important. Although optical channel monitoring and management are also important issues, they are beyond the scope of the present investigations.

1.2 Description of present work

The purpose of the work is to investigate the most important subsystems used in optical networks with emphasis on transmission characterization, cascadability and new implementation schemes.

In this Ph.D. thesis, a number of subsystems are studied, such as optical cross-connects, wavelength routers, wavelength converters, wavelength selectable light sources, chirped return-to-zero transmitters, crosstalk suppressors and dispersion managed fiber transmission links; some important issues are addressed, such as interferometric crosstalk, filtering effect, dispersion in optical components and fiber dispersion and non-linearity; Useful tools are developed: 1) crosstalk models to calculate the interferometric crosstalk induced power penalty; 2) method to measure dispersion in optical components or subsystems; 3) fiber re-circulating loop set-up to experimentally characterize the performance of subsystems after a number of cascades;

Interferometric crosstalk which originates from signals with a frequency difference less than the receiver bandwidth has stronger impact on system performance than so-called power-addition crosstalk from neighboring channels. A widely used Gaussian crosstalk model is improved by taking signal extinction ratio into account and by including optically pre-amplified receivers. The improved model gives a more accurate estimation of crosstalk induced power penalty with simple analytic expressions. The model was verified by an experiment and was used to analyze the crosstalk in a cascade of arrayed-waveguide grating (AWG) based wavelength routers and in a new modular 2×2 multi-wavelength cross-connect. Another more accurate numerical model is developed and used to validate the necessary number of crosstalk terms needed for the improved Gaussian crosstalk model to be a good approximation.

Dispersion in optical components might also induce degradation of optical signal at high bit-rates. An accurate method to measure dispersion in optical components is developed. It imposes no critical requirements on the amplitude transfer function of the optical devices under test.

A fiber re-circulating loop set-up was upgraded and used for investigation of cascadability of subsystems. The loop set-up associated with dispersion shifted fibers (DSF) was used to characterize optical components and subsystems [8, 9] and it works fine as far as having one wavelength channel in the loop. When more wavelength channels are re-circulated in the loop, four wave mixing between the channels becomes a problem. Different dispersion schemes are used in the loop to overcome the four wave mixing while it is still supporting transmission of high speed signal of 10Gb/s. Gain equalization is used in order to obtain

equal power for all channels. The loop set-up was used to investigate the cascadability of AWG routers limited by interferometric crosstalk, to study the cascadability improvement of wavelength converters based on cross-gain modulation in semiconductor optical amplifiers (SOAs) limited by the high frequency response, to transmit L-band signals using dispersion maps optimized for C-band, and to transmit chirped return to zero channels through dispersion managed normalized fiber sections. Besides characterization of subsystems, a few new subsystems are proposed. A modular 2×2 multiwavelength cross-connect scheme based on optical add/drop multiplexers (OADMs) and space switches is proposed, and its basic performance is analyzed and experimentally demonstrated. The scheme can be further extended to a fully reconfigurable 2×2 optical cross-connect with wavelength translation using wavelength tunable OADMs and tunable wavelength converters. A low crosstalk N×N wavelength router is constructed using 1×N AWG multi/demultiplexers; a crosstalk level of –53 dB is measured from such an 8×8 wavelength router. A wavelength selectable light source is made using DFB fiber lasers and space switches, the source features stable wavelength output due to the use of DFB fiber laser and low cost due to the use of only one shared pump laser. A wavelength converter based on cross-phase modulation in a reversely biased semiconductor modulator is demonstrated at 10 Gb/s for both NRZ and RZ formats in a commercially available transmitter module. Several schemes based on a saturated semiconductor amplifier (SOA) for suppression of interferometric crosstalk are developed. A simple chirped RZ transmitter is constructed using only one external modulator, and its performance is demonstrated in a single channel 10 Gb/s transmission over 3600 km and 8×10 Gb/s transmission over 2000 km. These new subsystems provide useful options for designing a more flexible and cost-effective optical transport network.

1.3 Thesis outline

The summary of this thesis presents the most important results and emphasizes the major conclusions from the papers [I-XX]. The papers are numbered according to the order in which they appear in this summary. The summary is organized as follows. Section 2 discusses the interferometric crosstalk models, their assumptions and results verified by experiments. Section 3 discusses the cascadability of AWG routers showing the limitation from interferometric crosstalk. A low crosstalk router is also proposed and experimentally demonstrated in this section. Section 4 investigates different schemes based on saturated SOAs to suppress interferometric crosstalk in a single optical channel as well as WDM channels. Section 5 studies the cascadability improvement of wavelength converter based on cross gain modulation in SOAs. A new wavelength converter based on cross-phase modulation in a reversely biased semiconductor modulator is proposed and demonstrated at 10 Gb/s for both NRZ and RZ formats. Section 6 discusses dispersion managed fiber sections for transmission of L-band signals and chirped return-to-zero (CRZ) signals. A simple scheme to generate CRZ signals is proposed and experimentally demonstrated. Section 7 discusses a modular fully re-arrangeable 2×2 multi-wavelength cross-connect with and without wavelength translation. Section 8 describes a cost-effective wavelength selectable light source based on DFB fiber lasers and optical space switches. Section 9 presents a method to measure small dispersion in optical components. Section 10 gives the conclusion of the thesis. Appendix I includes details of the improved Gaussian crosstalk model. Appendix II describes method to measure dispersion in optical components in more details.

2. Interferometric crosstalk models

The Gaussian crosstalk model is widely used to calculate power penalty induced by interferometric crosstalk [10, 11]. Among other assumptions, the model assumes: 1) perfect signal extinction ratio; 2) a large number of independent crosstalk terms contribute the total crosstalk power so that the signal crosstalk beat noise follows a Gaussian distribution. These two assumptions may not hold in most cases. Besides, the model is only valid for PIN type receivers. In this project, more accurate models were developed to calculate the interferometric crosstalk induced power penalty. The model developed in paper [I] includes the signal extinction ratio while the model in paper [II] takes both the signal extinction ratio and the number of crosstalk terms into account.

In paper [I], the Gaussian crosstalk model is improved by introducing signal extinction ratio so that the signal crosstalk beat noise on both “1” and “0” levels is taken into account. Signal spontaneous emission beat noise is also taken into account when the model is applied to optically pre-amplified receivers. The improved model can well explain why larger penalties than predicted by the Gaussian crosstalk model are measured in our experiments and found in the literature [10]. The improved model still gives simple analytical expressions of crosstalk-induced penalty for both PIN and optically pre-amplified receivers, with signal extinction ratio taken into account as a parameter. Detailed description of the improve crosstalk model is listed in Appendix I.

Experiments are made to verify the improved model for both receiver types using either average power decision threshold setting or optimum decision threshold setting. Very good agreement between calculated and measured results is found in all cases. The calculation and experiment also show that the signal extinction ratio is an important parameter when predicting the impact from interferometric crosstalk. Without taking it into account, the crosstalk influence will be underestimated, which could be disastrous for network design. For instance, an extinction ratio deterioration from $r = 0$ (perfect extinction ratio used in the Gaussian crosstalk model) to $r = 0.15$ (ITU-T requirement for STM 16) results in a reduction of tolerable crosstalk power of 4.8 dB at 1 dB penalty in an optically pre-amplified receiver with optimum decision threshold, which corresponds to a 65% cut of nodes in a network.

In order to answer the question how many independent interferometric crosstalk terms are needed to give a good approximation by the improved Gaussian model, a more accurate numerical model is developed in paper [II]. The numerical model calculates the penalty caused by interferometric crosstalk, taking both signal extinction ratio and number of crosstalk terms into account. The numerical model is also verified by experiment with excellent agreement.

The numerical model confirms that the improved Gaussian crosstalk model gives a very good approximation when crosstalk power is contributed by six or more independent crosstalk terms and still gives a safe boundary condition by overestimating the crosstalk induced penalty when the number of crosstalk terms is less than six.

3. Cascadability of AWG routers and a low crosstalk router construction

Wavelength routing is a very promising technology in future advanced DWDM networks because of its simple structure and high degree of wavelength reuse among the nodes [12]. Reconfigurable wavelength routing networks with throughput of more than 1 Tb/s have been demonstrated in laboratories[13]. The combination of fast tunable laser diodes and passive wavelength routers can be used to perform optical packet switching, a big step towards “IP

over WDM"[14, 15]. The key subsystem in the wavelength routing networks is a wavelength router, and an integrated optical N×N wavelength router based on an arrayed-waveguide-grating (AWG) is a good candidate.

Due to the non-ideal transfer function of a physical AWG router, a node will receive not only the signal from the node it is connected to, but also interferometric crosstalk from the other nodes. The interferometric crosstalk will further accumulate when the routers are used in cascade in the network.

In paper [III], interferometric crosstalk in a cascade of AWG routers is investigated experimentally using a re-circulating loop set-up at 10Gb/s. In the set-up, the wanted signal deteriorated by interferometric crosstalk from other input ports of an AWG router is re-circulated in the loop set-up. Four more crosstalk terms are added for each roundtrip to the wanted signal. The degradation of the wanted signal is measured in terms of power penalty. The experiment shows that even for a low crosstalk of -34.8 dB from each of the four input ports of an AWG router, a power penalty of 4.1 dB is measured when five routers are cascaded.

The improved Gaussian crosstalk model described in Section 2 is used to calculate the crosstalk induced penalty in the cascade of AWG routers; very good agreement is found between the calculated and measured results. The Gaussian crosstalk model without modification overestimates the crosstalk tolerance by 5 dB for the same 1 dB penalty.

The interferometric crosstalk from each input port needs to be very small in order that an AWG router with large size can be used in cascade. Although a significant amount of effort is put into reducing the crosstalk level in AWG routers [16, 17], it is also important to consider alternative structures with the same functionality as a wavelength router.

In paper [IV], it is proposed that an N×N wavelength router can be constructed using 1×N AWG multi/demultiplexers. The new router construction features the same routing table, but the interferometric crosstalk can be significantly reduced due to the combined transfer function of a multiplexer and demultiplexer. An 8×8 wavelength router is constructed using commercial 1×8 AWG multi/demultiplexers; the measured maximum crosstalk is -53 dB, which is much less than the crosstalk level in any AWG router reported so far. In paper [V], the 8×8 wavelength router is used to route 8 WDM channels at 10Gb/s, and no noticeable penalty is observed after the router. It is further pointed out that using reported 1×64 AWG multi/demultiplexers with crosstalk of –27 dB, a 64×64 wavelength router with crosstalk level of –54 dB can be constructed. Such low a crosstalk level enables the 64×64 wavelength router to be cascaded 10 times at 1 dB penalty in the term of crosstalk limitation. Hence rather large wavelength routing networks can be built.

The number of multi/demultiplexers used in the N×N wavelength router construction is 2N, which indicates that the construction of the wavelength router could be expensive in terms of number of components used when N is large. This is a major drawback of this scheme.

4. Suppression of interferometric crosstalk using a saturated SOA

As shown in the Section 2, interferometric crosstalk has a strong impact on the signal in transparent optical networks. To avoid the influence, crosstalk in the subsystems must be kept low, or alternatively, effective techniques to suppress the crosstalk need to be developed. Several techniques have been used for this purpose. A gain saturated laser diode amplifier can suppress interferometric crosstalk, but it is limited to low bit-rate [18]. A wavelength

converter based on cross gain modulation in an SOA has been used to suppress the crosstalk [19], but wavelength conversion is not always needed; Cross phase modulation in SOA based interferometers has been used to suppress the crosstalk [20, 21], but the structure is complicated.

In this work, a saturated SOA is used to suppress the crosstalk. When input power into a SOA is high enough, the gain of the SOA starts to saturate. Hence, the input power fluctuation caused by interferometric crosstalk will be suppressed at the output. The SOA also induces waveform distortion when it is operated in saturation because of the gain transient effect, so some further step needs to be taken when a saturated SOA is used to suppress the crosstalk.

In paper [VI], CW light is injected into the SOA counter-propagating with the input signal in the SOA. The SOA gain is held by the CW light to some extent, so waveform distortion of the output signal is relaxed while the SOA still exhibits saturation characteristics for the input signal. Experiments demonstrated that the saturated SOA with gain holding light could be used to reduce the impact from interferometric crosstalk at both 2.5 Gb/s and 10 Gb/s. 4 dB more crosstalk power can be tolerated at 1 dB penalty by using the SOA. Unfortunately, extinction ratio of the output signal is degraded because of saturation.

In paper [VII], a polarization multiplexing technique is introduced to remove the waveform distortion in the saturated SOA when it is used to suppress interferometric crosstalk. An optical dummy signal modulated by the data complementary is combined with the signal modulated by the data via a polarization combiner at the output of which we obtain two orthogonal polarization states. A constant optical power without bit transients is constructed after the polarization combiner, while a modulated signal is carried in each polarization state. A saturated SOA is used to suppress the power fluctuation on the polarization multiplexed signal caused by interferometric crosstalk. The combined signal is demultiplexed into two polarization states before the optical receiver. Since the saturated SOA only experiences a constant power without bit-transients, no waveform distortion will occur at the output.

Experiment shows the interferometric crosstalk can be effectively suppressed using a saturated SOA and the polarization multiplexing method. A 6 dB higher crosstalk level can be tolerated at 1 dB penalty using this technique. The technique is also pattern independent and bit-rate transparent, and gives no waveform distortion or extinction ratio degradation.

In paper [VIII], it is shown that this technique can be used to suppress crosstalk within a large input power dynamic range of 14 dB due to the large saturation range of the SOA. Suppression of in-band ASE noise is also demonstrated.

Most crosstalk suppression schemes published so far only work for a single channel, while a scheme to simultaneously suppress crosstalk for multiple channels is attractive and challenging.

In paper [IX], the saturated SOA and polarization multiplexing technique is used to suppress crosstalk for multiple WDM channels and crosstalk suppression for two channels is successfully demonstrated. It is found that the gain saturation of the SOA becomes shallower when more channels are present, hence the crosstalk suppression becomes less effective.

5. Cascadability of wavelength converters based on XGM in SOAs and wavelength conversion in a semiconductor MZ modulator

Wavelength converters are key elements in future advanced optical networks, and several technologies have been used to realize wavelength conversion [22, 23]. Wavelength conversion based on cross gain modulation (XGM) in a semiconductor optical amplifier

(SOA) is the simplest to realize and capable of converting the input signal also to the same wavelength which is favorable in many applications. An important issue is cascadability since the signal might be converted more than once in a network [24]. The cascadability of a wavelength converter based on XGM in an SOA has been found to be limited by signal extinction ratio degradation and accumulated ASE from the SOAs [25].

In paper [X], insufficient high frequency response is shown to be another severe limiting factor for conversion at high speed. It is also demonstrated that the high frequency response can be improved by filtering the converted signal from the SOA using a fiber Bragg grating based optical add/drop multiplexer (OADM), hence the cascadability of the wavelength converter can be improved.

The cascadability of the wavelength converter based on XGM in an SOA is investigated using the re-circulating loop set-up. The wavelength converter is placed in the loop set-up, converting the input signal to the same wavelength. The wavelength conversion at 10 Gb/s can be performed several times to the same original signal by re-circulating the converted signal in the loop, in order to simulate the wavelength converter used in cascade.

A 1.25 mm long SOA is used in paper [X], and it has a 3 dB frequency response of 10 GHz. Experiment shows that the wavelength converter can be cascaded up to 5 times with a penalty of 10 dB at BER of 10^{-9}. Eye closure after five roundtrips is observed; we believe the eye closure is due to insufficient frequency response.

Since the converted signal from the SOA has blue chirp on the rising edges and red chirp on the falling edges, a fiber Bragg grating based OADM is used after the SOA to re-shape the converted signal. By performing a kind of FM to AM conversion through the steep transfer function of the grating, the high frequency response is improved [26]. The measured 3 dB bandwidth is extended to 20 GHz. By using the OADM after the SOA, the wavelength converter can be cascaded up to 8 times with penalty of 4 dB at BER of 10^{-9}.

In paper [XI], the same method is applied to a 0.8 mm SOA. Without the OADM, the 3 dB frequency response is only 4GHz, and a cascade of two of such converters exhibits a penalty of 10 dB at BER of 10^{-9}. By adding the OADM after the SOA, the 3 dB frequency response is improved to 18 GHz, hence the converter can be cascaded up to 6 times.

Recently wavelength conversion based on cross-absorption modulation in saturated electroabsorption modulators (EAM) has been reported, showing high conversion speed up to 40 Gb/s, large wavelength range and regenerative capability [27-28]. However, the cross-absorption modulation in EAMs requires high input optical power, which restricts conversion to RZ format with short optical pulses (~10ps). A new scheme of wavelength conversion based on cross-phase modulation in a reversely biased semiconductor Mach-Zehnder modulator is proposed and demonstrated in paper [XII].

The InGaAsP waveguide under reverse bias absorbs input light and generates carriers, and hence the refractive index is changed. The absorption ratio is different under different bias voltages. When an intensity-modulated optical signal passes through such a waveguide, the refractive index will be modulated. The modulation depth of the index is also different under different bias voltages.

When the intensity-modulated optical input signal passes through an InGaAsP Mach-Zehnder interferometer with two arms being reversely biased at different voltages, the refractive index in two arms are modulated by the input signal at different depths. A CW probe light is injected into the M-Z interferometer from the other direction, counter-propagating with the input signal. The CW probe light experiences a phase difference between the two arms, and

hence becomes intensity-modulated at the output of the M-Z interferometer. The converted signal is coupled out via an optical circulator.

Wavelength conversion at 10 Gb/s for both NRZ and RZ formats is made in a semiconductor M-Z modulator designed for commercial transmitters. The extinction ratio of the converted signal is better than 13 dB, and penalty is less than 1.5 dB in both cases. Concerning the converted signal polarity, both non-inverted and inverted conversion are realized for NRZ format in the same device under different bias conditions. In comparison with wavelength conversion based on XPM in SOAs, this scheme gives no extra spontaneous emission noise.

As a new method to realize wavelength conversion, further work needs to be done to verify the conversion wavelength range, conversion efficiency, input power dynamic range, conversion speed and regenerative ability.

6. Optical cross-connects based on OADMs

Optical cross-connects are core elements in the optical path layer for development of cost effective and reconfigurable optical networks. Optical cross-connects can be classified into three categories in terms of rearrangeability [30]:

1) Fixed cross-connects, or referred to as wavelength router;
2) Rearrangeable cross-connects, also referred to wavelength path cross-connects;
3) Fully rearrangeable cross-connects with wavelength translation, also referred to as virtual wavelength path cross-connects.

According to ref [6], the requirements placed on the optical path cross-connect subsystems are as follows:

1) Strictly non-blocking;
2) Maximum modular growth capability;
3) Easy evolution from wavelength paths (WPs) to virtual wavelength paths (VWPs);
4) Low crosstalk and low optical loss;
5) Based on rather mature and reliable optical technologies.

In paper [XIII], a modular 2×2 multi-wavelength optical cross-connect is proposed. The basic unit in the OXC is a 2×2 wavelength switching block consisting of 2 optical add/drop multiplexers (OADMs) with identical drop wavelength and an optical space switch. The wavelength switching block cross-connects one pair of channels with the same drop wavelength between two fibers, and all other channels just bypass the block. Constructing a 2×2 multi-wavelength optical cross-connect can be done simply by cascading a number of such wavelength switching blocks with fixed wavelength. Since each wavelength switching block independently cross-connects a pair of channels between the two fibers, the 2×2 multi-wavelength cross-connect is strictly non-blocking. The modular structure enables a node to start with a small number of switching blocks and later to add more blocks when it is necessary. This is favorable in terms of initial investment.

The basic performance of the 2×2 multi-wavelength cross-connect is analyzed in paper [XIII]. The 2×2 OXC possesses a symmetric structure, hence all channels will experience the same loss in the full configuration. The excess loss of a single block is very low due to low loss in an OADM and an optical switch. Optical amplifiers can be put between blocks to compensate for the loss when the number of block is very large.

Crosstalk in both “drop-add” and “bypass” blocks is analyzed. When a wavelength channel passes through an OXC node, it experiences two types of switching blocks. In the “drop-add” block, the channel is dropped, switched and added back to the fiber; here the crosstalk is mainly due to the imperfect drop band reflection of the OADMs. In the “bypass” blocks, the channel simply bypasses the blocks; here crosstalk is mainly due to the imperfect extinction ratio of the specific type of OADM and the finite reflection outside the drop band of the OADMs. Given a perfect on-off ratio from optical switches, these parameters are quantified in order to get satisfactory performance in a 2×2 OXC with different number of wavelength switching blocks.

A 2×2 OXC node with two wavelength switching blocks is experimentally constructed in paper [XIV], using commercial components: fiber grating based Mach-Zehnder interferometric OADMs and mechanical optic switches. Two fibers each hosting 8 WDM channels at 10 Gb/s pass through the node with two wavelength switching blocks at 1556nm and 1559nm. The BER curves of each channel from one output fiber are measured in order to determine the signal degradation from the OXC node. It is shown that the main degradation stems from crosstalk, and the measured penalty is in good agreement with the calculated penalty caused by crosstalk.

A possible integration scheme of a wavelength switching block is also proposed in paper [XIV], using planar waveguide grating based OADMs and thermo-optic switches. If each wavelength switching block is fabricated as a planar waveguide module, low cost mass production of such modules is possible.

In paper [XV], a tunable 2×2 wavelength switching block is further developed using tunable OADMs, 2×2 optical space switch and tunable wavelength converters. A fully reconfigurable 2×2 optical cross-connect with wavelength translation can be constructed using such tunable wavelength switching blocks. In comparison with conventional constructions [6], this structure avoids the use of large size optical space switches and possesses a very high degree of modularity.

The basic concept of the 2×2 OXC is demonstrated experimentally, focusing on the tunable wavelength conversion. Tuning speed and cascadability of the modules need to be further studied.

7. Wavelength selectable light source based on DFB fiber lasers

Wavelength selectable light sources are needed in tunable wavelength converters, as well as in back-up transmitters in WDM transmission systems. In paper [XVI], a wavelength selectable light source based on DFB fiber lasers and space switches is proposed and experimentally demonstrated.

Stable single mode operation fiber DFB lasers were made by directly UV writing a Bragg grating into an Er^{3+}-doped fiber and inducing $\pi/2$ phase shift in the middle of the grating. A stable $\pi/2$ phase shift can also be created by UV exposure [31]. Fiber DFB lasers generate lasing signal around 1.55μm when it is pumped by either a 1480nm or 980nm pump laser. Fiber DFB lasers are good candidates for high quality light sources in high bit-rate optical systems due to their very high side-mode suppression ratio, single mode operation without mode hoping, high output power and inherent fiber compatibility. They are even more attractive in dense WDM systems owing to accurate wavelength setting and wavelength stability over a large temperature range [32-34]. Fiber DFB lasers with different wavelengths can be made in both C- and L-band and they have shown excellent performance in WDM

transmission experiments [35, 36]. However, the need of optical pump sources for lasing operation dramatically increases the cost of using DFB fiber lasers in transmission systems.

A cost-effective wavelength selectable light source is proposed using DFB fiber lasers and a single shared pump. A set of DFB fiber lasers with different wavelengths is connected between two optical switches. Pump power is guided into the desired DFB fiber laser via one of the optical space switches, and the lasing signal is guided out through the other space switch, and is further amplified in an extra erbium-doped fiber by the residual pump power. Wavelength selection is simply performed by selecting the corresponding DFB fiber laser between the two space switches.

A wavelength selectable source with two wavelengths is constructed experimentally, and output power higher than 5 dBm and signal to ASE ratio better than 40 dB are obtained for each wavelength. Experiment also shows that the switching speed is limited to about 11 ms by the combination of the optical switch, extra erbium-doped fiber and DFB fiber laser.

Since a very low wavelength temperature coefficient can be achieved using a special bi-metal package [32], no further wavelength monitoring and active wavelength servo are necessary. This is a major advantage in comparison with wavelength tunable semiconductor lasers. As only one shared pump laser is used to support many DFB fiber lasers with different wavelength, the proposed wavelength selectable light source is cost-effective.

8. Transmission over dispersion managed sections

As the size and capacity of optical networks increase, transmission of large capacity over long distance becomes an important issue. In order to transmit large number of WDM channels at high bit-rate over long distances, dispersion management must be adopted in the transmission fiber. It has been suggested that the design of future optical transparent networks could be facilitated by the use of so-called “normalized sections” [37]. Any path through the network would then consist of a cascade of identical normalized sections and both network scalability and management would rely on knowledge of the accumulated signal degradation after transmission through a certain number of these sections. Transmission over these normalized sections can be optimized by simulation [38].

The re-circulating loop set-up is again a powerful tool to investigate different cases of transmission over normalized fiber sections. The loop set-up was used to investigate normalized sections consisting of standard single mode fibers (SMF) and dispersion compensating fibers (DCF), including systematic optimization of input powers into SMF and DCF in normalized sections, optimization of dispersion compensation ratio, L-band signal transmission and transmission of chirped return-to-zero single channel and WDM channels.

Extension of the conventional C band transmission window (1530 to 1565nm) into the L-band (1570-1610) is one attractive way to increase the capacity in dense WDM systems. Terabit WDM transmission using both C- and L-bands has been demonstrated [39] and continuing progress in optimizing design of L-band EDFA is made [40]. Transmission of both C- and L-band signals over the same normalized section is important for simplifying the network design. In paper [XVII], a L-band signal at 1597nm is transmitted over normalized fiber sections designed for 1550nm.

Two normalized sections were used in the loop set-up. One consists of 50 km SMF and the other of 80 km SMF. Wideband DCFs were used to fully compensate the dispersion at 1550nm in the two sections. Due to the simultaneous dispersion and dispersion slope compensation feature from the wideband DCFs [41], the measured values of residual

dispersion at 1597 nm were –21.3 ps/nm and –13.4 ps/nm for the 50km and 80 km spans respectively. Transmission of the 1597 nm channel over 1000 km is realized in both kinds of sections using a pre-compensation scheme.

In order to transmit large capacity WDM channels over long distances in optical transparent networks, different modulation formats have been investigated. Among them, the chirped return-to-zero (CRZ) modulation format has become of great importance at high bit-rate, because of its robustness to fibre non-linearity and dispersion. Many of the transmission experiments achieving the longest distances with large capacity have used the CRZ format [42, 43].

Normally a CRZ signal is obtained by modulating CW light in a chain of external modulators: first the amplitude of the light is modulated using the NRZ signal; second the amplitude is modulated again using a bit-synchronized clock to get the RZ pulse shape; last the phase is modulated using a bit-synchronized clock to add a chirp on the pulse. The CRZ transmitters built in this way are complex and expensive.

In paper [XVIII], a new and simplified way to generate the CRZ pulses is proposed using only one external modulator and a CW light source. An electrical 2:1 selector is used to generate 10 Gb/s RZ electrical pulses by selecting a 10 Gb/s NRZ signal (2^{31}-1 pattern) at the rising edge of a synchronized 10 GHz clock and selecting a constant “space” at the falling edge. In principle, AND logic operation between a 10 Gb/s NRZ signal and a synchronized 10 GHz clock in an electrical gate can also generate a 10 Gb/s RZ signal. CW light from a DFB semiconductor laser is coupled into a Lithium Niobate (LN) Mach-Zehnder modulator via a polarization controller. When the RZ signal generated from the 2:1 selector is amplified by an electrical amplifier (E-amp), and applied to one electrode of the LN modulator with a proper DC bias, a 10 Gb/s RZ optical signal is generated. Since only one electrode of the LN modulator is used, a bit-synchronized chirp is automatically added to the RZ optical pulse. A maximum phase shift of $\pi/2$ can be added to the optical signal and the sign of the chirp can be adjusted.

Single channel transmission of the CRZ signal is performed in the fiber re-circulating loop. The loop contains an 80 km span of SMF and a 13 km DCF providing 100% dispersion compensation in a pre-compensation scheme. A 40 km SMF (so-called pre-distortion fiber) and a corresponding 6.5 km DCF are put after the transmitter and before the receiver, respectively, to reduce the maximum accumulated dispersion in the transmission. This dispersion pre-distortion scheme is demonstrated to be able to improve the transmission distance in computer simulations [38]. The power into SMF and DCF, respectively, is optimized at the 45th roundtrip. BER curves for different transmission distances are measured, and a 6 dB power penalty at BER=10^{-9} can be found after transmission over 3600 km of SMF.

In paper [XIX], eight channels of the CRZ signals are transmitted in the loop using the same dispersion map. Since the DCF provides both dispersion and dispersion slope compensation, no channel-by-channel dispersion compensation is used at the receiver. Non the less, the maximum residual dispersion after 2000 km transmission over SMF is less than 142.1 ps/nm for all channels. Two Mach-Zehnder type gain equalizers with different free spectral ranges are used before the DCF in the loop to equalize the overall gain of 3 EDFAs. The equalizers are carefully adjusted, so that the power variation between channels is kept less than 5 dB even after 25 roundtrips. The power penalties of all channels are measured after transmission of 2000 km of SMF and the maximum penalty is less than 5 dB.

These good transmission results are due to the use of the CRZ transmitters, advanced dispersion map, and precise gain equalization.

9. Measurement of dispersion in optical components

In dense WDM networks, the cascading of narrowband devices such as filters, multi/demultiplexers and OADMs might result in phase-induced degradation of optical signals, especially at high bit-rates [44]. Therefore, a precise method for measuring the dispersion characteristics of individual optical components is necessary. The phase-shift technique has previously been used to measure the group delay of optical devices [44]. Curve fitting and numerical differentiation are required to obtain the dispersion from the measured group delay, resulting in additional inaccuracy. The RF modulation method originally used to measure dispersion in optical fibers has a high accuracy, but the minimum measurable dispersion value is too large to exist in most optical components [45, 46].

The RF method relies on the fact that, due to the dispersive nature of optical components, the propagation constants of the two sidebands of an amplitude modulated signal are different. For a given dispersion value, modulation frequencies can be found where the components of the beat signal between the carrier and the sidebands are in counter-phase, resulting in cancellations of the photocurrent seen as dips in the small signal frequency response. The total dispersion can be calculated from these frequencies using a simple equation [46].

In paper [XX], the RF method is extended to measure small dispersion in optical components by adding a constant dispersion offset, stemming from a 50km of standard single mode fiber in our case. The total dispersion from the optical component and the fiber offset is large enough to be measured using the RF method, and the dispersion offset from the fiber can be measured using the same method. The dispersion from the optical component is the difference of the two measured values. Using the extended RF method, both positive and negative dispersion in optical components can be measured with an accuracy of 1.2 ps/nm. Uneven amplitude transfer function of optical components results in an imperfect cancellation of the two sidebands in the RF method, but our calculation shows that the frequencies of the dips are the same as in the devices with flat amplitude transfer functions so that the extended RF method is still applicable. A detailed calculation is given in Appendix II.

The fluctuation of the dispersion in the fiber offset is characterized to be 1.2 ps/nm over 40 minutes, and the dispersion in an OADM is successfully measured.

10. Conclusion

This thesis investigates some of the most important subsystems in terms of transmission characterization, cascadability in optical network, functionality and implementation.

Interferometric crosstalk in subsystems has been investigated comprehensively. An improved Gaussian crosstalk model is developed which takes the signal extinction ratio into account when calculating the crosstalk induced power penalty. A numerical model further developed also includes the number of crosstalk terms. Both models are experimentally verified. The improved Gaussian crosstalk model is used to analyze the crosstalk influence in a cascade of AWG routers and in a cascade of wavelength switching modules in an OXC. It is a fact that the interferometric crosstalk cannot be filtered out by optical filters, but the crosstalk induced fluctuation on the optical signal power can be suppressed by different non-linear devices.

Saturated SOAs are used to suppress the interferometric crosstalk, and gain holding light or polarization multiplexing technique is used to eliminate the side-effects from a saturated SOA, such as waveform distortion and extinction ratio degradation.

Filtering of high frequency components in a wavelength converter based on XGM in a SOA is the main limiting factor for its use in a cascade, due to its insufficient frequency response. The high frequency response of the wavelength converter is improved using an OADM filter at the output of the SOA, by performing an FM to AM conversion on the chirped output signal. The maximum cascaded number of a 0.8 mm long SOA converters is improved from 2 to 6 in a re-circulating loop set-up. In dense WDM networks, the cascading of narrowband devices such as filters, multi/demultiplexers and OADMs might result in phase-induced degradation of optical signals, especially at high bit-rates. An accurate measurement of small dispersion in optical components is developed by extension of the RF modulation method that was used to measure large dispersion in optical fiber. The method can be used for components with uneven amplitude transfer functions as well as flat ones.

The fiber re-circulating loop set-up is upgraded to investigate transmission over normalized fiber sections with dispersion compensation. An L-band signal at 1597 nm is successfully transmitted more than 1000 km at 10 Gb/s using a dispersion map optimized for 1550 nm in C-band; CRZ signals at 10 Gb/s is transmitted over 3600 km SMF for single channel and 2000 km for 8 channels in an advanced dispersion map which are the longest ever demonstrated in our laboratory.

Useful subsystems are proposed and demonstrated experimentally. A 2×2 multiwavelength OXC constructed using wavelength switching blocks shows a high degree of modularity. Wavelength translation can be added to the structure to realize a fully re-arrangeable optical cross-connect between two fibers. Wavelength conversion based on cross phase modulation in a reversely biased semiconductor MZ modulator has been realized. The wavelength converter shows a higher conversion efficiency than using cross absorption in electro-absorption modulators, and is less noisy than using forward biased MZ semiconductor interferometer. Wavelength selectable light source has been constructed using DFB fiber lasers and space switches. Since a single pump laser is shared by a large number of DFB fiber lasers with different wavelengths, the structure is cost-effective and wavelength stable. A simple CRZ transmitter scheme is proposed using only one external modulator. The transmitter is demonstrated in transmission over 3600 km of SMF. All these subsystems will give useful options in designing flexible and cost-effective optical networks.

From this study, it can be highlighted that: 1) interferometric crosstalk and filtering effect in subsystems are most important issues which determine the cascadability in transparent optical networks, and hence the size of the networks; 2) dispersion management is very important in high-speed (10Gb/s and above) WDM networks, and modulation formats should be taken into account in optimization of the dispersion maps; 3) fiber re-circulating loop set-up is a powerful tool to investigate the cascadability of subsystems in optical networks.

In order to facilitate a more comprehensive investigation of subsystems used in optical networks, quite a bit of work still needs to be done in the future. First, the fiber loop setup should be upgrade to a higher level: more wavelengths in both C- and L- band should be supported; longer loop span should be installed to minimize the influence from the loop switch; higher line rate, e.g., 40 Gb/s should be performed; Q factor measurement should be included. Second, the combined effect of impairments which an optical signal experienced in the optical network should be investigated. For instance, an optical signal might suffer interferometric crosstalk from some subsystems, and suffer signal filtering from some other

subsystems, and suffer influence of dispersion and non-linearity from transmission links. These issues cannot be treated independently unless one of them is the dominant effect. It is important in the future to investigate the interaction of different signal impairments in an optical network and find the joint impact from these impairments. Third, implementations of subsystems presented in this thesis, e.g., wavelength converter based on cross-phase modulation in a semiconductor MZ modulator, should be further investigated and optimized in order to get even better performance.

References:

[1] T. Ito, K. Fukuchi, K. Sekiya, D. Ogasahara, R. Ohhira, T.Ono: "6.4 Tb/s (160x40Gb/s) WDM transmission experiment with 0.8 bit/Hz spectral efficiency", ECOC'2000, PD 1.1.

[2] A. Farbert, G. Mohs, S. Spalter, J.-P. Elbers, C. Furst, A. Schopflin, E. Gottwald, C. Scheerer, C. Glingener, "7 Tb/s (176x40 Gb/s) bi-directional interleaved transmission with 50 GHz channel spacing", ECOC'2000, PD1.3.

[3] T.N. Nielsen, A.J. Stentz, K. Rottwitt, D.S. Vengsarkar, L. Hsu, P.B. Hansen, J.H. Park, K.S. Feder, T.A. Strassar, S. Cabot, S. Stulz, C.K. Kan and A.F. Judy: "3.28 Tb/s (82×40Gb/s) transmission over 3×100km nonzero-dispersion fiber using dual C- and L- band hybrid Raman/Erbium doped inline amplifiers", OFC'2000, paper PD-23.

[4] K. Yonenaga, Y. Miyamoto, H. Toba, K. Murata, M. Yoneyama, Y. Yamane and H. Miyazawa: "320-Gbit/s 100-km WDM repeatless transmission using fully encoded 40-Gb/s optical Duobinary channels with dispersion tolerance of 380 ps/nm", EOCO'2000, vol. I, pp. 75-76.

[5] ITU-T Recommendation, G. 803, "Architectures of transport networks based on the synchronous digital hierarchy (SDH) ", 03/93, 1993.

[6] K.I. Sato: "Advances in transport networks technologies: Photonic networks, ATM, and SDH", Chapter 4, Artech House, 1996.

[7] M. Koga, Y. Hamazumi, A. Watanabe, S. Okamoto, H. Obara, K.-I. Sato, M. Okuno and S. Suzuki: "Design and Performance of an Optical Path Cross-Connect Systen Based on Wavelength Path Concept", IEEE J. of Lightwave Technol., vol.14, 1996, pp.1106-1119.

[8] R.J.S. Pedersen, M. Nissov, B. Mikkelsen, H.N. Poulsen, K.E. Stubkjaer, M. Gustavsson, W. Van Berlo and M. Janson: "Transmission through a cascade of 10 all-optical interferometric wavelength converter spans at 10 Gb/S", Electronics Letters, vol. 32(11), 1996. pp. 1034-1035.

[9] M. Nissov, R.J.S. Pedersen and B.F. Jørgensen: "Transmission performance through cascaded 1-nm arrayed waveguide multiplexers at 10 Gb/s", IEEE Photonics Technology Letters, vol. 9(7), 1997, pp.1038-1040.

[10] E. L. Goldstein and L. Eskildsen, "Scaling limitations in transparent optical networks due to low-level crosstalk", IEEE Photo. Technol. Lett., vol. 7(1), 1995, pp.93-94,

[11] H. Takahashi, K. Oda and H. Toba, "Impact of crosstalk in an arrayed-waveguide multiplexer on N×N optical interconnection", IEEE J. Lightwave Technol., vol.14, pp.1097-1105, 1996.

[12] C.A. Brackett: "Dense wavelength division multiplexing networks: principles and applications", IEEE J. Sel. Areas Commun., vol. 8, 1990, pp.948-964.

[13] B.R. Hemenway, M.L. Stevens, B.A. Barry, C.E. Koksal, and E.A. Swanson: "Demonstration of a re-configurable wavelength-routed network at 1.14 terabits-per-second", OFC'97, PD26.

[14] M. Fukutoku, and N. Shibata: "16 WDM optical packet routing experiment over 640 km transtmission distance at data rate of 2.5 Gbit/s " OFC'99, pp.168-170.

[15] J. Gripp, P. Bernasconi, C. Chan, K.L. Sherman and M. Zirngbl: “Demonstration of a 1 Tb/s optical packet switch fabric and scalable to 128T/s ”, ECOC’2000, paper PD2.7.

[16] H. Yamada, K. Takada, Y. Inoue, Y. HiBino, and S. Mitachi: “Statically-phased-compensated 10GHz-spaced arrayed-waveguide grating multiplexer”, *Electron. Lett*., vol. 32(17), 1996, pp. 1580-1582.

[17] H. Yamada, K. Takada, Y. Inoue, K. Okamoto, and S. Mitachi,: “Low-crosstalk arrayed-waveguide grating multi/demultiplexer with phase compensating plate”, *Electron. Lett*., 33(20), 1997, pp. 1608-1609.

[18] K. Inoue: “Suppression of Signal Fluctuation Induced by Crosstalk Light in a Gain Saturated Laser Diode Amplifier”, IEEE Photonics Techn. Lett., 8(3), 1996, pp.458-460.

[19] S.I. Pegg, M.J. Fice, M.J. Adams and A. Hadjifotiou: “Noise in wavelength conversion by cross-gain modulation in a semiconductor optical amplifier”, IEEE Photonics Techn. Lett., 11(6), 1999, pp.724-726.

[20] H.N. Poulsen and K.E. Stubkjaer: “Reduced impact of interferometric cross-talk by using all-optical interferometric wavelength converters” Proc. of OAA'98, 1998. pp.181-183.

[21] D. Wolfson, S.L. Danielsen, H.N. Poulsen, P.B. Hansen and K.E. Stubkjaer: “Experimental and theoretical investigation of the regenerative capabilities of electrooptic and all-optical interferometric wavelength converters”, IEEE Photonics Techn. Lett., vol. 10(10), 1998, pp.1413-1415.

[22] S.J. Yoo, “Wavelength conversion technologies for WDM network applications”, IEEE J. of Lightwave Technology, vol. 14 (6), 1996, pp. 955-966.

[23] K. E. Stubkjaer, A. Kloch, P. B. Hansen, H. N. Poulsen, D. Wolfson, K. S. Jepsen, A. T. Clausen, E. Limal and A. Buxens: “Wavelength converter technology”, IEICE Transactions on Communications, vol. E82-B (2), 1999, pp.390-400.

[24] R. J. S. Pedersen, B. F. Jorgensen, B. Mikkelsen, M. Nissov, K.E. Stubkjaer, K. Wunstel, K. Daub, E. Lach, G. Lsube, W. Idler, M. Schilling, P. Doussiere, and F. Pommerau, “Cascadability of a nonblocking WDM crossconnect based on all-optical wavelength converters for routing and wavelength slot interchanging,” Electron. Lett., vol. 30(19), 1997, pp. 1647–1648.

[25] K. Oberman, D. Breuer, and K. Petermann, “Theoretical estimation of the cascadability of wavelength converters based on cross-gain modula-tion in semiconductor optical amplifiers”, CLEO’98, 1998, pp. 388–389.

[26] H.-Y. Yu, D. Mahgerefteh, P.-S. Cho, and J. Goldhar, “Optimization of the frequency response of a semiconductor optical amplifier wavelength converter using a fiber Bragg grating,” IEEE J. Lightwave Technol., vol. 17, pp. 308–313, 1999.

[27] N. Edagawa, M. Suzuki, S. Yamamoto, S. Akiba: “Novel wavelength converter using an electroabsorption modulator: conversion experiments at up to 40Gb/s”, OFC’97, pp.77-78.

[28] L.K. Oxenloewe, A.T. Clausen and H.N. Poulsen: “Wavelength conversion in an electroabsorption modulator”, ECOC’2000, Vol.3, pp.303-304.

[29] T. Miyazaki, N. Edagawa, M. Suzuki, and S. Yamamoto, "Novel optical regenerator using electroabsorption modulator", OFC'9*9*, vol.2, pp350-352.

[30] R. Sabella: "Tutorial: Key Elements for WDM Transport Networks", Photonic Network Communications, 2000, pp.7-14.

[31] M. Sejka, P. Varming, J. Hubner, M. Kristensen: "Distributed feedback Er^{3+}-doped fiber laser," Electron. Lett., vol. 31(17), 1995, pp.1445-1446.

[32] P. Varming, J. Hubner, and M. Kristensen: "DFB fiber laser as source for optical communication systems", OFC'97, pp169.

[33] J.J. Pan, and Y. Shi: "166-mW single –frequency output interactive fiber lasers with low noise", IEEE Photonics Technol. Lett., vol. 11(1), 1999, pp. 36-38.

[34] M. Ibsen, S. Alam, M.N. Zervas, A.B. Grudinin, and D.N. Payne: "All fiber DFB laser WDM transmitters with integrated pump redundancy", ECOC'99, Nice, France, 1999, pp. 74-75.

[35] M. Ibsen, A. Fu, H. Geiger, and R.I. Laming: "fiber DFB lasers in a 4×10 Gb/s link with a single sinc-sampled fiber grating dispersion compensator", ECOC'98, postdeadline paper, pp109-111.

[36] H.N. Poulsen, P. Varming, A. Buxens, A.T. Clausen, I. Munoz, P. Jeppesen, C.V. Poulden, J.E. Pedersen, and L. Eskildsen: "1607nm DFB fiber laser for optical communication in the L-band", ECOC'99, Vol. I, Nice, France, 1999, pp70-71.

[37] N. Hanik, A. Gladisch, and G. Lehr: "An effective method to design transparent optical WDM-networkts", in Technology and Infrastructure NOC'98, Manchesterm U.K., pp.190-197.

[38] C. Peucheret, N. Hanik, R. Freund, L. Molle and P. Jeppesen: "Optimization of pre- and post-dispersion compensation schemes for 10 Gbit/s NRZ links using standard and dispersion compensating fibers", Photonics Technology Letters, 2000, vol. 12(8), pp. 992-994.

[39] S. Aisawa, T. Sakamoto, M. Fukui, J. Kani, M. Jinno and K. Oguchi: "Ultra-wideband long distance WDM demonstration of 1 Tb/s (50×20Gb/s) 600km transmission using 1550 and 1580nm wavelength band", Electron. Lett., 1998, 34(11), pp. 1127-1129.

[40] H.S. Chung, M.S. Lee, D. Lee, N. Park, and D.J. Digiovanni: "Low noise high efficiency L-band EDFA with 980 pumping", Electron. Lett., 1999, 35(13), 1099-1100.

[41] L.G. Nielsen, S.N. Knudsen, T. Veng, B. Edvold and C.C. Larsen: "Design and manufacture of dispersion compensating fibre for simultaneous compensation of dispersion and dispersion slope", OFC'99, 1999, pp. 232-234.

[42] E.A. Golovchenko, N.S. Bergano, C.A. Davidson and A.N. Pilipestskii: "Modeling vs Experiments of 16X10 Gb/s WDM Chirped RZ Pulse Transmission over 7500 km", OFC'99, pp.246-248.

[43] C.R. Davidson, C.J. Chen, M. Nissov, A. Pilipetskii N. Ramanujam, H.D. Kidorf, B. Pedersen, M.A. Mills, C. Lin, M.I. Hayee, J.X. Cai, A.B. Puc, P.C. Corbett, R. Menges, H. Li, A. Elyamani, C. Rivers and N.S. Bergano: "1800 Gb/s transmission of

one hundred and eighty 10Gb/s WDM channels over 7000km using the full EDFA C-band", OFC'2000, paper PD25.

[44] C. Caspar, H.-M. Foisel, C. v. Helmolt, B. Strebel and Y. Sugaya, "Comparison of cascadability performance of different types of commercially available wavelength (de)multiplexers", Electronics Letters, vol. 33(19), 1997, pp. 1624-1626.

[45] B. Christensen, J. Mark, G. Jacobsen and E. Bødtker, "Simple dispersion measurement technique with high resolution", Electronics Letters, vol. 29(1), 1993, pp. 132-134.

[46] F. Devaux, Y. Sorel and J. F. Kerdiles: "Simple measurement of fiber dispersion and of chirp parameter of intensity modulated light emitter", IEEE Journal of Lightwave Technology, vol. 11(12), 1993, pp. 1937-1940.

IEEE PHOTONICS TECHNOLOGY LETTERS, VOL. 11, NO. 1, JANUARY 1999 137

Experimental Verification of a New Model Describing the Influence of Incomplete Signal Extinction Ratio on the Sensitivity Degradation Due to Multiple Interferometric Crosstalk

Fenghai Liu, *Member, IEEE*, Christian J. Rasmussen, and Rune J. S. Pedersen

***Abstract*—Larger optical penalties than predicted by a Gaussian crosstalk model are found both in our experiments and in the literature when investigating signals including multiple interferometric crosstalk contributions. We attribute this to an imperfect signal extinction ratio. In this letter, simple analytical relations for crosstalk induced power penalties are derived taking the signal extinction ratio into account and excellent agreement with 10-Gb/s experiments is obtained. Both theory and experiments show the importance of the signal extinction ratio in connection with interferometric crosstalk.**

***Index Terms*—Networks, noise, optical crosstalk, optical fiber communication, optical receivers.**

I. Introduction

THE INFLUENCE of interferometric crosstalk in optical transmission systems and optical networks has attracted a lot of attention [1]–[8]. This kind of crosstalk which originates from signals with a frequency difference less than the receiver bandwidth has stronger influence on system performance than the so-called power-addition crosstalk from neighboring channels.

When considering the choice of statistics for the interferometric crosstalk, two limiting cases are common in the literature: Arc-sine statistics for a single crosstalk contribution [1], [2], [6] and Gaussian statistics for multiple crosstalk contributions [4]–[6]. In optical networks, several independent crosstalk contributions with more or less identical power normally exist, and according to [5] only a few crosstalk contributions are necessary before the Gaussian statistics is a good approximation. Therefore, Gaussian statistics is used in this letter.

We present simple analytical expressions of crosstalk induced penalty for both PIN receivers and optically preamplified (OPA) receivers, taking into account the imperfect signal extinction ratio which has a significant influence. Furthermore, a comparison with experimental results is made for both receiver types using either average power decision threshold setting or optimum decision threshold setting. Excellent agreement between calculated and measured results are found in all cases. Therefore we believe that it is important to include the signal extinction ratio in order to model the impact of interferometric crosstalk accurately.

Manuscript received May 14, 1998; revised September 8, 1998.

F. Liu and C. J. Rasmussen are with the Department of Electromagnetic Systems, Technical University of Denmark, DK-2800, Lyngby, Denmark.

R. J. S. Pedersen is with Mikroelektronik Centret, Technical University of Denmark, DK-2800, Lyngby, Denmark.

Publisher Item Identifier S 1041-1135(99)00357-2.

II. Theory

In the following discussion, we employ Gaussian statistics to calculate the degradation in receiver sensitivity due to multiple interferometric crosstalk. This means that the signal crosstalk beat noise follows a Gaussian probability density distribution, and the total average crosstalk power determines the sensitivity degradation. In order to investigate the worst case, we assume that signal and crosstalk light have the same polarization state and that the total signal crosstalk beat noise falls within the receiver bandwidth. The signal photocurrent in the "1" level is denoted i_1, and the signal mark density is taken to be 0.5. We introduce the signal extinction ratio r defined as the optical power in the "0" level divided by the optical power in the "1" level, and define the relative crosstalk power ε as the ratio of total average crosstalk power to average signal power. Expressed in these quantities the variance of the signal crosstalk beat noise is $\varepsilon(1+r)i_1^2$ in the "1" level and $r\varepsilon(1+r)i_1^2$ in the "0" level.

A. p-i-n Receiver

In p-i-n receivers, only thermal noise with variance of σ_0^2 and signal crosstalk beat noise are considered. Under the Gaussian assumption, the probability of an erroneous detection of a bit, P_e, is given by

$$P_e = \frac{1}{4}\operatorname{erfc}\left(\frac{1}{\sqrt{2}}\,\frac{i_1 - i_d}{\sqrt{\sigma_0^2 + \varepsilon(1+r)i_1^2}}\right) + \frac{1}{4}\operatorname{erfc}\left(\frac{1}{\sqrt{2}}\,\frac{i_d - ri_1}{\sqrt{\sigma_0^2 + \varepsilon r(1+r)i_1^2}}\right) \quad (1)$$

where i_d is the decision threshold and erfc is the complementary error function.

When average power decision threshold is used, $i_d = (1+r)i_1/2$, the errors from the "1" level dominate the error probability. Following a procedure similar to the one used in

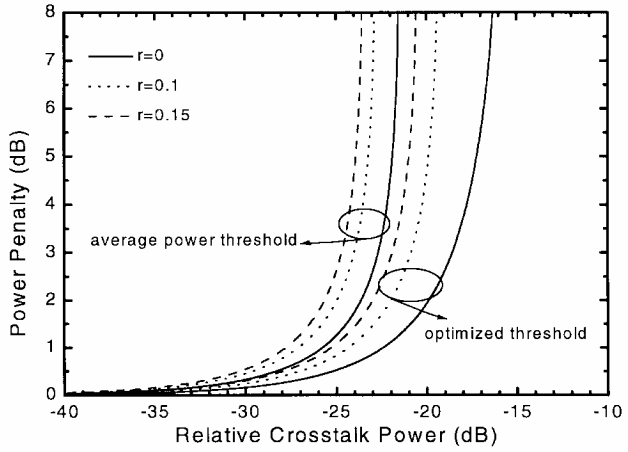

Fig. 1. Crosstalk induced power penalty versus relative crosstalk power for p-i-n receivers with signal extinction ratio as parameter.

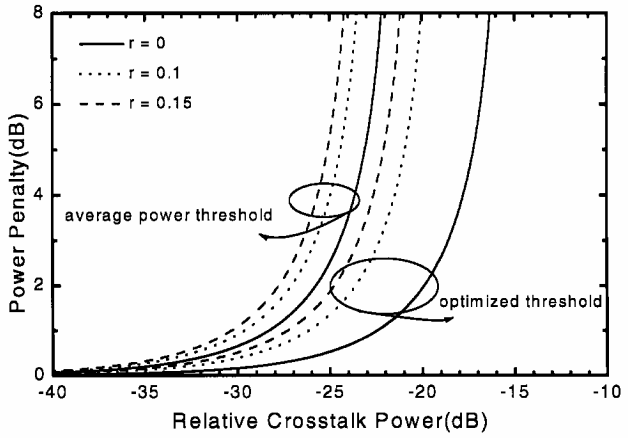

Fig. 2. Crosstalk induced power penalty versus relative crosstalk power for optically preamplified receivers with signal extinction ratio as parameter.

[5], the power penalty at $P_e = 10^{-9}$ can be written as

$$\text{Penalty (dB)} = -5\log\left(1 - 4\varepsilon Q'^2\frac{1+r}{(1-r)^2}\right) \quad (2)$$

where $Q' = 5.9$ is a constant and log is the base 10 logarithm. When $r = 0$, (2) takes the form of the widely quoted power penalty equation [3]–[5]. The crosstalk induced penalty as a function of total crosstalk power with signal extinction ratio as a parameter is plotted in Fig. 1.

A variable decision threshold can provide a lower penalty when adjusted for the minimum error probability. The optimum decision threshold is given by

$$i_{\text{opt}} = \frac{\sqrt{\sigma_0^2 + r\varepsilon(1+r)i_1^2} + r\sqrt{\sigma_0^2 + \varepsilon(1+r)i_1^2}}{\sqrt{\sigma_0^2 + r\varepsilon(1+r)i_1^2} + \sqrt{\sigma_0^2 + \varepsilon(1+r)i_1^2}} i_1. \quad (3)$$

The optimized decision threshold i_{opt} is slightly smaller than that of the average power decision threshold. By setting $i_d = i_{\text{opt}}$, the power penalty at $P_e = 10^{-9}$ can be written as

$$\text{Penalty (dB)} = -5\log\left(1 - 2\varepsilon Q^2\left(\frac{1+r}{1-r}\right)^2 + \varepsilon^2 Q^4\left(\frac{1+r}{1-r}\right)^2\right) \quad (4)$$

where $Q = 6$. The crosstalk induced penalty in case of optimized decision threshold is also plotted in Fig. 1.

Fig. 1 shows that a degradation of the signal extinction ratio means that less crosstalk power can be tolerated for a given power penalty. At 1-dB power penalty, an extinction ratio deterioration from $r = 0$ to $r = 0.15$ (ITU-T requirement for STM16)[1] results in a 2.0-dB reduction of tolerable crosstalk power in the case of average power decision threshold, and 2.8 dB in the case of optimized decision threshold.

B. Optically Preamplified (OPA) Receiver

For a well-designed OPA receiver, the main noise contributions are the signal spontaneous emission beat noise and the signal crosstalk beat noise. The error probability is then given as follows:

$$P_e = \frac{1}{4}\operatorname{erfc}\left(\frac{1}{\sqrt{2}}\frac{i_1 - i_d}{\sqrt{\varepsilon(1+r)i_1^2 + 2\frac{B_e}{B_o}i_{\text{sp}}i_1}}\right) + \frac{1}{4}\operatorname{erfc}\left(\frac{1}{\sqrt{2}}\frac{i_d - ri_1}{\sqrt{r\varepsilon(1+r)i_1^2 + 2r\frac{B_e}{B_o}i_{\text{sp}}i_1}}\right). \quad (5)$$

Here, B_e is the electrical bandwidth of the receiver, B_o is the bandwidth of the optical filter in the receiver and i_{sp} is the photocurrent corresponding to the spontaneous emission after the optical filter. Following the same procedure as for the p-i-n receiver, crosstalk induced power penalties at $P_e = 10^{-9}$ are

$$\text{Penalty (dB)} = -10\log\left(1 - 4\varepsilon Q'^2\frac{1+r}{(1-r)^2}\right) \quad (6)$$

$$\text{Penalty (dB)} = -10\log\left(1 - \varepsilon Q^2\frac{1+r}{(1-\sqrt{r})^2}\right) \quad (7)$$

for average power decision threshold and optimized decision threshold, respectively.

Equations (6) and (7) are plotted in Fig. 2, and the power penalty versus crosstalk power curves show a similar tendency as in the p-i-n receiver case when the signal extinction ratio is degrading.

For OPA receivers at 1-dB power penalty, an extinction ratio deterioration from $r = 0$ to $r = 0.15$ results in a reduction of tolerable crosstalk power of 2.0 dB for average power decision threshold, and 4.8 dB for optimized decision threshold.

III. Experiments

To measure the influence of multiple interferometric crosstalk, we have used the experimental setup shown in Fig. 3. A 10-Gb/s optical signal is generated by modulating the CW-light from a DFB laser with a linewidth of 24 MHz in a push-pull driven Mach–Zehnder modulator. The measured signal extinction ratio is -10 dB ($r = 0.1$). The modulated signal is divided into a signal part and a crosstalk part. The

[1] ITU-T Recommendation G.957 (07/95), STM-16 Optical Interface Specification, Application code L-16.2 and L-16.3.

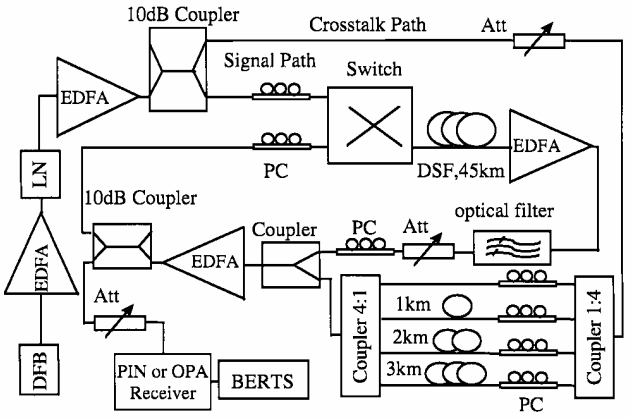

Fig. 3. Experimental setup for measuring crosstalk induced power penalty. LN: LiNbO3 external modulator. DSF: Dispersion-shifted fiber. Att: Attenuator. PC: Polarization controller. BERTS: Bit-error-rate test set.

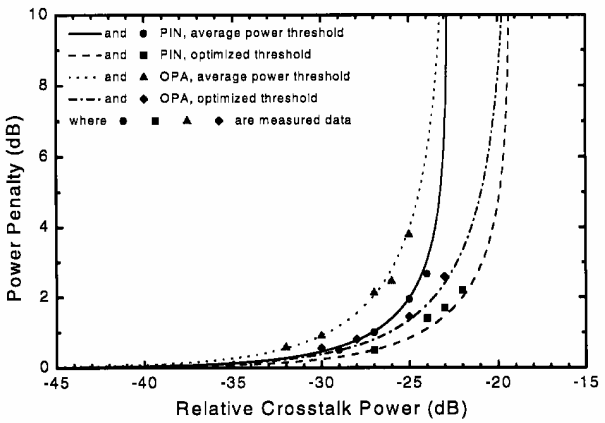

Fig. 4. Measured and calculated power penalties for a signal extinction ratio of −10 dB for different receivers. PIN: p-i-n receivers. OPA: Optically preamplified receivers.

signal part is launched via a loop switch into the loop which includes 45 km of dispersion shifted fiber, loop amplifiers and a spontaneous emission limiting optical bandpass filter. The crosstalk part is divided into four parts that are decorrelated using 0-, 1-, 2-, 3-km dispersion-shifted fiber delay lines in order to get independent crosstalk contributions. The main signal and the four crosstalk terms are combined by couplers and looped back through the loop switch. In order to simulate the worst case operation, the polarization controllers are used to align the polarization of signal and crosstalk light.

By recirculating the signal in the loop setup, four additional crosstalk contributions are added for each circulation. A fraction of the signal circulating in the loop is coupled into the receiver. Using a gated test-set, we measure the signal after three circulations, which corresponds to having 12 crosstalk contributions of equal power. The bit-error-rate (BER) performance is measured for a p-i-n receiver and an OPA receiver. Measurements are performed for the cases of average power decision threshold and optimized decision threshold in both receivers. The power penalty is defined as the difference between the receiver sensitivity with and without crosstalk at BER $= 10^{-9}$. In Fig. 4 the measured power penalties versus the relative crosstalk power are plotted together with the calculated curves in which the signal extinction ratio is 0.1. Very good agreement with the calculated curves is evident for all cases.

IV. Discussion

In all the cases discussed above, we find that the signal extinction ratio has a strong impact on crosstalk induced penalty. Figs. 1 and 2 show that if the signal extinction ratio degrades from $r = 0$ to $r = 0.15$, the total crosstalk power must be decreased more than 2.0 dB to maintain the same 1-dB power penalty. This corresponds to a reduction of more than 37% in network size. Furthermore, it can be seen from Fig. 4 that the OPA receiver with average power decision threshold is most sensitive to crosstalk (−30-dB crosstalk power induces 1-dB penalty @ $r = 0.1$), while the p-i-n receiver with optimized decision threshold is the least sensitive case (−24.5-dB crosstalk power induces 1-dB penalty @ $r = 0.1$).

V. Conclusion

We have investigated the performance degradation caused by multiple interferometric crosstalk in four cases: p-i-n receiver with average power and optimized decision threshold as well as OPA receiver with average power and optimized decision threshold. Imperfect signal extinction ratio is found to have strong influence on the crosstalk induced power penalty. Very good agreement is found between experimental results and power penalties calculated from the analytical expressions based on our extended Gaussian crosstalk model that includes signal extinction ratio.

References

[1] M. Tur and E. L. Goldstein, "Probability distribution of phase-induced intensity noise generated by distributed-feedback lasers," *Opt. Lett.*, vol. 15, no. 1, pp. 1–3, 1990.

[2] L. Eskildsen and P. B. Hansen "Interferometric noise in lightwave systems with optical preamplifier," *IEEE Photon. Technol. Lett.*, vol. 9, pp. 1538–1540, 1997.

[3] E. L. Goldstein, L. Eskildsen, and A. F. Elrefaie, "Performance implications of component crosstalk in transparent lightwave networks," *IEEE Photon. Technol. Lett.*, vol. 6, pp. 657–660, 1994.

[4] E. L. Goldstein and L. Eskildsen, "Scaling limitations in transparent optical networks due to low-level crosstalk," *IEEE Photon. Technol. Lett.*, vol. 7, pp. 93–94, 1995.

[5] H. Takahashi, K. Oda, and H. Toba, "Impact of crosstalk in an arrayed-waveguide multiplexer on $N \times N$ optical interconnection," *J. Lightwave Technol.*, vol. 14, pp. 1097–1105, 1996.

[6] P. J. Legg, M. Tur, and I. Andonovic, "Solution paths to limit interferometric noise induced performance degradation in ASK/direct detection lightwave networks," *J. Lightwave Technol.*, vol. 14, pp. 1943–1954, 1996.

[7] M. Gustavsson, L. Gillner, and C. P. Larsen, "Statistical analysis of interferometric crosstalk: Theory and optical network examples," *J. Lightwave Technol.*, vol. 15, pp. 2006–2019, 1997.

[8] K.-P. Ho "Analysis of co-channel crosstalk interference in optical networks," *Electron. Lett.*, vol. 19, pp. 383–384, 1998.

Optical Fiber Communication Conference, 1999, OFC'99

258 / TuR5-1

Theoretical and experimental studies of the influence of the number of crosstalk signals on the penalty caused by incoherent optical crosstalk

Christian J. Rasmussen[1], cr@emi.dtu.dk Fenghai Liu[1], lf@emi.dtu.dk
Rune J. S. Pedersen[2], rjp@mic.dtu.dk Bo F. Jørgensen[3], bjoergen@dscc.dk

[1]Technical University of Denmark, Department of Electromagnetic Systems, Building 348, DK-2800 Lyngby, Denmark, Phone +45 45881444, Fax +45 45931634; [2]Technical University of Denmark, Mikroelektronik Centret, Building 345East, DK-2800 Lyngby, Denmark, Phone +45 45934610, Fax +45 45887762; [3]DSC Communications A/S, Lautrupbjerg 7-11, DK-2750 Ballerup, Denmark, Phone +45 44732281, Fax +45 44733650

I. Introduction

Incoherent optical crosstalk, i.e. the crosstalk type where the crosstalk signals have the same wavelength as the wanted signal but all signals are uncorrelated, is one of the most detrimental phenomena in optical networks and has therefore been the subject of many studies, e.g. [1]-[3]. Most of these have focused on situations with many crosstalk signals, and Gaussian statistics have been used as an approximation to the statistics of the receiver process in order to find the crosstalk penalty. However, a few recent theoretical investigations [4],[5] have used more accurate statistics and have shown for PIN receivers that the penalty caused by a given total crosstalk power increases when this power is distributed among an increasing number of crosstalk signals. This phenomenon is not predicted by the Gaussian models.

To continue the investigations of how the number of crosstalk signals affects the incoherent crosstalk penalty, we have calculated the incoherent crosstalk penalty as a function of the total crosstalk power and the number of crosstalk signals for both PIN and optically preamplified receivers. Furthermore, we have verified the theoretical results experimentally. To our knowledge, neither calculations of the penalty for preamplified receivers nor experimental verifications of the influence of the number of crosstalk signals have been reported before. The calculated penalties are compared to the penalties obtained using the Gaussian approximation, and the difference is smaller than ¼ dB when the total crosstalk power does not exceed a level 24 dB below the power of the wanted signal and 6 or more crosstalk signals exist. We have also discovered that the penalty in dB in the case of a preamplified receiver is approximately twice the penalty for the PIN case. A network consequence of our results is that if the allowed crosstalk penalty is 1 dB, up to 3 dB more total crosstalk power can be tolerated in small networks with only 1 crosstalk signal compared to larger networks with many crosstalk signals.

II. Theory

We consider a situation where a wanted signal with a mean power of P_s is disturbed by N independent crosstalk signals each having a mean power of XP_s/N. The total crosstalk power is thus XP_s and X is denoted "total relative crosstalk power". Both the wanted signal and the crosstalk signals are assumed to have a mark density of 0.5 and extinction ratio e, where e is defined as the optical power in the "1"-level divided by the optical power in the "0"-level. In order to investigate the worst case with maximum crosstalk influence all signals are assumed to have identical polarization states. Because of the presence of crosstalk, the total received power at time t, $P(t)$, is a random variable even if it is known whether the wanted signal is "0" or "1". $P(t)$ can be written:

$$P(t) = P_s\left|\delta(t) + \sum_{i=1}^{N} A_i(t)e^{j\theta_i(t)}\right|^2$$

Here $\delta(t)$ is the amplitude of the wanted signal at time t and is either $\sqrt{2/(1+e)}$ or $\sqrt{2e/(1+e)}$ depending on whether the signal is "0" or "1". $A_i(t)$, $i\in\{1,\ldots,N\}$ is a random variable representing the amplitude of the ith crosstalk signal at time t. It takes the value $\sqrt{2X/(N(1+e))}$ or $\sqrt{2eX/(N(1+e))}$ with equal probability. $\theta_i(t)$, $i\in\{1,\ldots,N\}$ is the difference between the phase of the ith crosstalk signal and the wanted signal at time t. This random variable is uniformly distributed in $[0;2\pi]$. The $2N$ random variables $A_i(t)$ and $\theta_i(t)$ are mutually independent and also independent of $\delta(t)$.

Fig. 1 shows the probability density function (pdf) of $P(t)$ when the wanted signal is "1" and 1, 2, 4, 6 and an infinite number of crosstalk signals exist. The Gaussian pdf used in the Gaussian approximation is also shown. Mean and variance of this Gaussian are chosen to the mean and the variance of $P(t)$ when an infinite number of crosstalk signals exist.

Optical Fiber Communication Conference, 1999, OFC'99

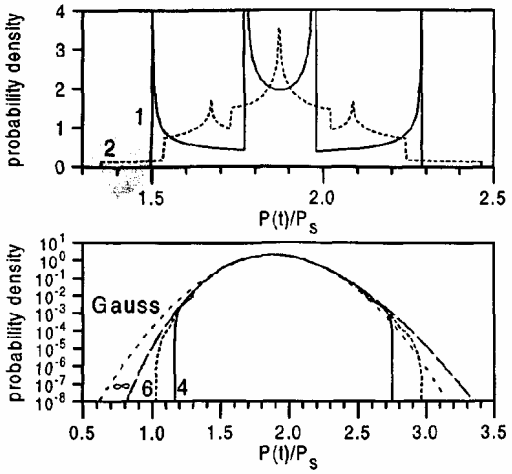

Fig. 1. pdf for $P(t)/P_s$ when the wanted signal is "1". The numbers next to the curves are the number of crosstalk signals. "Gauss": see text. The total relative crosstalk power is -20 dB, and the extinction ratio is 12 dB.

In order to determine the bit error probability and the receiver sensitivity, which is the total received optical average power that gives an error probability of 10^{-9}, the pdf of the input voltage to the decision circuit of the receiver is calculated. Since we study incoherent crosstalk, the vast majority of the spectrum of $P(t)$ falls within the bandwidth of the electrical amplifiers in the receiver. Consequently, the photocurrent proportional to $P(t)$ will be amplified but not significantly distorted in the electrical amplifiers. Therefore we assume that the input voltage to the decision circuit is the sum of a signal part $HP(t)$, where H is a constant, and a zero mean Gaussian noise with variance $a+bP(t)$. a is the power of the signal independent noise generated in the receiver (thermal noise, for optically preamplified receivers also spontaneous-spontaneous beat noise and shot noise from the spontaneous emission) and $bP(t)$ is the power of the signal dependent noise (signal shot noise, for optically preamplified receivers also signal-spontaneous emission beat noise).

Fig. 2 shows the calculated crosstalk penalty as a function of the total relative crosstalk power and the number of crosstalk signals for both a PIN receiver and an optically preamplified receiver whose dominant receiver noise contribution is signal spontanous beat noise. It is clear from fig. 2 that the penalty increases when a given amount of total crosstalk power is distributed among a larger number of crosstalk signals. As an example we see that a total relative crosstalk power of -20 dB distributed over 1, 6 and an infinite number of crosstalk signals gives penalties of 1.1 dB, 2.1 dB or 2.7 dB, respectively, in the PIN case. In the case of an optically preamplified receiver, the penalties are approximately two times higher (namely 1.9 dB, 3.8 dB and 5.0 dB), and fig. 2 shows that this relation between PIN receiver penalty and preamplified receiver penalty is general.

Fig. 2 can also be used to determine how much total relative crosstalk power that can be tolerated if the penalty must be smaller than, say, 1 dB. In the PIN case, the tolerable amount of total relative crosstalk power decreases from -20.4 dB in the case of 1 crosstalk signal to -23.3 dB in the case of an infinite number of crosstalk signals. This shows that up to 3 dB more crosstalk power can be tolerated in small networks with only 1 crosstalk signal than in larger networks with many crosstalk signals.

The curves called "Gauss" on fig. 2 show the penalties calculated using the Gaussian pdf's from the Gaussian approximation instead of the exact pdf's. The Gaussian approximation is seen to give results which are accurate within ¼ dB if 6 or more crosstalk signals exist and if the total relative crosstalk power is smaller than -24 dB.

III. Experiments

In order to verify the theoretical results, the incoherent crosstalk penalty has been measured in the set-up shown on fig. 3: CW light from a DFB laser (wavelength 1555 nm, linewidth 48 MHz) is modulated with a 5 Gbit/s 2^{31}-1 PRBS in a Mach-Zehnder modulator and then split into a crosstalk part and wanted signal part. The former is further split into 6 crosstalk signals whose powers are controlled by attenuators. After decorrelation in delay lines consisting of 0.5, 1, 2, 3, 4 and 23 km of dispersion shifted fiber, the crosstalk signals and the wanted signal are combined again, and a small fraction of the combined signal is coupled into a polarization analyzer. The rest is attenuated in an attenuator that controls the total power into the PIN or the optically preamplified receiver. A bit error rate test set connected to the receiver measures the bit error rate. Identical polarization states of all signals arriving at the receiver input are obtained using the polarization analyzer and the polarization controllers.

The measured incoherent crosstalk penalties for different values of total relative crosstalk power distributed on 1,2,4 and 6 crosstalk signals with equal powers are shown on fig. 2 for both a PIN and an optically preamplified receiver. The agreement between the theoretical predictions and the measurements is very good.

Optical Fiber Communication Conference, 1999, OFC'99

260 / TuR5-3

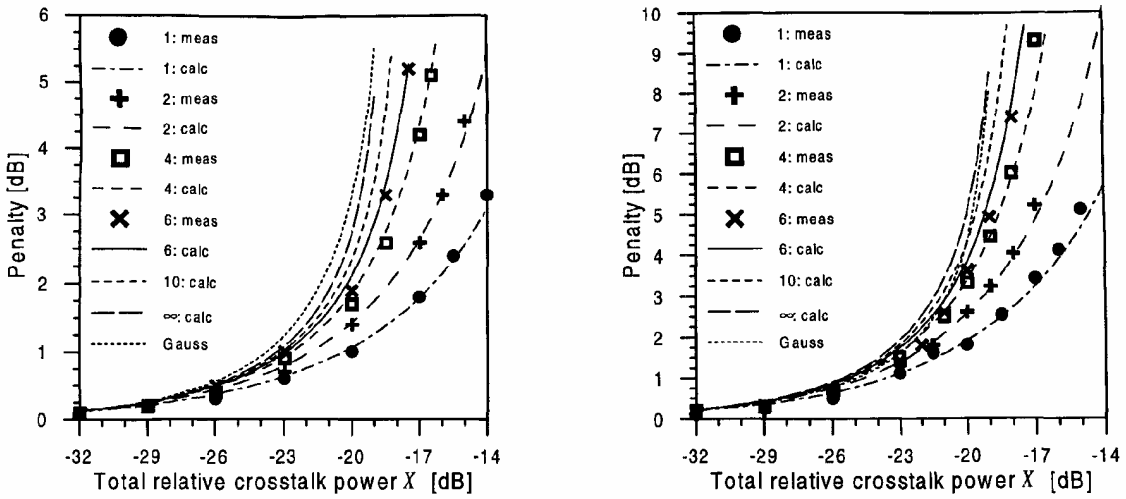

Fig. 2. Calculated and measured incoherent crosstalk penalty for a PIN receiver (to the left) and an optically preamplified receiver (to the right) as a function of the total relative crosstalk power with the number of crosstalk signals as parameter. Gauss: See text. The extinction ratio is 11.7 dB in the PIN case and 12.0 dB in the optically preamplified case.

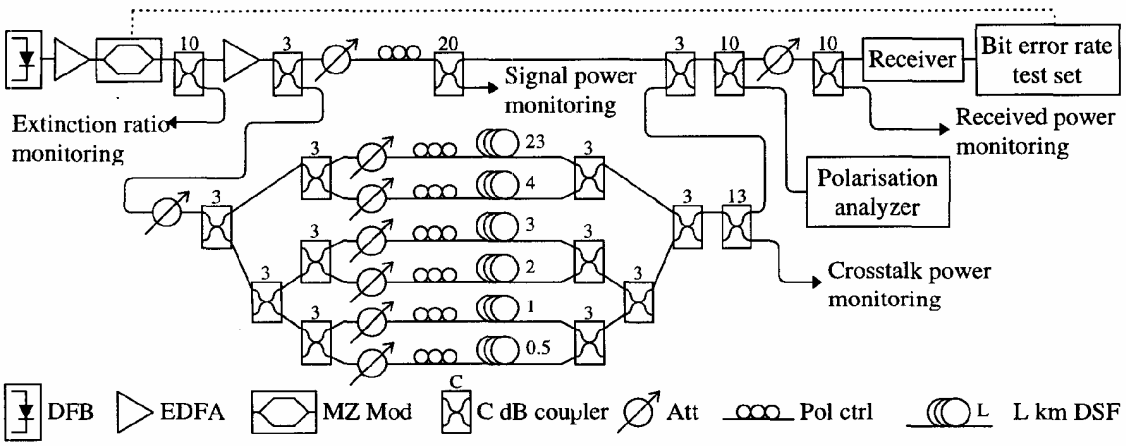

Fig. 3. Set-up for measurements of incoherent crosstalk penalty. DFB: DFB laser; EDFA: Erbium Doped Fibre Amplifier; MZ Mod: Mach-Zehnder modulator; Att: Attenuator; Pol ctrl: Polarization controller; DSF: Dispersion shifted fibre.

IV. Conclusion

The penalty caused by incoherent crosstalk has been calculated and measured for both PIN and optically preamplified receivers. Measured and calculated penalties agree excellently, and they show that the penalty is not only a function of the total crosstalk power but also of the number of crosstalk signals among which the power is distributed. As an example, the penalty caused by a total relative crosstalk power of -20 dB increases in the preamplified case from 2 dB to 4 dB when 6 instead of 1 crosstalk signals exist. As to the relation between the penalty in the PIN and the preamplified case, a rule of thumb is derived: The penalty in dB in the preamplified case is two times the penalty in the PIN case. Finally, the penalty calculations based on the exact pdf of the received optical power show that the often used Gaussian approximation is accurate within ¼ dB if 6 or more crosstalk signals having a total relative power smaller than -24 dB exist.

References

[1] Goldstein et al.: IEEE Phot. Technol. Lett. **1**, 93-94 (1995)
[2] Takahashi et al, IEEE J. Lightwave Techn. **6**, 1097-1105 (1996)
[3] Legg et al., IEEE J. Lightwave Technol. **9**, 1943-1954 (1996)
[4] Mitchell et al., OFC98 Technical Digest, WD3
[5] Danielsen et al.:"Analysis of interferometric crosstalk in optical switch blocks using moment generating funcrions", to appear in IEEE Phot. Technol. Lett.

Conference on Lasers and Electro-Optics, 1998, CLEO'98

/ CLEO'98 / WEDNESDAY AFTERNOON / ***318***

Influence of interferometric crosstalk in a cascade of 10Gb/s wavelength routers and an improved Gaussian crosstalk model

Fenghai Liu, Christian J. Rasmussen and Rune J.S. Pedersen
Dept. of Electromagnetic Systems, Building 348, Technical University of Denmark, DK-2800, Lyngby, Denmark.
Phone: +45 45253800, Fax: +45 45931634, Email: lf@emi.dtu.dk

Integrated optical N×N wavelength routers based on arrayed-waveguide gratings (AWGs) are likely to become key devices in future wavelength division multiplexing (WDM) networks [1,2]. A cascade of wavelength routers is formed when several N×N networks are interconnected as shown in Figure 1. Due to the non-ideal transfer function of physical AWGs, a node will receive not only the signal from the node it is connected to, but also crosstalk at the same wavelength from the other nodes. In a cascade of AWG-routers, the crosstalk will accumulate and thereby limit the number of stages. The Gaussian crosstalk model is considered to be a worst-case model when investigating multiple independent crosstalk sources [2-4], but higher power penalties than predicted by this model is found in [4] as well as in our work. We extend the model by including the signal extinction ratio and spontaneous emission from the optical pre-amplifier in our receiver. Experimentally, a re-circulating loop is used for investigation of router cascades. Very good agreement is demonstrated between the measured penalty and the penalty predicted from our improved Gaussian crosstalk model.

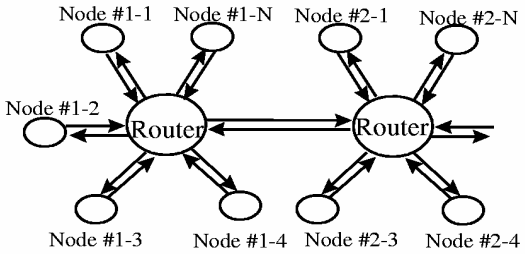

CWT3 Fig. 1. Architecture of network using a cascade of routers

In our crosstalk model which includes signal-crosstalk beat noise and signal-spontaneous emission beat noise, we assume that (1) the signal and all the crosstalk contributions have the same polarization state (worst case); (2) the noise contributions are independent and can be described by Gaussian probability density functions; (3) optimized threshold is used. This leads to a new equation for power penalty versus relative crosstalk ε and signal extinction ratio r:

$$Penalty(dB) = -10\log\left[1 - \frac{(1+r)Q^2\varepsilon}{(1-\sqrt{r})^2}\right] \qquad (1)$$

Q is equal to 6 at BER=10^{-9}.

Figure 2 shows the re-circulating loop set-up used for the investigation of the AWG-router cascadability. The light from the transmitter modulated externally at 10Gb/s is divided into a signal part and a cross talk part. The crosstalk part is amplified in an EDFA, split into four, and decorrelated using four fibers of different length in order to obtain independent crosstalk contributions. The signal part is launched via the switch into the loop which includes 45 km of dispersion shifted fiber. Polarization controllers and an attenuator are put before the AWG router to achieve identical polarization states and approximately equal power at all inputs. The loop contains two EDFAs to compensate for the loss. A part of the signal (including crosstalk) circulating in the loop is coupled into the optically pre-amplified receiver. Bit-error-rate is measured at optimized threshold.

Optical Fiber Communication Conference, 1999, OFC'99

/ CLEO'98 / WEDNESDAY AFTERNOON / ***319***

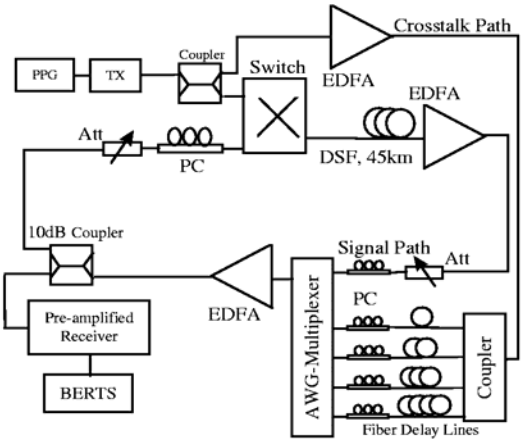

CWT3 Fig. 2. Experimental setup for measuring the cascadability of routers. PPG: pulse pattern generator. TX: transmitter. Att: attenuator. PC: polarization controller. BERTS: bit error rate test set. DSF: dispersion shifted fiber. AWG: arrayed waveguide grating.

Wavelength routers used in cascade should be carefully designed, since all crosstalk contributions are accumulated in the cascade. Even for a low crosstalk power of -34.8dB per contribution, a power penalty of 4.1dB is measured when cascading 5 routers, each adding 4 crosstalk contributions. The measured penalty as a function of accumulated crosstalk power is shown in Figure 3 together with the penalty calculated from (1) assuming an extinction ratio of 0.12 (solid). Excellent agreement between experimental result and the new Gaussian model is observed. To show the influence of the signal extinction ratio, a curve of r = 0 (dashed) is also plotted in the same figure. It can be seen that for a penalty of 1dB there is a 5dB difference of crosstalk power. This clearly shows the importance of including the signal extinction ratio.

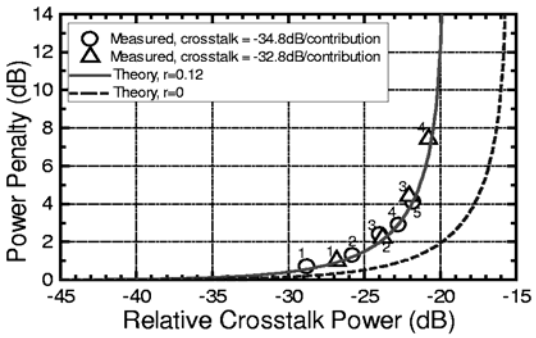

CWT3 Fig. 3. Relation between power penalty and relative crosstalk power. The number related to the symbols indicates the loop roundtrips corresponding to the number of cascaded AWG routers.

Reference:

[1] Hiroshi Takahashi, et al, IEEE J. Lightwave Technol. 13, 447-455, 1995.
[2] Hiroshi Takahashi, et al, IEEE J. Lightwave Technol. 14, 1097-1105, 1996.
[3] E.L.Goldstein, et al, IEEE J. Photonics Technology Letters 6, 657-660, 1994
[4] E.L.Goldstein, L.Eskildsen, IEEE J. Photonics Technology Letters 7, 93-94, 1995

Very low crosstalk wavelength router construction using arrayed-waveguide grating multi/demultiplexers

F. Liu, R.J.S. Pedersen and P. Jeppesen

A very low crosstalk $N \times N$ wavelength router construction using $1 \times N$ arrayed-waveguide grating multi/demultiplexers is described. A crosstalk level of < −53dB has been measured in such an 8×8 wavelength router. Even a 64×64 wavelength router can be built with a large crosstalk margin.

Introduction: Dense wavelength division multiplexing (DWDM) technology not only offers a flexible way to increase the transmission capacity, but also provides a new dimension for optical networking. Wavelength routing is very promising for future DWDM networks because it can be realised using simple structures and enables a high degree of wavelength reuse among the nodes to be obtained [1]. As the key elements in wavelength routing networks, various kinds of wavelength routers have been investigated [2 – 4]. Interferometric crosstalk, i.e. crosstalk with the same wavelength as the signal, is a critical issue when implementing wavelength routing networks because the crosstalk will accumulate from all the input ports and also accumulate when the channel passes through a cascade of wavelength routers. This kind of crosstalk cannot be filtered at the receiver, and its influence has been thoroughly studied [5, 6]. As an example, if the full connectivity is used in a 32×32 wavelength router, the crosstalk level from each input port must be reduced to < −40dB in order to meet the common 1dB power penalty criteria [5, 6]. This crosstalk requirement is far from being met even by the best published results for 32×32 arrayed waveguide grating (AWG) wavelength routers [4].

Although a significant amount of effort is involved in reducing the crosstalk level in AWG components [7 – 9], it is important to consider alternative structures with the same functionality as a wavelength router. In this Letter, we clarify that very large (64×64) $N \times N$ wavelength routers can be constructed so that they are not limited by interferometric crosstalk. Compared to a single component $N \times N$ AWG wavelength router a substantial reduction in crosstalk is obtained in an $N \times N$ wavelength router structure that is based on $1 \times N$ AWG multi/demultiplexers and takes advantage of double filtering. We demonstrate a very low crosstalk level of −53dB for such an 8×8 wavelength router which comprises commercial 1×8 AWG multi/demultiplexers.

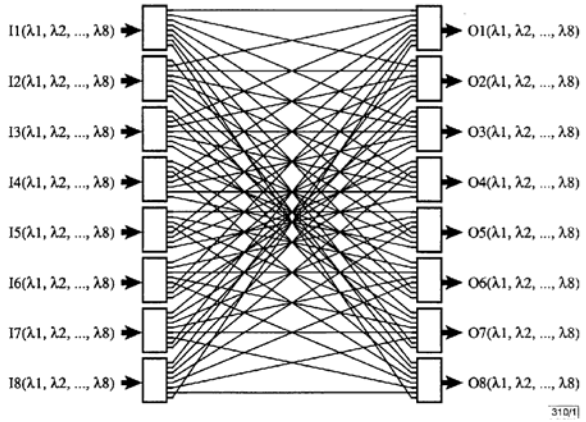

Fig. 1 *Structure of 8× 8 wavelength router*

Construction: Fig. 1 shows the structure of an 8×8 wavelength router using eight pairs of 1×8 multi/demultiplexers interconnected according to the connection table of a wavelength router [1]. The wavelength channels are first demultiplexed from the input ports using AWG demultiplexers. The demultiplexed channels contain crosstalk from adjacent channels according to the transfer function of the demultiplexers. The adjacent channel crosstalk turns into interferometric crosstalk in channels with the same nominal wavelength when these channels are combined in the multiplexers. However, owing to the combined transfer function of the AWG demultiplexer and multiplexer, the adjacent channel crosstalk is filtered twice before resulting in interferometric crosstalk at the output ports. Such interferometric crosstalk suppression cannot be realised in a single component AWG wavelength router.

The number of $1 \times N$ AWG multi/demultiplexers needed to build an $N \times N$ wavelength router is $2N$, and hence scales linearly with the size of the router. The loss in $1 \times N$ AWG multi/demultiplexers can be as low as 2.5dB [4]. So even though the proposed construction includes the loss of an AWG multi/demultiplexer pair, the total loss is still low. The crosstalk level is significantly decreased at the same time due to the double filtering.

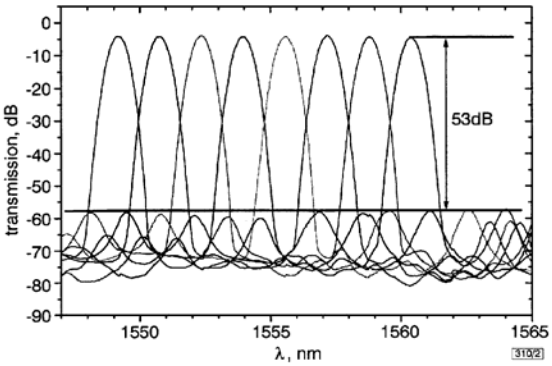

Fig. 2 *Transfer functions of 8× 8 wavelength router*

Characterisation: To verify the expected crosstalk improvement from the double filtering in the proposed wavelength router structure, an 8×8 wavelength router was constructed using commercial 1×8 AWG multi/demultiplexers with a wavelength spacing ot 200GHz as shown in Fig. 1. We measured the transfer functions from input ports I1, I2, ..., I8 to output port O1 using a scanning wavelength laser source. From the measured transfer functions shown in Fig. 2, a loss of < 4.5dB was observed for all channels and the crosstalk suppression was better than 53 dB for all channels.

Discussion: The measured crosstalk level in the 8×8 wavelength router means that, in this configuration, the connectivity is no longer limited by crosstalk and actually a cascade of 40 routers would be tolerable. Concerning large routers, 1×64 AWG multi/demultirlexers with crosstalk < −27dB have been reported [4], which can be used to build a 64×64 wavelength router. Actually, in this case, the resulting crosstalk is still 11dB below the level required for 1dB power penalty, which allows a cascade of up to 10 such routers to be used in networks. Hence, rather large wavelength routing networks can be built.

Conclusion: In this Letter, a very low crosstalk $N \times N$ wavelength router construction using $1 \times N$ AWG multi/demultiplexers has been proposed. The crosstalk requirement for the individual AWG multi/demultiplexers is significantly relaxed compared to that for an AWG wavelength router. It is clarified that a crosstalk value of −27dB reported for a 1×64 AWG multi/demultiplexer is sufficient to construct a full connectivity 64×64 wavelength router with a large crosstalk margin.

30 March 1999
Electronics Letters Online No: 19990568
DOI: 10.1049/el:19990568

F. Liu, R.J.S. Pedersen and P. Jeppesen (*Research Center COM, Technical University of Denmark, Building 349, Lyngby, DK-2800, Denmark*)

E-mail: lf@com. dtu.dk

References

1 BRACKETT, C.A.: 'Dense wavelength division multiplexing networks: principles and applications', *IEEE J. Sel. Areas Commun.*, 1990, **SAC-8**, pp. 948–964

2 HEMENWAY, B.R., STEVENS, M.L., BARRY, R.A., KOKSAL, C.E., and SWANSON, E.A.: 'Demonstration of a re-configurable wavelength-routed network at 1.14 terabits-per-second'. Dig. Conf. Opt. Fiber Commun., 1997, Paper PD26

3 BAMBRIDGE, J.D., WHITE, I.H., PENTY, R.V., ASGHARI, M., THOMPSON, G.H.B., CLEMENTS, S.J., ROGERS, C.B., MELVILLE, D., and SHEPHERD, F.R.: 'Demonstration of integrated 12 × 12 InGaAsP grating wavelength router at 2.5 Gbit/s channel bit rates', *Electron. Lett.*, 1997, **33**, pp. 1458–1459

4 OKAMOTO, K., INOUE, Y., TANAKA, T., and OHMORI, Y.: 'Silica-based planar lightwave circuits for WDM application', *IEICE Trans. Electron.*, 1998, **E81-C**, pp. 1176–1186

5 TAKAHASHI, H., ODA, K., and TOBA, H.: 'Impact of crosstalk in an arrayed-waveguide multiplexer on $N \times N$ optical interconnection', *J. Lightwave Technol.*, 1996, **LT-14**, (6), pp. 1097–1105

6 LIU, F., RASMUSSEN, C.J., and PEDERSEN, R.J.S.: 'Influence of interferometric crosstalk in a cascade of 10 Gb/s wavelength routers and an improved Gaussian crosstalk model'. Conf. Lasers and Electro-Optics (CLEO), 1998, pp. 318–319

7 YAMADA, H., TAKADA, K., INOUE, Y., HIBINO, Y., and MITACHI, M.: 'Statically-phased-compensated 10 GHz-spaced arrayed-waveguide grating multiplexer', *Electron. Lett.*, 1996, **33**, pp. 1580–1582

8 YAMADA, H., TAKADA, K., INOUE, Y., OKAMOTO, K., and MITACHI, S.: 'Low-crosstalk arrayed-waveguide grating multi/demultiplexer with phase compensating plate', *Electron. Lett.*, 1997, **33**, pp. 1608–1609

9 OKAMOTO, K., KANEKO, A., and ITOU, M.: 'Array waveguide grating routers for 50 GHz applications'. Dig. Conf. Opt. Fiber Commun., 1999, pp. 190–192

1999 Digest of the LEOS summer Topical Meetings

TuA1.3
9:30am-9:50am

Experimental verification of a very low crosstalk wavelength router construction using arrayed- waveguide grating multi/demultiplexers

Fenghai Liu, Rune J.S. Pedersen, Christophe Peucheret and Palle Jeppesen
Research Center COM, Technical University of Denmark,
Building 349, Lyngby DK-2800, Denmark, Email: lf@com.dtu.dk

Introduction: Dense Wavelength Division Multiplexing (DWDM) technology not only offers a flexible way to increase the transmission capacity, but also provides a new dimension for optical networking. Wavelength routing is very promising in future DWDM networks because of its simple structure and high degree of wavelength reuse among the nodes[1]. As the key elements in wavelength routing networks, various kinds of wavelength routers have been investigated[2,3,4].

Interferometric crosstalk, i.e., crosstalk with the same wavelength as the signal, is a critical issue when implementing wavelength routing networks because the crosstalk will accumulate from all the input ports and also accumulate when the channel passes through a cascade of wavelength routers. This kind of crosstalk cannot be filtered at the receiver, and its influence has been thoroughly studied[5,6]. As an example, if the full connectivity is used in a 32×32 wavelength router, the crosstalk level from each input port must be reduced to less than -40 dB in order to meet the common 1dB power penalty criteria[5,6]. This crosstalk requirement is far from being met even by the best published results of 32×32 arrayed waveguide grating (AWG) wavelength router[4].

Although a significant amount of effort is put into reducing the crosstalk level in the AWG components[7,8,9], it is important to consider alternative structures with the same functionality as a wavelength router. In this letter, we clarify that very large (64×64) N×N wavelength routers can be constructed so that they are not limited by interferometric crosstalk. Compared to the N×N AWG wavelength router a substantial crosstalk reduction is obtained in a N×N wavelength router structure based on 1×N AWG multi/demultiplexers due to double filtering. We demonstrate a very low crosstalk level of -53 dB for such an 8×8 wavelength router based on commercially available 1×8 AWG multi/demultiplexers.

Construction: Figure 1 shows the structure of an 8×8 wavelength router using 8 pairs of 1×8 multi/demultiplexers interconnected according to the connection table of a wavelength router[1]. The wavelength channels are first demultiplexed from the input ports using AWG demultiplexers. The demultiplexed channels contain crosstalk from adjacent channels according to the transfer function of the demultiplexers. The adjacent channel crosstalk turns into interferometric crosstalk in channels with same nominal wavelength when these channels are combined in the multiplexers. However, due to the combined transfer function of the AWG demultiplexer and multiplexer, the adjacent channel crosstalk is filtered twice before resulting in interferometric crosstalk at the output ports. Such a good crosstalk suppression cannot be realized in a single component AWG wavelength router.

The number of 1×N AWG multi/demultiplexers needed to build an N×N wavelength router is 2N, and hence scales linearly with the size of the router. The loss of 1×N AWG multi/demultiplexers can be as low as 2.5dB[4]. So even though the proposed construction includes the loss of an AWG multi/demultiplexer pair, the total loss is still low. The crosstalk level is significantly decreased at the same time due to the double filtering.

Characterization: In order to verify the expected crosstalk performance from the double filtering in the new wavelength router structure, an 8×8 wavelength router is constructed using commercial 1×8 AWG multi/demultiplexers with 200GHz wavelength channel spacing as shown in Figure 1.

Experiments have been made to identify the crosstalk induced power penalty in the 8×8 wavelength router. Figure 2 shows the experimental setup. 8 lasers with a wavelength spacing of 200GHz are combined together after polarization alignment. The combined wavelength channels are modulated at 10Gb/s in a Mach-Zehnder modulator. 2 EDFAs are used before and after the modulator. The combined wavelength signal passes through a pair of inter-connected 1×8 multi/demultiplexer with fiber delay lines in between; this setup simulates the crosstalk influence from the proposed 8×8 wavelength router. All channels are demultiplexed again at the receiver end. Bit error rate (BER) versus received power has been measured for each channel with and without the 1×8 multi/demultiplexer pair and is shown in Figure 3. From Figure 3, we can find that the penalty introduced by the 8×8 wavelength router for each channel is less than 0.1dB at BER=10^{-9} and the maximum variation of sensitivity for all cases is within 0.3dB at BER=10^{-9}. This shows that the crosstalk induced penalty in the proposed 8×8 wavelength router is negligible.

We have measured the transfer functions of the 8×8 wavelength router from input ports I1, I2,…,I8 to output port O1 using a scanning wavelength laser source. From the measured transfer functions shown in Figure 4 , a loss smaller than 4.5dB can be found for all channels and the crosstalk suppression is better than 53dB for all channels. This confirms the low power penalty from the router.

1999 Digest of the LEOS summer Topical Meetings

TuA1.3
9:30am-9:50am

Discussion: The measured crosstalk level in the 8×8 wavelength router shows that in this configuration, connectivity is no longer limited by crosstalk and actually a cascade of 40 routers would be tolerable[6]. In terms of large routers, 1×64 AWG multi/demultiplexer with crosstalk less than -27dB has been reported[4], which can be used for a 64×64 wavelength router construction. Even in this case, a cascade of 10 such routers would be possible[6]. Hence, rather large wavelength routing networks can be built using this kind of wavelength router construction.

As mentioned, the number of 1×N multi/demultiplexers needed to construct a N×N wavelength router increases linearly with the number of ports as 2N. However, the relaxed requirements and the fabrication of multi/demultiplexers rather than routers will both contribute to a low cost per device.

Conclusion: A very low crosstalk N×N wavelength router construction based on 1×N AWG multi/demultiplexers has been proposed. The peak crosstalk level of -53dB is measured in such an 8×8 wavelength router and power penalty from the router is negligible. Rather large wavelength routing networks can be built using the wavelength router construction presented here.

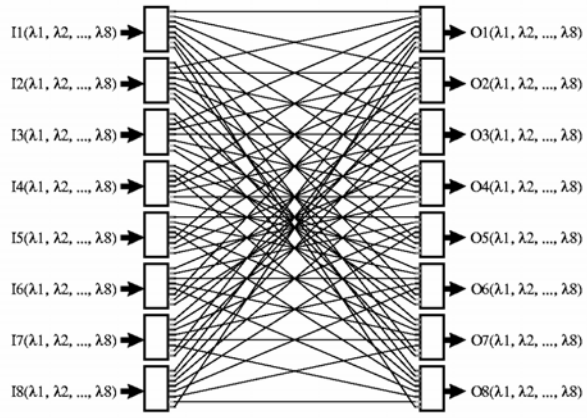

Figure 1. Structure of an 8×8 wavelength route

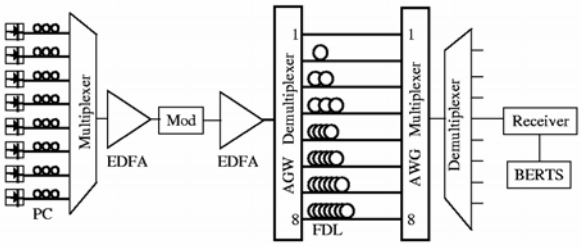

Figure 2. Experimental setup for crosstalk induced penalty measurement in the 8×8 wavelength router.
PC: polarization controller. Mod: modulator. FDL: fiber delay lines. BERTS: bit error rate test set.

References

[1] Brackett, C.A., *IEEE J. Sel. Areas Commun.*, 1990,8, pp.948-964.

[2] Hemenway, B.R., et al, Technical Digest of Conference on Optical Fiber Communications, 1997 , PD26.

[3] Bainbridge, J.D., et al., *Electron. Lett.*, 1997, 33, pp. 1458-1459.

[4] Okamoto, K., et al., *IEICE Trans. Electron.,* 1998, E81-C, pp. 1176-1186.

[5] Takahashi, H., et al., *J. Lightwave Technol.*, 1996, 14,(6), pp. 1097-1105.

[6] Liu, F., Rasmussen, C.J., and Pedersen, R.J.S., , *Conference on Lasers and Electro-Optics,* 1998, pp. 318-319.

[7] Yamada, H., et al., *Electron. Lett.*, 1996, 33, pp. 1580-1582.

[8] Yamada, H., et al., *Electron. Lett.*, 1997, 33, pp. 1608-1609.

[9] Okamoto, K., et al., *Dig. Conf. Opt. Fiber Commun.*, 1999, pp190-192.

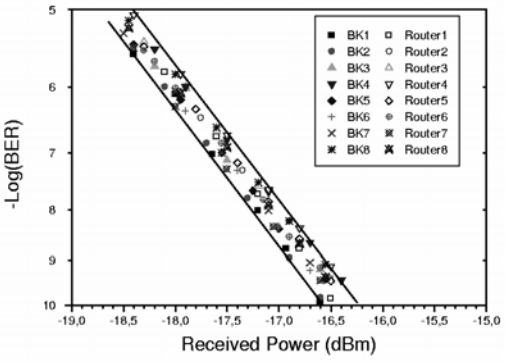

Figure 3. BER vs. Received power with/without the 8×8 wavelength router.

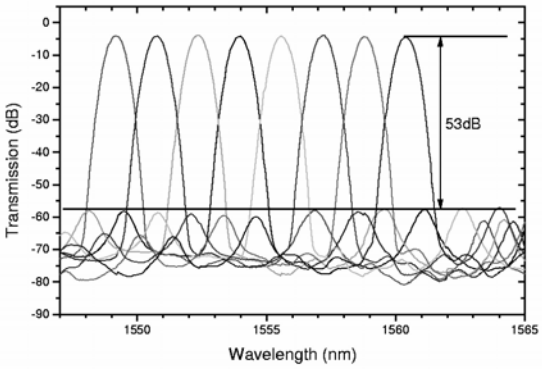

Figure 4. Transfer functions of the 8×8 wavelength router.

IEEE/LEOS Annual Meeting, 2000,

2:00pm-2:15pm
TuR2

Reduction of interferometric crosstalk induced penalty using a saturated semiconductor optical amplifier

Fenghai Liu, Xueyan Zheng, Henrik N. Poulsen, David Wolfson, Palle Jeppesen
Research Center COM, Technical University of Denmark, Building 349, Lyngby, DK-2800, Denmark
Telephone: +45-45253845, Fax: +45-45936581, Email: lf@com.dtu.dk

Introduction

WDM networks have been installed on a global scale to satisfy the ever-increasing demand of communication capacity. As the number of wavelength increases, the interferometric crosstalk is becoming critical. Strong requirements on crosstalk are imposed to the components used in large-scale transparent optical networks.[1,2]

Components with low crosstalk are important, but other effective techniques to suppress the impact of crosstalk are also needed. Several techniques can be used for this purpose, e.g., using a gain saturated laser diode amplifier [3], wavelength conversion based on cross-phase-modulation [4] or cross-gain-modulation [5,6] in semiconductor optical amplifiers (SOA).

The gain saturated laser diode amplifier needs a filter to suppress the lasing signal from the diode and it is limited to low bit-rate. To suppress the crosstalk, wavelength conversion is not always necessary. For instance, a tunable source is needed to track the wavelength of input signal in the wavelength converter in order to keep the same wavelength for the input and output signals, which is complex and expensive. SOA has a fast gain saturation, which can be used to suppress the fluctuation on the optical amplitude. A holding CW light counter-propagating with the input signal is used to overcome waveform distortion in the saturated SOA. This scheme avoids wavelength conversion. Since the SOA is of simple structure and bit-rate transparent at high speed, it is promising in reduction of crosstalk impact in transparent optical networks.

Experiment and results

Fig.1 shows the experimental set-up to demonstrate the capability of reducing the crosstalk induced power penalty using a saturated SOA.

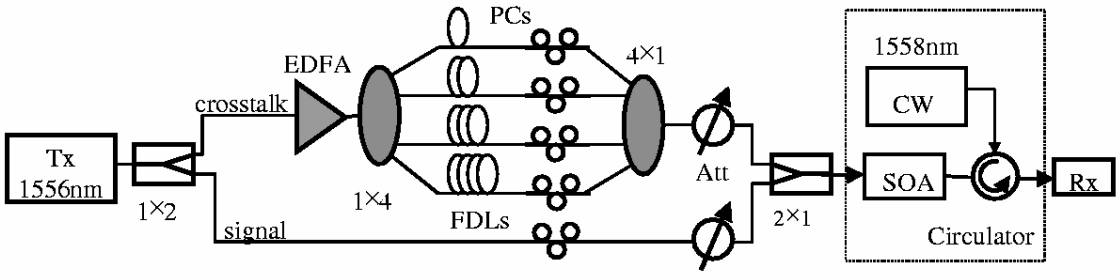

Fig.1. Experimental set-up. Tx: transmitter; 1×2 and 2×1: 3dB coupler; 1×4 and 4×1: star coupler; PC: polarisation controller; FDL: fibre delay line; Rx: PIN receiver.

The power from the transmitter is split into two parts; one part serves as signal, and the other part as crosstalk. The crosstalk part is amplified by an EDFA and further divided into four parts using a 1×4 star coupler in order to simulate four crosstalk terms. The four crosstalk terms are de-correlated by different lengths of fibre delay lines, aligned in the same polarisation state as the signal for maximum impact using polarisation controllers and combined again using a 4×1 star coupler. The crosstalk contributions are attenuated and combined with the signal. Another attenuator is used to control the power into the saturated SOA. Bit error rate (BER) curves are measured with and without the SOA before the PIN receiver. Optimal decision threshold is used in the BER measurement.

IEEE/LEOS Annual Meeting, 2000,

In order to overcome the waveform distortion when the SOA is saturated, a holding light in CW operation at 1558 nm is injected into the SOA through a circulator, counter-propagating with the input signal, as shown in a dashed frame in Fig.1.

The transfer characteristic of the saturated SOA is shown in Fig.2 when the power of CW light is 6.1 dBm. From the transfer characteristic, it can be found that the SOA is highly saturated when the input power is higher than 0 dBm. The average input power into the SOA is 1 dBm in our experiment in order to suppress the crosstalk-signal beat noise on the "1" level.

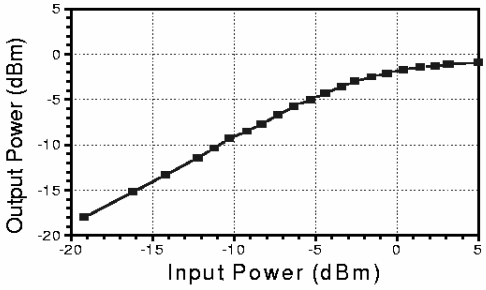

Fig.2. Transfer characteristic of the SOA saturated by a CW light of 6.1dBm

Since SOA is bit-rate transparent, the saturated SOA is used to reduce the crosstalk impact at both 2.5Gb/s and 10Gb/s. Fig.3 shows the eye-diagrams with -15 dB crosstalk before (a) and after (b) the SOA at 2.5Gb/s. A clearer eye can be seen after using the SOA. Fig.4 shows the penalty curves versus relative crosstalk power at 10 Gb/s. A 4 dB more crosstalk power can be tolerated at 1 dB penalty when the saturated SOA is used.

Using saturated SOA will significantly relax the crosstalk requirement on the components used in cascade in transparent optical networks where interferometric crosstalk accumulates.

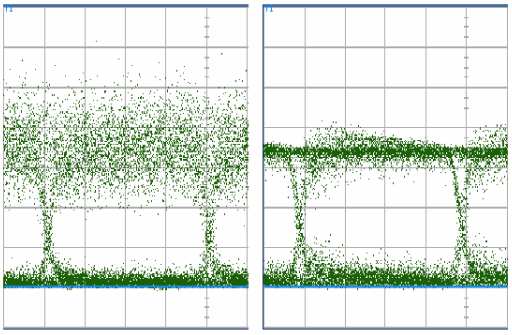

(a) (b)

Fig.3. Eye-diagrams before (a) and after SOA. Time scale: 100ps/div

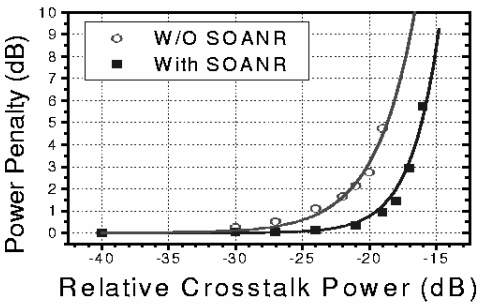

Fig.4. Penalty vs. relative crosstalk power with and without SOA at 10Gb/s

Conclusion

We successfully demonstrated that a simple saturated SOA could be used to reduce the impact from the interferometric crosstalk at 2.5Gb/s and 10Gb/s. It is shown that 4 dB more crosstalk power can be tolerated at 1 dB penalty by using the SOA. This will greatly reduce the crosstalk requirement on components, especially these used in cascade in large-scale transparent optical networks.

Reference:

[1] Ho K.P., et al., IEEE J. Lightwave Techn. 14, 1127-1135(1996)
[2] Liu F., et al., Technical Digest. of CLEO'98, 318-319(1998)
[3] Inoue K., IEEE Photonics Techn. Lett., 8(3), 458-460(1996)
[4] Poulsen H.N., et al., Proc. of OAA'98, 181-183(1998)
[5] Pegg S.I., et al., IEEE Photonics Techn. Lett., 11(6), 724-726(1999)
[6] Stephens M.F.C., et al., IEEE Photonics Techn. Lett., 11(8), 979-981(1999)

Conference on Lasers and Electro-Optics, 2000, CLEO'2000

91 / *CLEO'2000 / MONDAY AFTERNOON*

Interferometric crosstalk suppression using polarization multiplexing technique and an SOA

Fenghai Liu, Xueyan Zheng, Rune J.S. Pedersen and Palle Jeppesen
Research Center COM, Technical University of Denmark, Lyngby, DK-2800, Denmark
Telephone: +45-4525-3845, Fax: +45-45936581, Email: LF@com.dtu.dk

Abstract: Interferometric crosstalk can be greatly suppressed at 10Gb/s and 20Gb/s by using a gain saturated SOA and a polarization multiplexing technique that eliminates impairments like waveform distortion and extinction ratio degradation from the SOA.

Introduction

Interferometric crosstalk is one of the biggest issues in transparent WDM networks, and should be overcome by either decreasing the crosstalk level from the components, or employing effective techniques to suppress its impact [1].

A gain saturated laser diode amplifier has been reported to suppress crosstalk, but it can't be used for high speed signals and the output signal suffers from extinction ratio degradation and waveform distortion [2].

In this paper, we use a gain saturated semiconductor optical amplifier (SOA) to suppress the impact of interferometric crosstalk, and show that 6dB more crosstalk can be tolerated for 1 dB penalty at 10Gb/s. Using polarization multiplexing of optical signals modulated by data and the complementary, impairments like waveform distortion and extinction ratio degradation are eliminated, and the method is also bit rate transparent.

Principle and experimental set-up

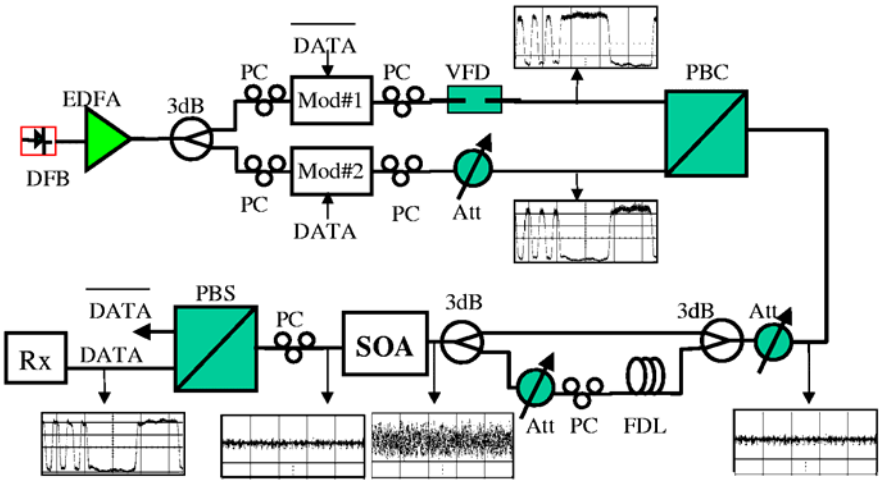

Fig. 1. Experimental set-up. 3dB: 3dB coupler; PC: polarization controller; Mod: Lithium Niobate modulator; VFD: variable fiber delay line; PBC: polarization beam combiner; Att: variable optical attenuator; FDL: fiber delay line; SOA: semiconductor optical amplifier; PBS: polarization beam splitter; Rx: optical receiver

Fig.1. shows the experimental set-up and waveforms at different points. Light from a DFB laser is divided into two parts after being amplified by an EDFA. Each part is modulated by data or the complementary in an external modulator, and then set to one of two orthogonal polarization states. The two parts are combined in the polarization beam combiner (PBC). A variable fiber delay line and a variable optical attenuator are used before the PBC, in order to obtain a constant power of the combined signal without bit transition patterns. Crosstalk is added to the combined signal by adding a fraction of the original signal delayed by 500 m of fiber. The signal-crosstalk beat noise causes amplitude fluctuations, but these fluctuations are significantly suppressed after the SOA because of the gain saturation. The 3 dB saturation

Conference on Lasers and Electro-Optics, 2000, CLEO'2000

input power of the SOA is -10dBm, and the input power into the SOA is -2dBm in our experiment. The two orthogonally polarized signals are separated by the polarization beam splitter, and one of them is detected.

Results and discussions

Since the SOA only experiences constant optical power of the combined signal, no waveform distortions will be generated by the SOA. Furthermore, since amplitude fluctuations are suppressed by the saturated SOA, crosstalk-induced penalty can be reduced. Fig.2.shows the penalties versus relative crosstalk power with and without the SOA; it can be seen that 6dB more crosstalk power can be tolerated using the SOA at 1dB penalty (BER=10^{-9}). The inlets show eye-diagrams of the 10Gb/s signal before and after the SOA when -13.8dB crosstalk is introduced. A clear eye is restored after the SOA.

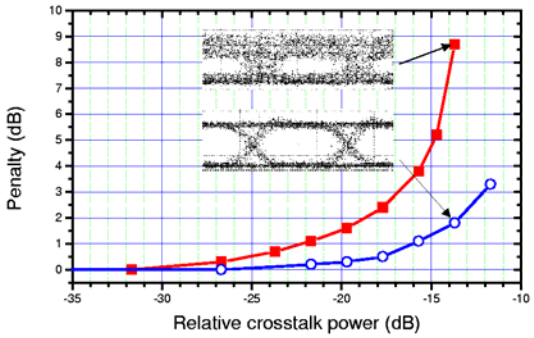

Fig. 2. Penalty vs. relative crosstalk power with (circles) and without (squares) gain saturated SOA

Because of the constant optical power in the SOA, this method is pattern independent and bit rate transparent, and there is no extinction ratio degradation. Fig.3. shows the eye-diagrams at 20Gb/s before and after the SOA when the relative crosstalk power is -17.8dB; also here a clear eye can be found after the SOA. Due to lack of a 20Gb/s receiver, no BER curves are measured in this case.

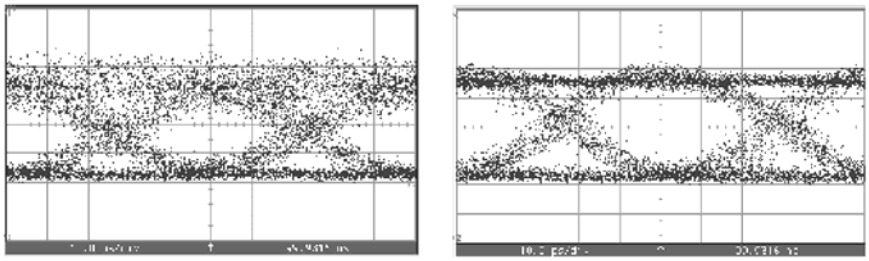

(a) (b)

Fig. 3. Eye-diagrams before (a) and after (b) gain saturated SOA at 20Gb/s. Relative crosstalk power is –17.8dB

Conclusion

We successfully demonstrate that the impact of interferometric crosstalk can be suppressed using a saturated SOA and a polarization multiplexing technique. The method is pattern independent and bit-rate transparent and gives no waveform distortion or extinction ratio degradation. A 6dB higher crosstalk level can be tolerated at 1 dB penalty using this method.

References

[1] P.J. Legg, M. Tur and I. Andonovic, "Solution paths to limit interferometric noise induced performance degradation in ASK/direct Detection lightwave networks", J. Lightwave Technol., Vol **14**, 1943-1954 (1996)

[2] K. Inoue, "Suppression of signal fluctuation induced by crosstalk light in a gain saturated laser diode amplifier", IEEE Photonics Technol. Lett., Vol.**8**, 458-460 (1996)

IEEE PHOTONICS TECHNOLOGY LETTERS, VOL. 12, NO. 8, AUGUST 2000 1091

Suppression of Interferometric Crosstalk and ASE Noise Using a Polarization Multiplexing Technique and an SOA

Xueyan Zheng, Fenghai Liu, David Wolfson, and Allan Kloch

***Abstract*—Noise suppression at 10 Gbit/s and 20 Gbit/s is demonstrated using a gain saturated semiconductor optical amplifier (SOA) and a polarization multiplexing technique, where no impairments like waveform distortion and extinction ratio degradation caused by the gain saturation of the SOA appear. Moreover, the method is bit rate transparent and the input power dynamic range is very large. Furthermore, the SOA can provide a high gain.**

***Index Terms*—Interferometric crosstalk, noise suppression, polarization multiplexing, semiconductor optical amplifier.**

I. Introduction

WAVELENGTH-DIVISION-MULTIPLEXING (WDM) networks have been installed on a global scale to satisfy the ever-increasing demand for communication capacity. In WDM networks, amplified spontaneous emission (ASE) from optical amplifiers and crosstalk at the signal wavelength (interferometric crosstalk) are serious problems [1]. So, it is very important to find effective techniques to suppress the impact of ASE noise and interferometric crosstalk. Several schemes have been demonstrated for noise suppression, including Mach–Zehnder interferometers [2], a wavelength converter based on cross gain modulation in a laser diode [3] and a gain saturated laser diode amplifier [4]. However, the Mach–Zehnder interferometer structure is complicated and the input power dynamic range is small. The method used in [3] inherently performs wavelength conversion and the conversion speed is limited by the recovery time of the carrier in the optical amplifier, moreover, there is a large undesired chirp is added to the signal. The method in [4] does not need wavelength conversion, but it suffers from extinction ratio (ER) degradation, waveform distortion at high input powers and it does not work at high bit rates because of the limited relaxation time.

In this paper, it is shown that signal fluctuations caused by interferometric crosstalk or ASE can be suppressed greatly at 10 or 20 Gbit/s using a gain saturated semiconductor optical amplifier (SOA) and a polarization multiplexing technique. Using polarization multiplexing of optical signals modulated by data and the complementary, the SOA experiences a constant input power instead of a transient power from the bit pattern and consequently impairments like waveform distortion and extinction ratio degradation from the SOA are eliminated. Moreover, the method is bit rate transparent and the input power dynamic range is very large. In addition, the SOA can also provide high gain.

Manuscript received January 1, 2000; revised April 12, 2000.

The authors are with the Research Center COM, Technical University of Denmark, Lyngby DK-2800, Denmark (e-mail: zx@com.dtu.dk).

Publisher Item Identifier S 1041-1135(00)06287-X.

II. Principle of the Method

When an SOA is gain saturated, the signal fluctuation caused by interferometric crosstalk or ASE noise can be reduced [3]. However, the ER of the output signal is reduced and the waveform is also distorted at high input power level due to the gain saturation. In order to avoid the above shortcomings, we multiplex the two optical signals with orthogonal polarization states which are modulated with data and the complementary respectively using a polarization beam combiner (PBC), hereby, obtain the multiplexed signals with a constant power as described in [5]. Since the SOA only experiences the constant optical power of the combined signals, no waveform distortions and ER degradation will be generated by the SOA. A polarization beam splitter (PBS) is used to demultiplex the signal. Fig. 1 shows the waveforms of the signals before the PBC, before and after the SOA and after the PBS when the input power into the SOA is -2 dBm, which is much higher than the 3-dB gain saturated power. It can be seen from Fig. 1 that no ER degradation and waveform distortion is induced. Furthermore, the method is pattern independent and no chirp is added to the signal due to the constant input power to the SOA.

III. Experimental Setup

Fig. 2 shows the experimental setup. Light from a DFB laser is divided into two parts after being amplified by an EDFA. Each part is modulated by data (2^{31-1} PRBS) or the complementary in an external modulator, and then set to one of two orthogonal polarization states. The two parts are combined in the PBC. A variable fiber delay line and a variable optical attenuator (Att1) are used before the PBC, in order to obtain a constant power of the combined signal without bit transition patterns. Two kinds of noise are generated to add fluctuation to the signal before launched into the SOA, one is interferometric crosstalk, the other is ASE noise. The interferometric crosstalk is added to the combined signal by adding a fraction of the original signal delayed by 500-m fiber. Att2 before the 3-dB coupler is used to control the input power to the SOA and Att3 is used to control the relative crosstalk power. ASE noise is generated by an EDFA. The signal is transmitted through in-line EDFA2, and then an optical filter with 1.3-nm bandwidth. Att4 before EDFA2 is used to control the input power. Thus, the optical signal-to-noise ratio at the input of the SOA can be controlled.

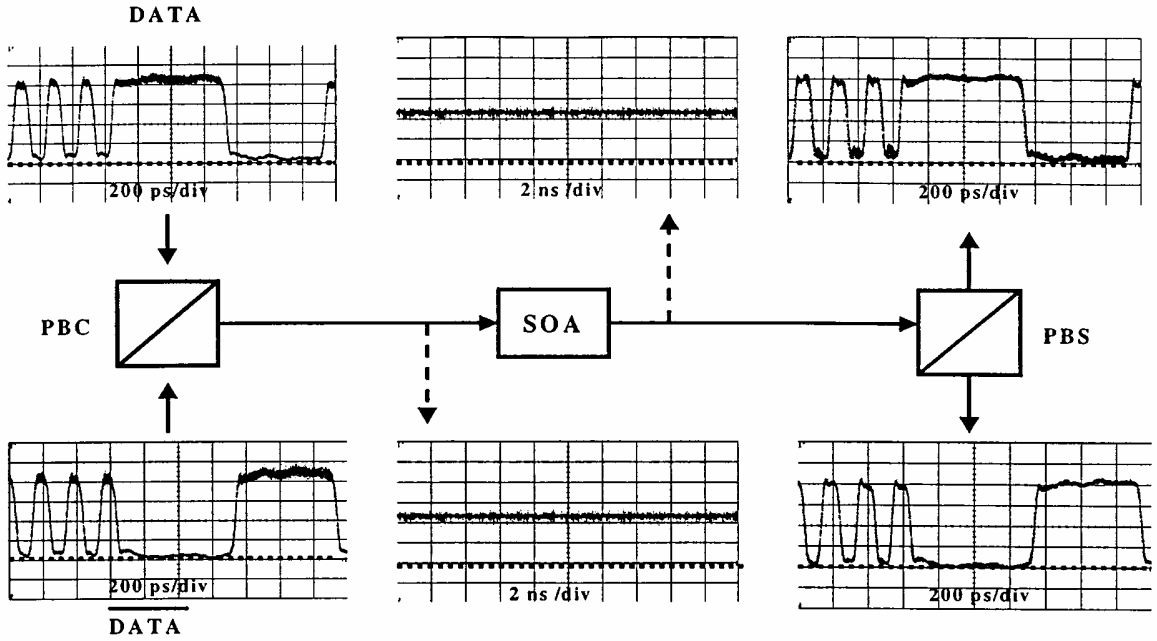

Fig. 1. Waveforms of the signal before polarization multiplexing, before and after the SOA and after the PBS. The input power into the SOA is −2 dBm. PBC: Polarization beam combiner. PBS: Polarization beam splitter. SOA: Semiconductor optical amplifier.

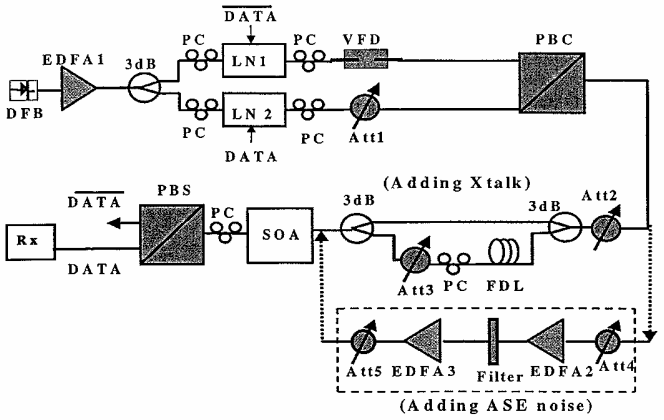

Fig. 2. Experimental setup. 3dB: 3-dB coupler. PC: Polarization controller. LN: Lithium Niobate modulator. VFD: Variable fiber delay line. PBC: Polarization beam combiner. Att: Variable optical attenuator. FDL: Fiber delay line. SOA: Semiconductor optical amplifier. PBS: Polarization beam splitter. Rx: Optical receiver.

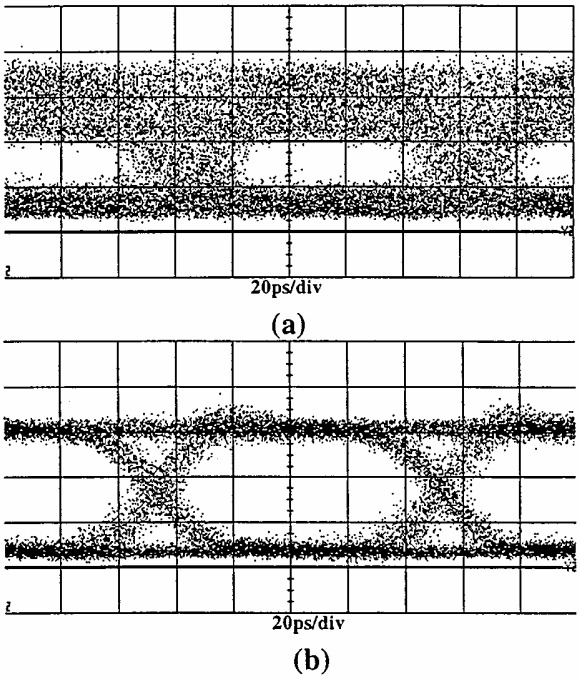

Fig. 3. Eye-diagrams of the signal with −13.8 dB crosstalk before (a) and after (b) the SOA at 10 Gb/s.

The Att5 after EDFA3 is used to control the power into the SOA. The 3-dB saturation input power of the SOA is −10 dBm, the gain peak of the SOA is at 1550 nm and the gain polarization-dependence of the SOA is 0.5 dB. The two orthogonal polarized signals are separated by the PBS, both of them have the same performance and one of them is detected in a PIN receiver.When the crosstalk is added to the signal, the amplitude fluctuations caused by the beat noise between the signal and the crosstalk are suppressed significantly by the saturated SOA. Fig. 3(a) and (b) shows eye-diagrams of the 10 Gb/s signal with −13.8 dB crosstalk before and after the SOA. Seen from Fig. 3, a clear eye is restored after the SOA. Fig. 4.shows the penalties versus relative crosstalk power with and without the SOA at different input power levels. It can be seen from Fig. 4 that a 6 dB more crosstalk power can be tolerated using the SOA at a penalty of 1 dB (BER = 10^{-9}) when the input power to the SOA is −6 dBm. Because the ER degradation and waveform distortion are avoided, the input power dynamic range is very large. Seen from Fig. 4, when the input power changes from −10 to 4 dBm, 4–6 dB more crosstalk power can be tolerated by using the SOA at a penalty of 1 dB (BER = 10^{-9}). Since the saturated output power of the SOA is +7 dBm, the SOA can also provide high gain. When the input power to the SOA is −10 dBm, the gain is +17 dB, meanwhile, 4 dB more crosstalk can be tolerated.

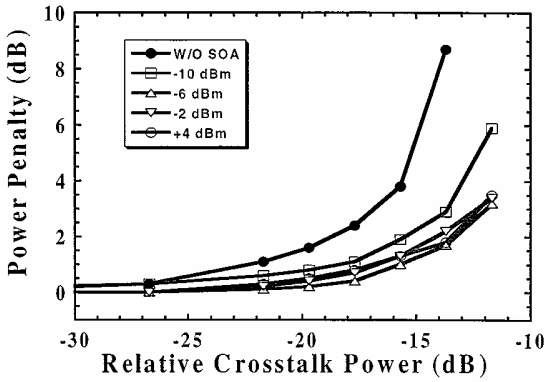

Fig. 4. Penalty as a function of relative crosstalk power for different input power level.

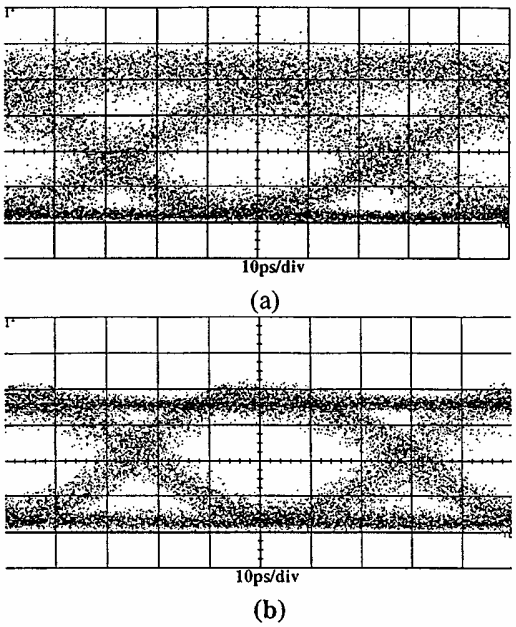

Fig. 5. Eye-diagrams of the signal with −17.8 dB crosstalk before (a) and after (b) the SOA at 20 Gb/s.

IV. Results and Discussions

In general, this method can reduce any amplitude fluctuation with the frequency to which the SOA can respond, on the other hand, the electronical filter in the receiver will filter the noise with high frequency. Moreover, the waveform distortion and ER degradation are avoided, so, we can say that this method is bit rate transparent. The length of the SOA used in the experiment is 1.2 mm, and the 3-dB modulation bandwidth is larger than 30 GHz. So, effective noise suppression can be realized at very high bit rate using this method. Fig. 5(a) and (b) shows the eye-diagrams at 20 Gb/s before and after the SOA when the relative

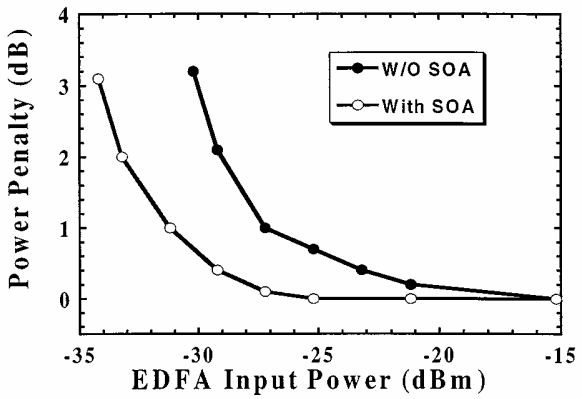

Fig. 6. Penalty as a function of the EDFA input power with and without the SOA at 10 Gbit/s. The input power to the SOA is −3 dBm.

crosstalk power is −17.8 dB; also here a clear eye can be found after the SOA. Due to lack of a 20 Gb/s receiver, no BER curves are measured in this case.

ASE noise is also suppressed effectively using the same method. Fig. 6 shows the receiver penalty at 10 Gb/s with and without the SOA as a function of the in-line EDFA input power. The input power to the SOA is −3 dBm. As seen, the noise is suppressed and 4 dB lower input power to the EDFA is allowed at a penalty of 1 dB (BER = 10^{-9}).

V. Conclusion

We have successfully demonstrated that the impact of interferometric crosstalk and ASE noise can be suppressed using a saturated SOA and a polarization multiplexing technique. The method gives no waveform distortion or extinction ratio degradation. Besides the method is bit rate transparent and the input power dynamic range is very large, the SOA can also provide a high gain.

References

[1] P. J. Legg, M. Tur, and I. Andonovic, "Solution paths to limit interferometric noise induced performance degradation in ASK/direct detection lightwave networks," *J. Lightwave Technol.*, vol. 14, pp. 1943–1954, Sept. 1996.

[2] D. Wolfson, P. B. Hansen, T. Fjelde, A. Kloch, C. Janz, A. Coquelin, I. Guillemot, F. Gaborit, F. Poingt, and M. Renaud, "40 Gbit/s all-optical 2R regeneration in an SOA-based all-active Mach–Zehnder interferometer," in *Proc. OECC'99*, Beijing, China, 1999, pp. 456–457.

[3] K. Inoue, "Noise transfer characteristic in LD wavelength conversion," *J. Lightwave Technol.*, vol. 14, pp. 2763–2770, Dec. 1996.

[4] ——, "Suppression of signal fluctuation induced by crosstalk light in a gain saturated laser diode amplifier," *IEEE Photon. Technol. Lett.*, vol. 8, pp. 458–460, Aug. 1996.

[5] S. Banerjee, A. K. Srivastava, B. R. Eichenbaum, C. Wolf, Y. Sun, J. W. Sulhoff, and A. R. Chraplyvy, "Polarization multiplexing technique to mitigate WDM cross-talk in SOAs," in *Proc. ECOC'99*, vol. PD, 1999, pp. 62–63.

European Conference on Optical Communication, Munich, Germany, 2000

SIMULTANEOUS INTERFEROMETRIC CROSSTALK SUPPRESSION IN WDM CHANNELS USING POLARIZATION MULTIPLEXING TECHNIQUE AND SOA

Xueyan Zheng, Fenghai Liu, Jianjun Yu, David Wolfson, Allan Kloch and Tina Fjelde
Research Center COM, Technical University of Denmark, Lyngby, DK-2800, Denmark
Telephone: +45-4525-3777, Fax: +45-45936581, Email: zx@com.dtu.dk

Abstract: *For the first time, interferometric crosstalk suppression of 2 WDM channels are realized simultaneously using a gain-saturated SOA and polarization multiplexing technique. The characteristics of interferometric crosstalk suppression in WDM channels using the method are discussed.*

Introduction

Wavelength division multiplexing (WDM) networks have been installed on a global scale to satisfy the ever-increasing demand for communication capacity. In WDM networks, crosstalk at the signal wavelength (interferometric crosstalk) raises serious problem [1]. So, it is very important to find effective techniques to suppress the impacts caused by interferometric crosstalk. However, all the schemes for crosstalk suppression, which have been demonstrated so far, can only work for a single channel, such as: Mach-Zehnder interferometers based on SOAs [2], wavelength converters based on cross gain modulation in a laser diode [3] and gain saturated laser diode amplifiers [4]. So, WDM channels have to be demultiplexed before crosstalk suppression, while it will increase the complexity and cost of a WDM network with a large number of channels.

In this paper, for the first time, simultaneous interferometric crosstalk suppression is realized experimentally for 2 channel using a gain saturated SOA and a polarization multiplexing technique (PMT). The characteristics of interferometric crosstalk suppression for WDM channels system using this method are discussed.

Working principle and experimental results

When an SOA is gain saturated, the fluctuation of the input signal caused by interferometric crosstalk or ASE noise can be reduced [3]. However, the extinction ratio of the output signal from the SOA is reduced and the waveform is also distorted at high input power levels due to the gain saturation. In order to avoid the above shortcomings, we multiplex the two optical signals in the orthogonal polarization states, which are modulated by data and the complementary, respectively, using a polarization beam combiner (PBC). Hereby, a multiplexed signal with a constant power is obtained as described in Ref [5]. Since the SOA only experiences the constant optical power of the combined signals, no waveform distortions and ER degradation will be generated by the SOA. Furthermore, the method is bit rate transparent and the SOA can also provide high gain [5]. In this paper, we extend the method to realize simultaneously interferometric crosstalk suppression for WDM channels. It should be pointed out, because the constant light is launched into the SOA, the crosstalk between the two channels caused by cross-gain modulation in the SOA is avoided [6].

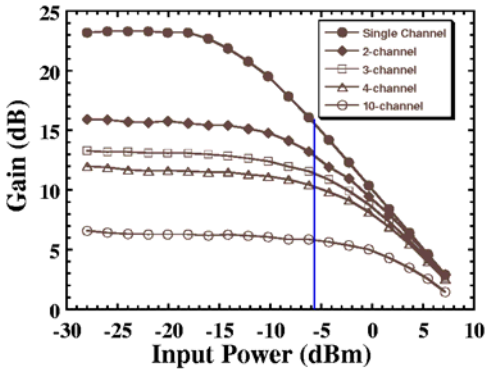

Fig.3. Gain curves of the SOA under different number of input channels.

We know that all the input channels should be in the state of deep saturation if we want to obtain effective noise suppression. Fig. 1 shows the gain of each channel versus the input power of each channel, when 1, 2, 3, 4 and 10 channels are launched into the SOA respectively. The gain curves for more than one channel is obtained by keeping the power of each channel to be -5.7 dBm, except for the measured channel whose input power is changed from -28 dBm to 7 dBm. As seen from the gain curve of single channel in Fig. 1, the gain is reduced 7 dB at an input power of -5.7 dBm, compared to the unsaturated gain. The deep saturation make interferometric crosstalk be suppressed effectively. When two channels are launched into the SOA, it can be seen from Fig. 1, that the gain is suppressed 2.7 dB for each channel at an input power of -5.7 dBm, compared to the unsaturated gain. So, the crosstalk can be suppressed for two channels simultaneously if two channels with power of -5.7 dBm is launched into the SOA. It means that the scheme works for multiple channels. However, we can also see that, for two channels situation, the saturation state is less than that when a single channel is used. So, the efficiency of noise suppression should be reduced comparing to the case of a single channel. It also can be seen from Fig. 3 that when more channels are launched into the SOA, each channel becomes less gain saturation.

European Conference on Optical Communication, Munich, Germany, 2000

Consequently, noise suppression should become less efficient. When 10 channels are used, each channel works in the linear area, no noise suppression will be obtained. In the next, we will show the experimental results of interferometric crosstalk suppression for two channels.

Experimental Set-up and Results

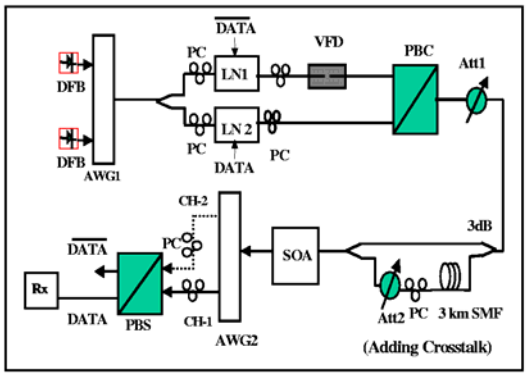

Fig.1. Experimental set-up. PC: polarization controller; LN: Lithium Niobate modulator; VFD: variable fiber delay line; PBC: polarization beam combiner; Att: variable optical attenuator; SOA: semiconductor optical amplifier; PBS: polarization beam splitter; Rx: optical receiver.

Fig.1 shows the experimental set-up. CW light from two DFB lasers with wavelengths of 1553.73 nm (channel one) and 1555.35 nm (channel two) is split into two parts after being multiplexed by AWG1. Each part is modulated by data or the complementary in an external modulator, and then set to one of two orthogonal polarization states. The two parts are combined in the PBC. A variable fiber delay line are used before the PBC, in order to obtain a constant power of the combined signal without bit transition patterns. The interferometric crosstalk is added to the combined signal by adding a fraction of the original signal delayed by 3 km of fiber. Att1 is used to control the input power to the SOA and Att2 is used to control the relative crosstalk power. After de-multiplexed by AWG2, the two orthogonal polarized signals are separated by the polarization beam splitter (PBS), both of them have the same performance and one of them is detected in a PIN receiver.

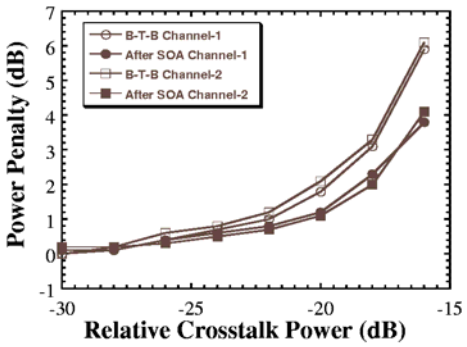

Fig. 2. Penalty as a function of relative crosstalk power for the two channels.

Fig. 2 shows the penalties for the two channels versus the relative crosstalk power with and without the SOA. The input power level to the SOA for each channel is -5.7 dBm. For the two channels, it can be seen from Fig. 3 that 1.3 and 2.3 dB more crosstalk power can be tolerated, respectively, at a penalty of 1 dB (BER=10^{-9}) by using the SOA. This indicates that the interferometric crosstalk is suppressed simultaneously for two channels with good performance. Furthermore, the SOA can also provide 13 dB gain for each channel, since the saturated output power of the SOA is +10 dBm.

Conclusion

We have demonstrated that the impact of interferometric crosstalk can be suppressed simultaneously for two channels using a gain saturated SOA and a polarization multiplexing technique. When more channels are launched into the SOA, the efficiency of noise suppression will be reduced. However, for large number of wavelengths, it can be divided into small groups in order to realize efficient crosstalk suppression. This method makes simultanous interferometric crosstalk suppression for WDM channels be promising in WDM networks.

References

1. P. J. Legg, M. Tur and I. Andonovic, "Solution paths to limit interferometric noise induced performance degradation in ASK/direct Detection lightwave networks", J. Lightwave Technol., Vol 14, 1943-1954 ,1996.
2. H. N. Poulsen, et al., "Reduced Impact of Interferometric Cross-talk by using All-Optical Interferometric Wavelength Converters" Proc. of OAA'98, 181-183, 1998.
3. K. Inoue, "Noise Transfer Characteristic in LD Wavelength Conversion", IEEE J. Lightwave Techn. 14, 2763-2770, 1996.
4. K. Inoue, "Suppression of signal fluctuation induced by crosstalk light in a gain saturated laser diode amplifier", IEEE Photonics Technol. Lett., Vol. 8, 458-460, 1996.
5. F. Liu, X. Zheng, R. J. Pedersen and P. Jeppesen, "Interferometric crosstalk suppression using polarization multiplexing technique and an SOA", 2000 CLEO/QELS 2000, San Francisco, California, CMR1.
6. S. Banerjee, A. K. Srivastava, B. R. Eichenbaum, C. Wolf, Y. Sun, J. W. Sulhoff and A. R. Chraplyvy, "Polarization Multiplexing Technique to Mitigate WDM Cross-talk in SOAs", Proc. ECOC'99, PD, pp62-63, 1999.

272 IEEE PHOTONICS TECHNOLOGY LETTERS, VOL. 12, NO. 3, MARCH 2000

Experimental Investigation of the Cascadability of a Cross-Gain Modulation Wavelength Converter

Xueyan Zheng, Fenghai Liu, and Allan Kloch

Abstract—**The cascading characteristics of a wavelength converter based on cross-gain modulation (XGM) are studied experimentally using a recirculating loop at 10 Gb/s. The maximum cascaded number of the wavelength converter converting the signal to the same wavelength is improved from five to eight by adding a fiber grating-based optical add–drop multiplexer after the semiconductor optical amplifier (SOA) to enhance the high-frequency response of the wavelength converter. However, the low-frequency degradation of the signal together with amplified spontaneous emission (ASE) noise and jitter accumulation finally limits the wavelength converter to be cascaded for more times.**

Index Terms—**Cascadability, cross-gain modulation (XGM), semiconductor optical amplifier (SOA), wavelength conversion.**

I. Introduction

ALL-OPTICAL wavelength converters (AOWC's) will be key components in future broad-band wavelength-division-multiplexed (WDM) optical networks. Among several AOWC's already demonstrated, the AOWC based on cross-gain modulation (XGM) in a semiconductor optical amplifier (SOA) is the simplest to realize and capable of converting the input signal to the same wavelength, which is favorable in all-optical networks [1], [2]. An important issue for the AOWC to be used in the WDM networks is its cascadability. However, up to now, only a few theoretical results have been reported, which do not consider the pattern effect [3], [4]. Actually, in practical systems, the cascadability of this kind of AOWC is limited seriously by the insufficient high-frequency response of the AOWC, which is caused by the slow gain recovery time of the SOA when it works at high bit rate. Recently, it has been reported that the frequency response of the AOWC can be improved by adding a fiber grating after the SOA, which reshapes the chirped converted signal [5].

In this paper, for the first time, the cascadability of the XGM-AOWC is studied experimentally using a recirculating loop setup at 10 Gb/s. The experiment shows that the maximum number of cascaded AOWC's converting the signal to the same wavelength is 5 mainly due to the degradation of the high-frequency components of the signal. By adding a Mach–Zehnder optical add–drop multiplexer (OADM) based on fiber gratings after the SOA, the maximum cascading round-trips in the loop is increased to eight due to the improved high-frequency response in the AOWC. However, the inherent low-frequency degradation in the cascaded signal together with the accumulation of ASE noise and jitter limits the AOWC to be cascaded for more times.

Manuscript received September 30, 1999; revised November 16, 1999.

The authors are with the Research Center COM, Technical University of Denmark, Lyngby DK-2800, Denmark (e-mail: zx@com.dtu.dk).

Publisher Item Identifier S 1041-1135(00)01993-5.

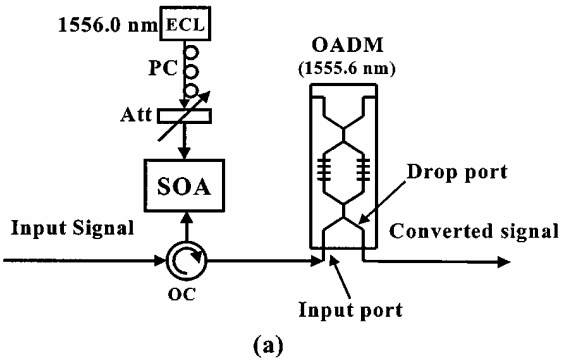

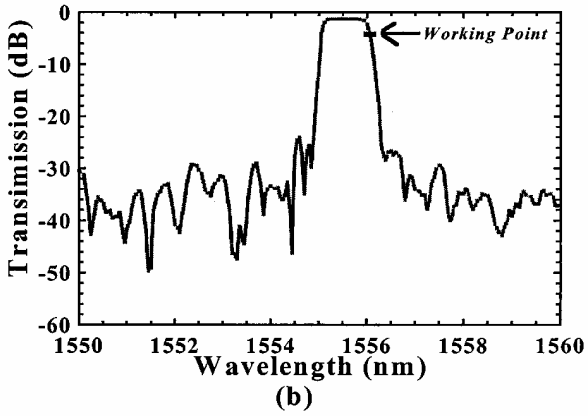

Fig. 1. (a) Structure of the AOWC. (b) In-drop transfer function of the OADM. PC: Polarization controller. Att: Tunable attenuator. OC: Optical circulator. ECL: External cavity laser.

II. Experimental Setup

In the experiment, the AOWC performs the conversion to the same wavelength. The structure of the counterpropagating AOWC is shown in Fig. 1(a). The CW light is provided by an external cavity laser (ECL) and the power into the SOA is −1 dBm after a polarization controller and an attenuator. The input signal with a power of +8 dBm is launched into the SOA through an optical circulator (OC). The converted signal from the SOA comes into the OADM from the input port and comes out from the drop port. The OADM with a center wavelength of 1555.6 nm and a 3-dB bandwidth of 1 nm is used to reshape the converted signal when the wavelength of the converted signal is at the red side of the in-drop transfer function [6], which is 1556.0 nm in the experiment. The in-drop transfer function of

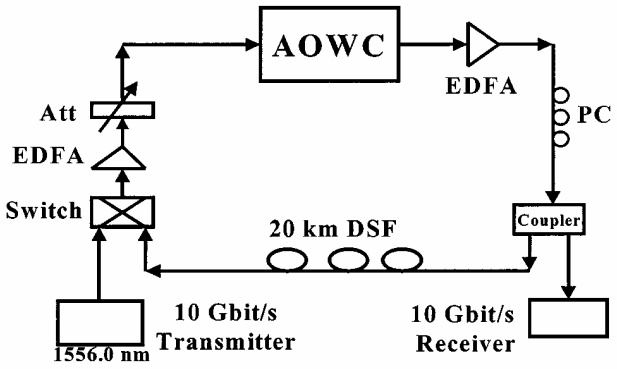

Fig. 2. Loop experimental setup. PC: Polarization controller. Att: Tunable attenuator. DSF: Dispersion-shifted fiber.

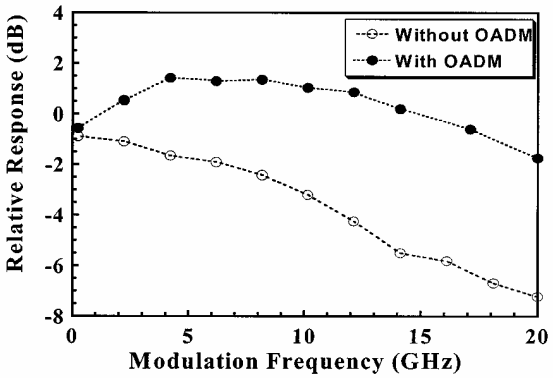

Fig. 3. Small signal bandwidths of the AOWC without and with the OADM.

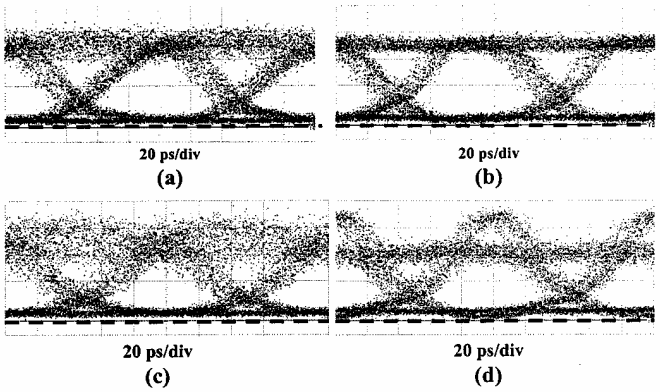

Fig. 4. The eye diagrams of the converted signal (a), (c) without and (b), (d) with the OADM after the second and fifth round-trips in the loop experiment, respectively.

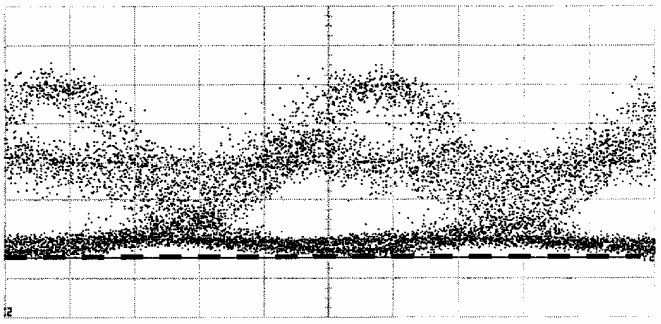

Fig. 5. The eye diagrams of the converted signal after the tenth round-trips.

the OADM and the working point in the experiment are shown in Fig. 1(b). The cascadabilities of the AOWC both with and without the OADM are measured in the loop experiment. The AOWC without the OADM actually means that the wavelength of the continuous-wave (CW) light is located at the center of the OADM in order to keep the same ASE level as when the OADM is used to reshape the converted signal. The SOA used in the experiment has a chip length of 1250 μm, and the fiber-to-fiber gain is 20 dB at a bias current of 250 mA, which is used in our experiment. The reflection from the facets of the SOA is smaller than -26 dB. The loop setup used in the experiment is shown in Fig. 2. An externally modulated 10 Gb/s [pseudorandom binary signal (PRBS) $2^{31} - 1$] tuneable transmitter provides the input signal to the AOWC in the loop, as shown in Fig. 2. The power of input signal and the CW light to the AOWC are kept constant for every round-trip. The polarization controllers in the setup are used to keep the interference between the converted signal and the reflected signal be minimum, so, the impact of crosstalk from the reflection can be neglected. Only 20 km of dispersion shifted fiber is used in the loop, so the dispersion can be neglected. The signal is coupled out via a 10-dB coupler and launched into a 10-Gb/s receiver.

III. Results and Discussions

Fig. 3 shows the relative responses of the AOWC versus the modulation frequency at 1556.nm with and without the OADM. Owing to the carrier density variation in the SOA, the converted signal from the SOA has blue chirp on the rising edge and red chirp on the falling edges [1]. After the OADM, the falling edge of the converted signal with red chirp is suppressed by the steep edge of the transfer function of the OADM, and consequently the response of the AOWC at high frequency is improved [5]. It can be seen from Fig. 3 that the high-frequency response is improved significantly and the 3-dB bandwidth is larger than 20 GHz when the OADM is added. Fig. 4(a) and (b) shows the optical eye diagrams after the second conversion without and with the OADM, respectively. The dashed lines indicate the zero optical power level. It can be seen from Fig. 4(a) and (b) that the rising and falling edges are improved by using the OADM due to the improved response bandwidth. Fig. 4(c) and (d) shows the eye diagrams after the fifth round-trip in the loop without and with the OADM, respectively. From Fig. 4(c), we can see that the insufficient response of the high-frequency components (single "mark" and "space" bits) in the AOWC without the OADM is the most important factor limiting the cascadability. From Fig. 4(d), it can be seen that the degradation of low-frequency components (long row of "mark" and "space" bits) in the converted signal becomes the limiting factor since there is no chirp on the low-frequency components, the amplitude cannot be changed by the OADM. Fig. 5 shows the optical eye diagram of the converted signal after the tenth round-trip. It can be seen from Fig. 5 that the degradation of low-frequency components together with the accumulation of ASE noise and jitter caused by the AOWC limits the AOWC to be cascaded for more round-trips.

The cascadability can be improved from five to eight round-trips without an error floor at a bit-error rate (BER) of 10^{-9}

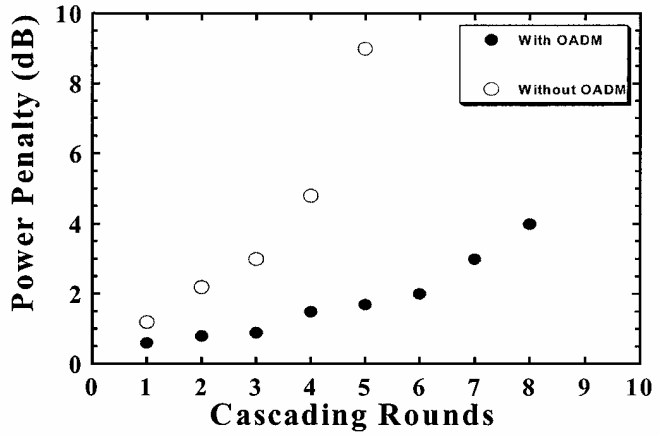

Fig. 6. Power penalty of the converted signal versus the cascading round-trips in the loop.

by adding the OADM after the SOA. Fig. 6 shows the power penalty of the converted signal with and without the OADM, respectively, as a function of different round-trips in the loop. It should be pointed out that there is a tradeoff among the parameters, like extinction ratio (ER), pattern effect, jitter and noise accumulation, all the parameters are optimized in our experiment. The power ratio between the signal and CW light used in the experiment corresponds to the theoretical predication in [4], which assures a small amount of jitter and a high extinction ratio (ER). However, the maximum number of cascaded AOWC's in the experiment is less than the theoretical predication in [4]. This is because the SOA used in the experiment is shorter than that in [4], the ER degradation is more severe. Furthermore, the ASE noise is not considered in [4]. It should also be stressed that using a loop configuration to test cascadability of the XGM-AOWC prevents any individual adjustments of the operation conditions for the cascaded AOWC's. So it is expected that the cascadability of the AOWC with the OADM can be improved further if a straight-line transmission or a longer SOA is used. Furthermore, it is expected that the cascadability of the XGM-AOWC converting to both longer wavelength and shorter wavelength can be improved by adding the OADM with a corresponding center wavelength.

IV. Conclusion

The cascadability of the XGM-AOWC converting the signal to the same wavelength is studied experimentally at 10 Gb/s using a loop setup. The poor high-frequency response of the AOWC limits it to be cascaded only five times in the loop experiment. By adding an OADM after the SOA, the maximum number of cascaded AOWC reaches eight due to the improved high-frequency response. However, the degradation of low-frequency components in the converted signal together with the accumulation of ASE and jitter become the most important limiting factors in the cascading experiment. It is expected that the cascadability of the AOWC with the OADM can be improved further if a straight-line transmission or a longer SOA is used.

References

[1] T. Durhuus, B. Mikkelsen, C. Joergensen, S. Danielsen, and K. Stubkjaer, "All-optical wavelength conversion by semiconductor optical amplifiers," *J. Lightwave Technol.*, vol. 14, pp. 942–953, June 1996.

[2] R. J. S. Pedersen, B. F. Jorgensen, B. Mikkelsen, M. Nissov, K. E. Stubkjaer, K. Wunstel, K. Daub, E. Lach, G. Lsube, W. Idler, M. Schilling, P. Doussiere, and F. Pommerau, "Cascadability of a nonblocking WDM crossconnect based on all-optical wavelength converters for routing and wavelength slot interchanging," *Electron. Lett.*, vol. 30, no. 19, pp. 1647–1648, Sept. 1997.

[3] K. Oberman, D. Breuer, and K. Petermann, "Theoretical estimation of the cascadability of wavelength converters based on cross-gain modulation in semiconductor optical amplifiers," in *Proc. CLEO'98, OSA Tech. Dig. Series*, vol. 6, 1998, pp. 388–389.

[4] A. Kloch and K. E. Stubkjaer, "Accumulation of jitter in cascaded wavelength converters based on semiconductor optical amplifiers," in *Proc. OFC'99, FB4-1*, 1999, pp. 33–35.

[5] H.-Y. Yu, D. Mahgerefteh, P.-S. Cho, and J. Goldhar, "Optimization of the frequency response of a semiconductor optical amplifier wavelength converter using a fiber Bragg grating," *J. Lightwave Technol.*, vol. 17, pp. 308–313, Feb. 1999.

[6] X. Zheng, F. Liu, A. Clausen, and A. Buxens, "High performance wavelength converter based on semiconductor optical amplifier and Mach–Zehnder interferometer optical add/drop multiplexer," in *Proc. 10th Optic. Amplifiers Their Appl., OSA Tech. Dig.*, 1999, pp. 132–134.

Optical Fiber Communication Conference, 2000, OFC'2000 TuF4-1

Cascadability improvement of a cross-gain modulation wavelength converter using a grating based optical add/drop multiplexer

Xueyan Zheng and Fenghai Liu
Research Center COM, Technical University of Denmark, DK-2800, Lyngby, Denmark
Telephone: +45-45253777, Fax: +45-45936581, Email: zx@com.dtu.dk

Introduction:

All-optical wavelength converters (AOWC) will be key components in future broadband wavelength division multiplexed (WDM) optical networks. Among several AOWCs already demonstrated, the AOWC based on cross-gain modulation (XGM) in semiconductor optical amplifier (SOA) is the simplest to realise and conversion to the same wavelength is possible using counter-propagating configuration which is also needed in the all-optical networks [1]. An important issue for the AOWC to be used in the WDM networks is cascadability [2], however, up to now, only a few theoretical results of the cascading XGM-AOWC have been reported [3] [4]. This is mainly due to the insufficient high frequency response of the AOWC caused by the finite gain recovery time of the SOA. Recently, it has been reported that the response frequency of the AOWC can be improved by filtering the chirped converted signal using a fiber grating after the SOA [5].

In this paper, for the first time, the cascadability of the XGM-AOWC converting optical signal to the same wavelength is studied experimentally in a re-circulating loop at 10 Gbit/s. By adding Mach-Zhender optical add/drop multiplexer (OADM) based on fiber gratings after the SOA, the maximum cascading rounds in the loop is improved from two to six. This is because the chirped signal from the SOA is reshaped by the steep edge of the transfer function of the OADM, consequently the frequency response of the AOWC is improved.

Experimental setup:

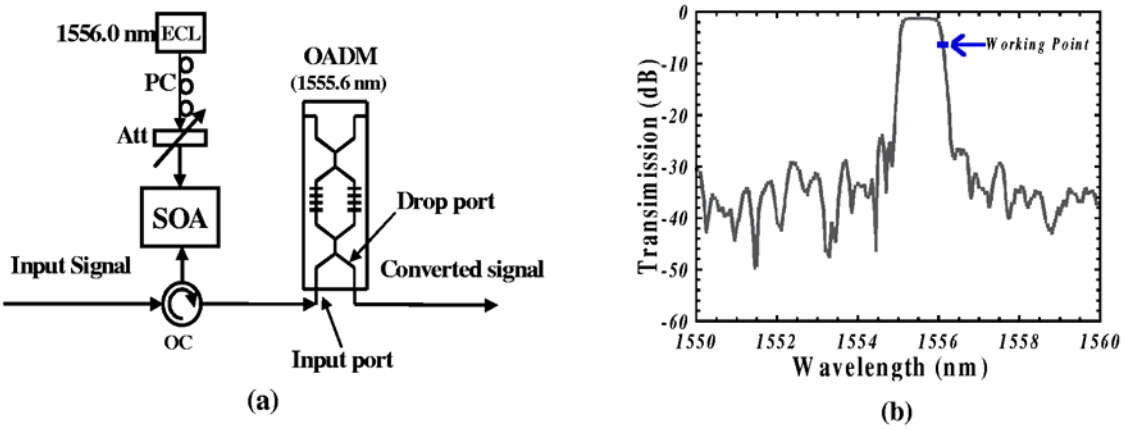

Fig.1 (a) Structure of the AOWC and (b) In-Drop transfer function of the OADM.

The structure of the counter-propagating AOWC is shown in Fig. 1 (a). The CW light with the wavelength of 1556.0 nm is provided by an external cavity laser (ECL) and its power into the SOA is -1 dBm after a polarization controller and an attenuator. The input signal is launched into the SOA through an optical circulator (OC). The OADM with certer wavelength of 1555.6 nm and the 3-dB bandwidth of 1 nm is used to reshape the converted signal when the wavelength of the converted signal is at the red side

Optical Fiber Communication Conference, 2000, OFC'2000 TuF4-2

of its In-Drop transfer function [6]. The converted signal from the SOA comes into the OADM from the Input port and comes out from the Drop port. The In-Drop transfer function of the OADM and the working point in the experiment is shown in Fig. 1 (b). The SOA used in the experiment has a chip length of 800 μm, and the fiber-to-fiber gain is 20 dB at a bias current of 180 mA, which is used in our experiment.

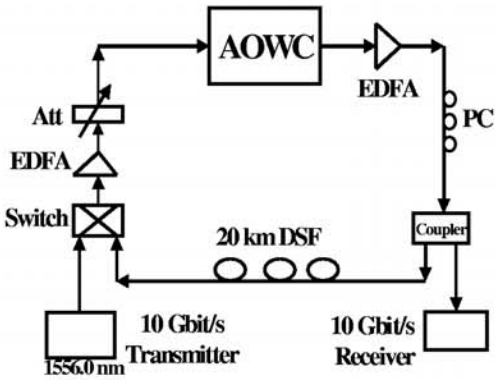

Fig.2 Experimental setup.

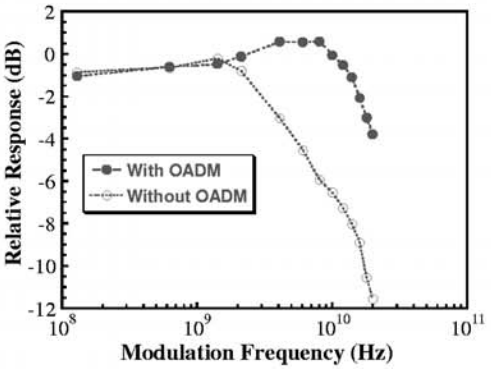

Fig.3 Small signal bandwidths for the same wavelength conversion in the AOWC without and with the OADM.

The loop set-up used in the experiment is shown in Fig.2. An externally modulated 10 Gbit/s (PRBS 2^{31}-1) transmitter emitting at the same wavelength as the CW light provides the input signal to the AOWC in the loop, as shown in Fig. 2. The input power into AOWC is +8 dBm, and kept constant for every round trip. Only 20 km DSF fiber is used in the loop, so the dispersion is neglected. The signal is coupled out via a 10 dB coupler and launched into a 10 Gb/s receiver.

Results and discussions:

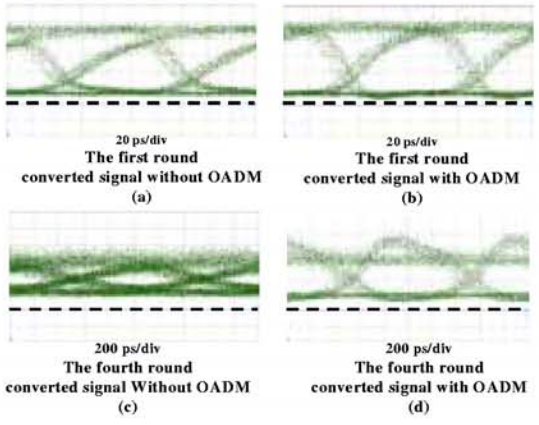

Fig.4 The eye diagrams of the converted signal without (a), (c) and with (b), (d) the OADM after the first and fourth round in the loop experiment respectively.

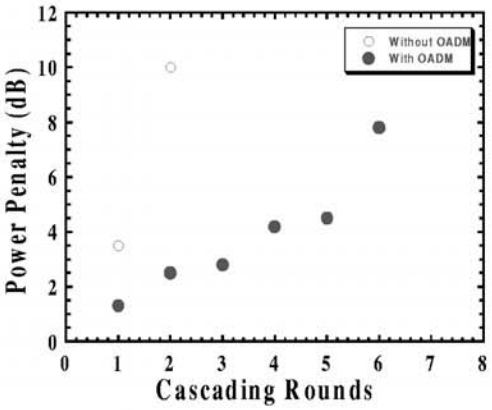

Fig. 5 Power penalty of the converted signal versus the cascading rounds in the loop.

Fig.3 shows relative response of the AOWC versus the modulation frequency at the wavelength of 1556.0 nm with and without the OADM. As we know, the converted signal after the SOA has blue chirp on the rising edge and red chirp on the falling edge which are caused by the carrier density changing in the SOA [1]. After the OADM, the falling edge of the converted signal with red chirp is suppressed by the steep edge of the transfer function of the OADM, and consequently the response of the AOWC at high

frequency is improved [5]. It can be seen from Fig. 3 that the high frequency response is increased significantly and 3-dB bandwidth is improved from 4 GHz to 18 GHz by adding the OADM. Fig.4 (a) and (b) show the optical eye diagrams of the converted signal without and with the OADM respectively after the first conversion. It can be seen from Fig. 4 (a) and (b) that the rising and falling edges are improved by using the OADM due to the improved response bandwidth. It can also be seen from Fig. 3, the OADM has no influence on the degraded low frequency response of the AOWC which is determined by the gain changing curve of the SOA [1]. Fig. 4 (c) and (d) show the eye diagrams of the converted signal without and with the OADM respectively after the fourth cascading round in the loop. From Fig. 4 (c), we can see that the insufficient response of the high frequency in the AOWC is the most important factor limiting the AOWC without the OADM to be cascaded. From Fig.4 (d), it can be seen that the low frequency response degradation in the converted signal becomes the most important limiting factor in the cascading experiment because the OADM can compensate the high frequency degradation but it has little influence on the low frequency components. So, the cascadability of the AOWC can be improved by adding the OADM but not infinite, it is determined by the low frequency response of the SOA.

The AOWC without the OADM can only to be cascaded two rounds in the loop experiment, but the cascadability can be improved to six rounds without error floor at BER of 10^{-9} by adding the OADM. Fig. 5 shows the power penalty of the converted signal with and without the OADM after different rounds in the loop transmission respectively.

If the SOA has sufficient responding time, theory shows that the maximum cascaded stages are seven [2] for the XGM-AOWC converting to the same wavelength due to the degraded ER and accumulated ASE noise which can not be improved by the OADM. So, our experimental result is close to this limit. However, in our experiment, the minimum power penalty of the converted signal without the OADM is 3.5 dB after the first conversion. It should also be stressed that using a loop configuration to test cascadability of the XGM-AOWC prevents any individual adjustments of the operation conditions for the cascaded AOWCs. Furthermore, it is expected that the cascadability of the XGM-AOWC converting to both longer wavelength and shorter wavelength can be improved by adding the OADM with corresponding center wavelength.

Conclusion:

The cascadability of the XGM-AOWC converting to the same wavelength is studied experimentally at 10Gb/s in a loop setup. The maximum cascaded round of the XGM-AOWC is improved from two to six in the loop experiment by adding the OADM due to the improved high frequency response. The low frequency response degradation in the converted signal becomes the most important limiting factor in the cascading experiment. The result is close to the theoretical limit, which is determined by the degradation of ER and accumulation of ASE noise.

Reference:

[1] T. Durhuus, B. Mikkelsen, C. Joergensen, S. Danielsen, and K. Stubkjaer, "All-Optical Wavelength Conversion by Semiconductor Optical Amplifiers", J. Lightwave Technol., 1996, vol 14 (6), pp 942-953.

[2] B. Ramamaurthy and B. Mukherjee, "Wavelength Conversion in WDM Networking", IEEE J. Select. Areas Commun., vol. 16, pp1061-1073, Sept, 1998

[3] K. Oberman, D. Breuer and K. Petermann, "Theoretical estimation of the cascadability of wavelength converters based on cross-gain modulation in semiconductor optical amplifiers", CLEO'98, Vol. 6, 1998 OSA Technical Digest Series, pp388-389.

[4] M. E. Bray and M. J. O'Mahony, "Cascading gain.satuation semiconductor laser-amplifier wavelength translators", Optoelectronics, IEE Proceedings- Volume: 143 1, Feb. 1996, pp 1 -6.

[5] H-Y. Yu, D. Mahgerfteh, P-S. Cho, and J. Goldhar, "Optimization of the Frequency Response of a Semiconductor Opticl Amplifier Wavelength Converter Using a Fiber Bragg Grating", J. Lightwave Technol., 1999, vol 17 (2), pp 308-313.

[6] X. Zheng., F. Liu, A. Clausen and A. Buxens, "High Performance Wavelength Converter Based on Semiconductor Optical Amplifier and Mach-Zehnder Interferometer Optical add/drop Multiplexer", in 10th Optical Amplifiers and Their Applications, OSA Technical Digest (Optical Socity Of America, Wasshington DC, 1999), p132-134.

Optical Fiber Communication Conference, 2001, OFC'2001

WK4

Wavelength conversion based on cross-phase modulation in a semiconductor Mach-Zehnder modulator

Fenghai Liu, Xueyan Zheng, Leif Oxenloewe, Rune J.S. Pedersen* and Palle Jeppesen

Research Center COM, Technical University of Denmark, Building 349, DK-2800 Lyngby, Denmark
Phone: +45-45253845, Fax: +45-45936581, Email: lf@com.dtu.dk
** Now with Tellabs Denmark A/S*

Jim Fraser, John D. Bainbridge and Mike Cox

High Performance Optical Component Solutions, Nortel Networks, Brixham Road, Paignton, Devon TQ47BE, United Kingdom
Phone: +44-1803-662649, Fax: +44-1803-662917, Email: jimfrasr@nortelnetworks.com

Abstract: Wavelength conversion based on cross-phase modulation in a reversely biased semiconductor Mach-Zehnder modulator is proposed and successfully demonstrated in a commercial device. The converted signals exhibit extinction ratio >13 dB and penalty <1.5 dB at 10Gb/s for both NRZ and RZ formats.

1. Introduction:

Wavelength converters are key components for future advanced optical networks, and several technologies have been used to realize wavelength conversion: opto-electronic conversion, optical wave mixing including four wave mixing and difference frequency generation, optically controlled gating including cross-gain and cross-phase modulation in semiconductor optical amplifiers [1,2]. Recently wavelength conversion based on cross-absorption modulation in saturated electroabsorption modulators (EAM) has been reported, showing high conversion speed up to 40Gb/s, large wavelength range and regenerative capability [3-5]. However, cross-absorption modulation in EAMs requires high input optical power, which restricts conversion to RZ format with short optical pulses (~10 ps) [3,4], and no wavelength conversion of NRZ format has been reported so far using cross-absorption modulation.

In this paper, we explore phase modulation in a reversely biased semiconductor Mach-Zehnder structure and demonstrate wavelength conversion in a commercial InGaAsP Mach-Zehnder modulator (MZM) originally designed as a 10Gb/s transmitter. The converted signals exhibit an extinction ratio better than 13 dB and a penalty less than 1.5 dB at 10Gb/s for both NRZ and RZ formats.

2. Principle and basic characteristics:

Fig. 1(a) shows the schematic diagram of the wavelength converter; the core part is a multiple quantum well (MQW) based InGaAsP Mach-Zehnder modulator. The MZ modulator, which is originally designed as a 10Gb/s transmitter, is fabricated by low-pressure metal organic chemical vapor deposition (MOCVD), and has an active length of the MZ arms of 600 μm [6].

An intensity modulated input signal with wavelength λ_i is coupled into the asymmetrically biased MZM through an optical circulator, and travels in two arms of the MZM. One of the MZM arms is reversely biased while the other arm is applied a 0 volt bias. The input optical signal in the reversely biased arm is partly absorbed and generates carriers, and the carriers further change the index of that arm. Since the carriers generated by the input signal is roughly proportional to the optical intensity, the intensity modulation of the input signal is transferred into a phase modulation in this arm. The input optical signal in the non-biased arm induces less index change since less light is absorbed. A CW probe light at λc, counter-propagating with the input signal, experiences a phase difference between the two arms, and hence becomes intensity modulated at the output of the MZM. The modulated light with wavelength λc, i.e., the converted signal, is guided out through the circulator.

An optical isolator is put between the DFB laser and the MZM to prevent the input light from going into the laser. The MZM, DFB laser and optical isolator shown in the dashed frame of Fig. 1(a) are integrated into a compact fibre-pigtailed package together with a wavelength locking scheme. Fig. 1(b) shows a photograph of the packaged device.

Fig. 2 shows the static characteristics of the wavelength converter under different bias conditions. The wavelengths of the CW probe-light and the input signal are 1557.36 nm and 1550.00 nm, respectively, in all

experiments. When the left bias is set to - 4.2V and right bias to 0V, the output power of the probe light increases as the input power increases, and the output power changes 10 dB when the input power increases from 5.8 dBm to 13.8 dBm. This indicates a non-inverted wavelength conversion capability with an improvement of the signal extinction ratio. When the right bias is set to - 4.47 V and the left bias to 0 V, the output power of the probe light decreases as the input power increases. This conversion possibility clearly shows the difference between cross-phase modulation and cross-absorption modulation where the output power always increases as the input power increases.

3. Wavelength conversion of 10Gb/s NRZ

The wavelength converter is used to convert a 10Gb/s NRZ signal, which has not been reported using cross-absorption modulation in an EAM. The 10 Gb/s optical NRZ signal is generated by a Lithium Niobate external modulator with a pattern length of 2^{31}-1. After being amplified to an average power of 13.8 dBm, the signal is fed into the wavelength converter. The converted eye-diagrams and waveforms detected by a fast photo detector are shown in Fig. 3.

From Fig. 3(a), we can see that the converted 10Gb/s NRZ signal has a wide open eye-diagram and the extinction ratio is better than 13 dB, which is optimised by the bias setting. From Fig. 3(b) and (c), we can see that the converted signal can have either inverted (b) or non-inverted (c) polarity in comparison with the input signal by changing the bias settings of the MZ, which again confirms the phase modulation effect in the MZ modulator. Bit-error-rates (BERs) of the converted signal and the input signal measured using an optically pre-amplified receiver are shown in Fig. 4. Power penalties less than 1.5 dB at BER=10^{-9} can be found from Fig.4.

4. Wavelength conversion of 10Gb/s RZ

The wavelength converter is also used to convert a 10Gb/s RZ signal. The 10Gb/s optical RZ signal is obtained by externally modulating the optical light source with an electrical RZ signal using the Lithium Niobate modulator [7]. The FWHM pulse-width of the 10Gb/s RZ optical signal is about 40 ps. The converted signal is detected using the same photo detector. Fig. 5 shows the eye-diagrams of input signal in (a) and converted signal in (b). Comparing the two eye-diagrams, no obvious pulse-broadening after wavelength conversion can be found, which indicates a fast conversion feature of the device. The extinction ratio of the converted signal is also better than 13 dB. Measured BER curves of input signal and converted signal are shown in Fig. 6 using the same receiver, and power penalties less than 1.5 dB at BER=10^{-9} can be found.

5. Conclusion

Wavelength conversion based on cross-phase modulation in a reversely biased semiconductor MZ modulator has been proposed and successfully demonstrated at 10Gb/s for both NRZ and RZ formats using a compact wavelength stabilised commercially available 10Gb/s transmitter. The experimental results show that wavelength conversion based on cross-phase modulation in reversely biased semiconductor MZ modulators can be realized at high speed for both NRZ and RZ.

Reference

[1] S.J. Yoo, "Wavelength conversion technologies for WDM network applications", *J. of Lightwave Technology*, vol. 14 (6), 1996. pp. 955-966.

[2] K. E. Stubkjaer, A. Kloch, P. B. Hansen, H. N. Poulsen, D. Wolfson, K. S. Jepsen, A. T. Clausen, E. Limal and A. Buxens: "Wavelength converter technology", *IEICE Transactions on Communications*, vol. E82-B (2), 1999. pp.390-400.

[3] N. Edagawa, M. Suzuki, S. Yamamoto, S. Akiba: "Novel wavelength converter using an electroabsorption modulator: conversion experiments at up to 40Gb/s", *OFC'97*, pp.77-78.

[4] L.K. Oxenloewe, A.T. Clausen and H.N. Poulsen: "Wavelength conversion in an electroabsorption modulator", *ECOC'2000*, Vol.3, pp.303-304.

[5] T. Miyazaki, N. Edagawa, M. Suzuki, and S. Yamamoto, "Novel optical regenerator using electroabsorption modulator", *OFC'99,* vol.2, pp350-352.

[6] C. Rolland: "InGaAsP-based Mach-Zehnder modulators for high-speed transmission systems",*OFC'98*, 1998, pp.283-284.

[7] F. Liu, C. Peucheret, X. Zheng, R.J.S. Pedersen and P. Jeppesen: "A novel chirped RZ transmitter and transmission experiments", *ECOC'2000.* pp. 113-114.

Optical Fiber Communication Conference, 2001, OFC'2001

WK4

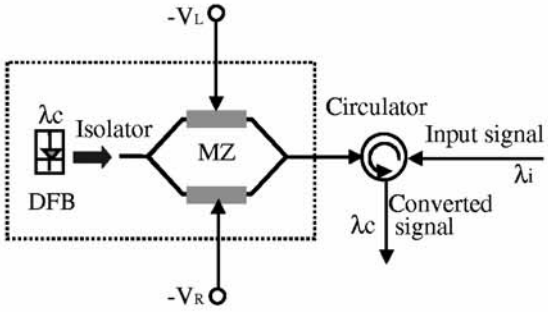

(a)

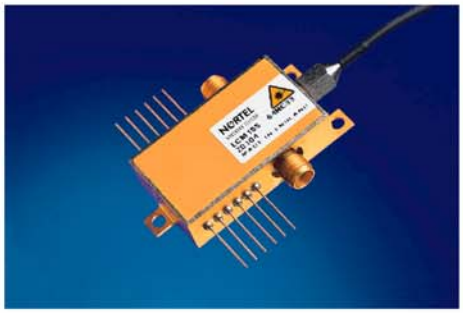

(b)

Fig. 1. Schematic diagram (a) and photograph (b) of the wavelength converter. MZ: InGaAsP Mach-Zehnder modulator.

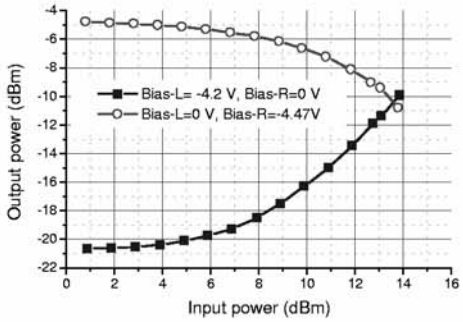

Fig. 2. Static characteristics of the wavelength converter.

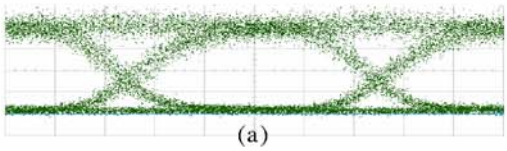

(a)

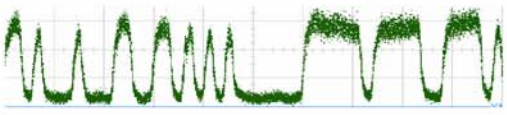

(b)

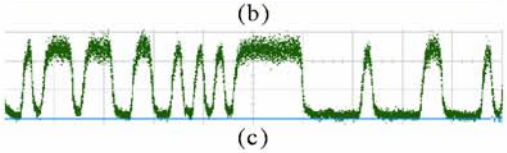

(c)

Fig. 3. Eye-diagrams (a) and waveforms (b, c) of the converted signals of 10Gb/s NRZ. (b) Inverted conversion. (c) Non-inverted conversion.

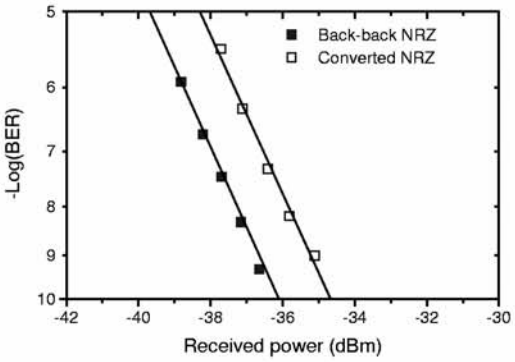

Fig. 4. BER curves of wavelength conversion of 10Gb/s NRZ signal.

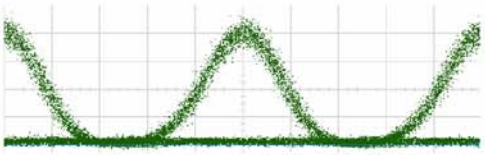

(a)

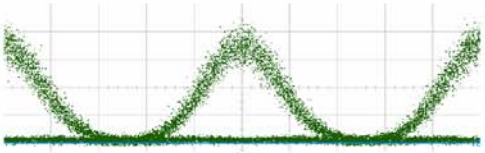

(b)

Fig. 5. Eye-diagrams of input signal (a) and converted signal (b).

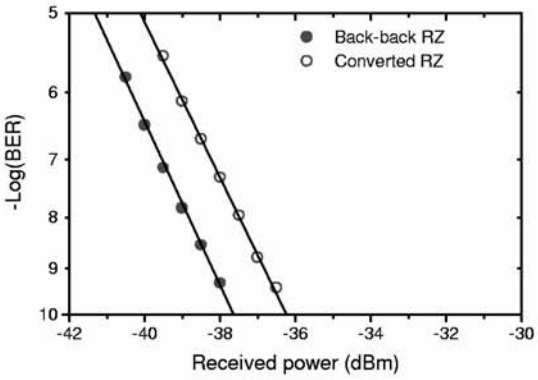

Fig. 6. BER curves of wavelength conversion of 10Gb/s RZ signal.

European Conference on Optical Communication, 1999, ECOC'99

Performance analysis of a novel multiwavelength cross-connect based on optical add/drop multiplexers

Fenghai Liu, Rune J.S. Pedersen and Palle Jeppesen
Research Center COM, Technical University of Denmark
Building 349, Lyngby DK-2800, Denmark, Email: LF@COM.DTU.DK

Abstract: A novel architecture of multiwavelength optical cross-connects based on optical add/drop multiplexers and optical switches is described. The performance of such a multiwavelength optical cross-connect is analyzed.

Introduction

Dense Wavelength Division Multiplexing (DWDM) technology is well-known for its dramatic increase in transmission capacity, and its flexibility in optical networking[1]. Multiwavelength Optical Cross-Connecting (OXC) is one of the key techniques for developing cost efficient and reconfigurable DWDM networks, and different structures of OXC have been proposed[2-4]. Essential requirements to an OXC are: strictly non-blocking nature, high modular growth capability, low crosstalk and low loss[5].

A novel OXC architecture based on optical add/drop multiplexers (OADM) and optical switches is presented in this letter. This structure is strictly non-blocking, which means that any input can always be connected in any viable way to any output without disturbing existing connections[5]. It is highly modular and can be integrated as a planar device, which makes upgrading to larger networks both in wavelength and port dimensions easy. It can be made to have low loss, low crosstalk and low difference between channel losses using available technology.

Multiwavelength optical cross-connect construction

2×2 wavelength switching block: The basic unit in the new OXC is a 2×2 wavelength switching block shown in Figure1. It consists of two OADMs with identical drop wavelength and an optical switch. When the switch is in "bar" state as shown in Figure1a, the DROP ports are connected to the ADD ports of the same OADM and all wavelength channels pass through the block without exchanging information. When the switch is in "cross" state as shown in Figure 1b, each of the two DROP ports is connected to the ADD port of the other OADM, which results in the drop channels being interchanged and all other channels being bypassed by the block.

Figure 1: Structure of 2×2 wavelength switching block. (a) in "bar" state. (b) in "cross" state

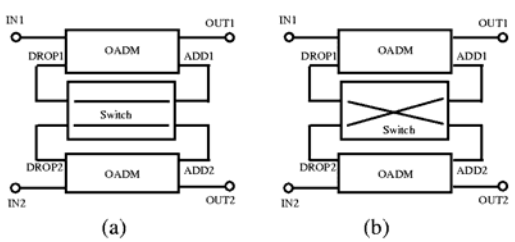

2×2 multiwavelength optical cross-connect block:

Constructing a 2×2 optical cross-connect block can be done simply by cascading a number of wavelength switching blocks each with a fixed wavelength as shown in Figure 2. Channels with the same wavelength from the two input ports can be interchanged via an independent wavelength switching block without disturbing the other existing connections, i.e., the cross-connect is strictly non-blocking for all wavelength channels.

When the network needs more channels, the corresponding wavelength switching blocks can be added to the already existing blocks. This is favorable in terms of initial investment.

Figure 2: Structure of 2×2 optical cross-connect block

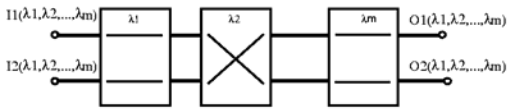

Similarly to building a large scale strictly non-blocking N×N switch using 2×2 switches described in [6], a strictly non-blocking N×N optical cross-connect can be constructed using 2×2 OXC blocks.

Figure 3: M-Z interferometric OADM structure and transfer functions

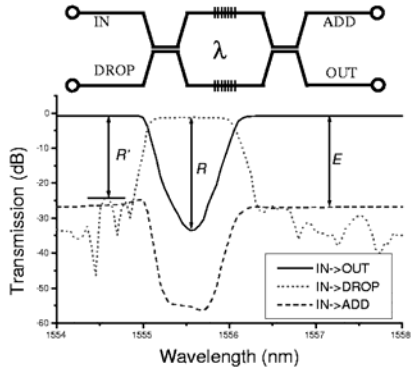

Realization and performance analysis

Many types of OADM [7-10] can be used in the proposed OXC structure and some of them are commercially available. Optical switches that provide high on-off ratio, such as mechanical and thermo-optic types, can be used here. A combination of planar grating based Mach Zehnder interferometer(MZI) OADMs and a thermo-optic switch is promising for the

proposed structure, since it can be integrated on a single chip, and thus enable low-cost mass production. Hence, the grating based MZI-OADM shown in Figure 3 with its typical transfer functions [7,8] is used as an example in the following discussion. From Figure 3, we define the drop band rejection R as the ratio between IN-OUT and IN-DROP at the drop wavelength, the pass band reflectivity R' as the ratio between IN-DROP and IN-OUT in the passing region, the extinction ratio E of the MZI as the ratio between the IN-ADD and IN- OUT.

The excess loss in an optical switch and an OADM can be very low. Due to the symmetric structure of the OXC, all channels will experience the same loss in all configurations, so no power equalizers are needed. However, optical amplifiers may be needed to compensate the total loss in case of a large optical cross-connect.

The interferometric crosstalk, i.e., crosstalk with the same wavelength as the signal, is always a critical issue in optical cross-connects[11], and will now be discussed for the proposed OXC structure.

In a 2×2 OXC, each wavelength channel will be dropped and added in one wavelength switching block ("drop-add" block) and be bypassed in all other wavelength switching blocks ("bypass" blocks). Interferometric crosstalk from each block will add up at the output ports and distort the signal. Without loss of generality, let us assume that all 2×2 wavelength switching blocks are in the "bar" state.

Figure 4: Crosstalk illustration in (a) "drop-add" block and (b) "bypass" block

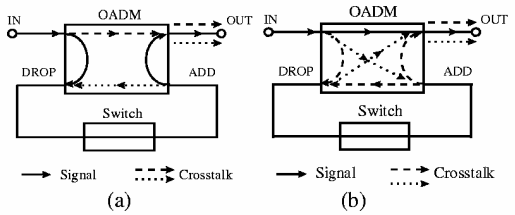

In the "drop-add" block shown in Figure 4a, the crosstalk is mainly due to the imperfect drop band rejection R. The signal is reflected from IN-DROP, passes through the optical switch, and then is reflected from ADD-OUT. One part of the crosstalk is the leaking signal from IN-OUT, and another part is the leaking signal from ADD-DROP, which travels through the optical switch, and then is reflected from ADD-OUT, higher order crosstalk terms are neglected.

In the "bypass" block shown in Figure 4b, the signal passes from IN-OUT. The crosstalk is mainly due to the imperfect extinction ratio E of the M-Z interferometer and the finite reflection outside the drop band of the OADMs. The crosstalk from IN-ADD passes through the switch, and is then coupled from DROP-OUT. The crosstalk from IN-DROP also passes through the switch, and is then coupled from ADD-OUT. Since the loss of optical switch and loss from ADD-DROP is low, crosstalk will circulate several times with decreasing power in the ADD-Switch-DROP-ADD loop, and will thus generate more crosstalk terms.

Considering all these crosstalk terms, Figure 5 shows the requirement of R, R' and E in OADMs for a 2×2 OXC with different wavelength channels under the assumptions of : 1) Gaussian probability distribution of signal-crosstalk beat noise and 1dB power penalty introduced by crosstalk, 2) perfect switch on-off ratio, 3) 1dB excess loss for all OADMs and optical switches. From Figure 5, we can see that in to order to build a 2×2 OXC with 32 channels, the drop band rejection R, pass band reflectivity R' and extinction ratio E of the M-Z interferometer in the OADMs need to be -33.3dB, -23.5dB and -24.5dB, respectively. These values can be reached by OADMs either based on fiber Bragg grating or planer waveguide grating [8,9]. For large N×N OXCs, better values are needed to keep the same overall performance, since each wavelength channel passes more than one stage of such a 2×2 OXC.

Figure 5: Required drop band rejection R, pass band reflectivity R' and Extinction ratio E in a 2×2 OXC with different wavelength channels.

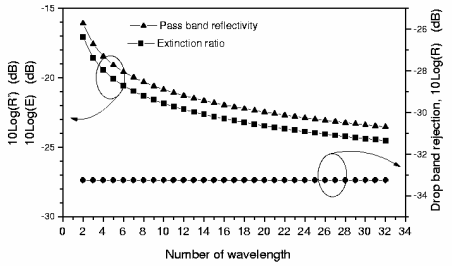

Conclusion

The authors have presented a new architecture of a multiwavelength optical cross-connect which is strictly non-blocking, has high degree of modularity and is easy to integrate. Performance of a realization of such an OXC based on MZI-OADMs has been analyzed, showing that 2×2 OXC with 32 wavelength channels can be built using the available components.

References

/1/ C.A.Brackett, *IEEE J. Sel. Areas Commun.*, 1990, 8, pp. 948-964.

/2/ A.Jourdan, et al., *J. of Lightwave Technol.*, 1996, 14, (6), pp.1198-1206.

/3/ E.Iannone, et al., *J. of Lightwave Technol.*, 1996, 14, (6), pp.2184-2196.

/4/ Y.K.Chen, and C.C.Lee, *J. of Lightwave Technol.*, 1998, 16, (10), pp.1746-1756.

/5/ K.I.Sato,: 'Advances in transport networks technologies: Photonic networks, ATM, and SDH', *Artech House*, 1996, pp. 175-199.

/6/ J.Y.Hui,: 'Switching and traffic theory for integrated broadband networks', *Kluwer Academic Publishers*, 1994.

/7/ F.Bilodeau, et al., *IEEE Photon. Technol. Lett.*, 1995, 7, (4), pp.388-390.

/8/ J.-M.Jouanno, et al., *Electron. Lett.*, 1997, 33, pp. 2120-2121.

/9/ T..Mizuochi, et al., *J. of Lightwave Technol.*, 1998, 16, P265-276.

/10/ A.Jourdan, *et al.*, *IEEE J. on Selected Areas in Communication,* 1998,16, (7) pp.1286-1297.

/11/ J.Zhou, et al., *J. of Lightwave Technol.*, 1996, 14, (6), pp.1423-1435.

1246 IEEE PHOTONICS TECHNOLOGY LETTERS, VOL. 12, NO. 9, SEPTEMBER 2000

Novel 2 × 2 Multiwavelength Optical Cross Connects Based on Optical Add/Drop Multiplexers

Fenghai Liu, *Student Member, IEEE*, Rune J. S. Pedersen, and Palle Jeppesen

***Abstract*—A novel architecture of 2 × 2 multiwavelength optical cross connects based on optical add/drop multiplexers and optical switches is described. The structure is strictly nonblocking with a high degree of modularity. Its basic performance is experimentally demonstrated.**

***Index Terms*—Optical cross-connect, optical add/drop multiplexer, strictly nonblocking, modularity.**

I. Introduction

DENSE wavelength-division-multiplexing (DWDM) technology is well-known for its dramatic increase in transmission capacity, and its flexibility in optical networking [1]. A multiwavelength optical cross connect (OXC) is one of the key devices for developing cost efficient and reconfigurable DWDM networks, and different structures of OXCs have been proposed [2], [3]. Essential requirements to an OXC are strictly nonblocking nature and high modular-growth capability [4].

A novel 2 × 2 multiwavelength OXC architecture based on optical add/drop multiplexers (OADMs) and optical switches is presented in this letter. This structure is strictly nonblocking, which means that any channel interchange will not disturb other existing connections. It is highly modular, and each building block can be integrated as a planar device, which makes OXC nodes flexible and allows an easy upgrade to a larger number of wavelengths. It can be made to have low-loss, low-difference, between channel losses and low-crosstalk, using available technologies. An experimental demonstration is performed to verify the concept of the proposed 2 × 2 multiwavelength OXC.

II. Multiwavelength OXC Construction

A. 2 × 2 *Wavelength Switching Block*

The basic unit in the new OXC is a 2 × 2 wavelength-switching block, shown in Fig. 1. It consists of two OADMs, with identical drop wavelength and an optical switch. When the switch is in "bar" state, as shown in Fig. 1(a), the drop ports are connected to the add ports of the same OADM, and all wavelength channels bypass the block without exchanging information. When the switch is in "cross" state, as shown in Fig. 1(b), each of the drop ports is connected to the add port of the other OADM. This results in the two drop channels being interchanged, while all other channels remain unchanged. Hence, a 2 × 2 wavelength switching block is capable of switching one wavelength channel between 2 fibers, and is transparent for all other wavelength channels.

The loss for bypass channels is equal to the out-of-band loss of the OADM, and an OADM with out-of-band loss of 1.8 dB was reported in [5]. The loss for the switched channel is the sum of losses from in to drop and add to out in the OADM and the loss of an optical switch, which all amounts to 4.2 dB, using the same OADM and a mechanical optical switch with a typical loss of 0.6 dB. The crosstalk of the 2 × 2 wavelength switching block depends on the on–off ratio of the optical switch and the transfer functions of the OADMs. Mechanical optical switches with on-off ratio larger than 60 dB are commercially available, and the OADM mentioned above exhibits drop band rejection ratio of 45 dB and out-of-band reflection of −45 dB. This leads to a crosstalk less than −60 dB from the 2 × 2 wavelength switching block, according to the analysis in [6].

B. 2 × 2 *Multiwavelength Optical Cross Connect*

Constructing a 2 × 2 multiwavelength optical cross connect can be done simply by cascading a number of wavelength switching blocks each with a fixed wavelength, as shown in Fig. 2. Channels with the same wavelength from the two input ports can be interchanged via an independent wavelength switching block without disturbing the other existing connections, i.e., the cross connect is strictly nonblocking for all wavelength channels.

In a given OXC node, it is only necessary to use the 2 × 2 wavelength switching blocks corresponding to the wavelengths that are to be cross-connected rather than a full cross connection between two fibers. When more wavelengths need to be cross-connected, the corresponding wavelength switching blocks can be added to the already existing OXC. This is favorable in terms of initial investment.

The loss which a channel experiences through a 2 × 2 multiwavelength OXC is the sum of the losses in each 2 × 2 wavelength switching block. Different channels will experience the same loss in a fully cross-connected 2 × 2 multiwavelength OXC if the OADMs have uniform loss for bypassing channels. Since the 2 × 2 OXC is built by modules, loss can be compensated by optical amplifiers, when necessary.

We have described that a 2 × 2 wavelength switching block is capable of switching one wavelength between two fibers, and is transparent for all other wavelength channels. In a 2 × 2 OXC, channels with different wavelengths are treated independently, like using 2 × 2 optical space switches in parallel. This not only results in the strictly nonblocking feature of a 2 × 2 OXC, but also in possible constructions of strictly nonblocking $N \times N$ OXCs (N input ports and N output ports) using proper growth

Manuscript received June 15, 1999; revised October 26, 1999.

The authors are with the Research Center COM, Technical University of Denmark, Lyngby DK-2800, Denmark (e-mail: LF@COM.DTU.DK).

Publisher Item Identifier S 1041-1135(00)07874-5.

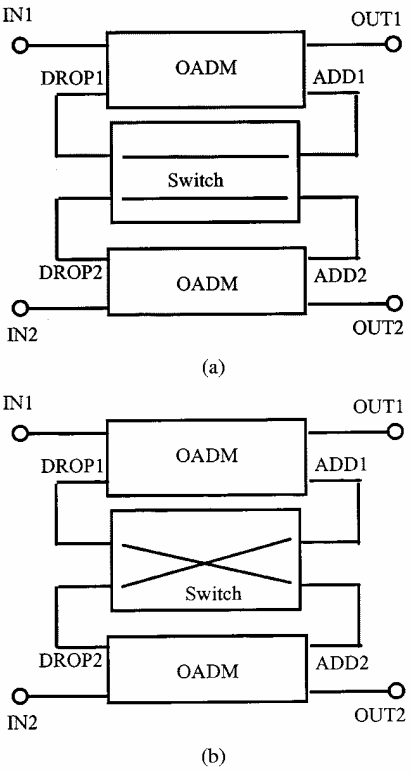

Fig. 1. Structure of 2 × 2 wavelength switching block. (a) in "bar" state. (b) in "cross" state.

paths. For example, if the 2 × 2 switch elements in [7] are replaced by the proposed 2×2 OXC, a strictly nonblocking $N \times N$ OXC can be built following the same growth path.

III. Experimental Demonstration

An experiment is made to demonstrate the concept and basic performance of the proposed 2 × 2 multiwavelength OXC, using fibergrating-based Mach–Zehnder interferometer (MZI) OADMs and a mechanical optical switch. Fig. 3 shows the experimental setup. Eight DFB lasers, with channel spacing of 1.6 nm, are combined through an arrayed-waveguide grating multiplexer, and modulated by a lithium niobate external modulator at 10 Gb/s. EDFAs are used to overcome the loss from all passive components. The extinction ratio of the modulated signals is 10 dB. The power of the eight channels is then divided into 2 parts, and decorrelated by a 5 km fiber delay line, in order to simulate the 2 inputs into a 2 × 2 multiwavelength OXC. The 2 × 2 multiwavelength OXC contains two wavelength switching blocks. One is working at 1555.7 nm, with a connection of two fiber grating based MZI-OADMs and a mechanical optical switch in "cross" state, and the other is working at 1559.0 nm and contains one MZI-OADM, with a connection from drop port to add port to simulate a block in "bar" state. From one output of the 2 × 2 multiwavelength OXC, all eight channels are demultiplexed and, in turn, put into a PIN receiver. Bit-error-rate (BER) curves are measured using a BER test-set, with optimal threshold setting. Polarization controllers are used to maximize the influence of the crosstalk in the BER measurement.

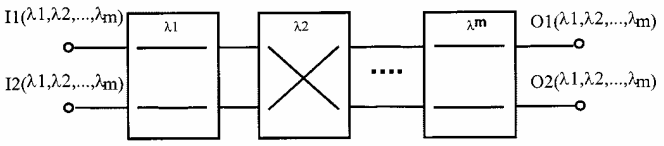

Fig. 2. Structure of 2 × 2 multiwavelength optical cross-connect block.

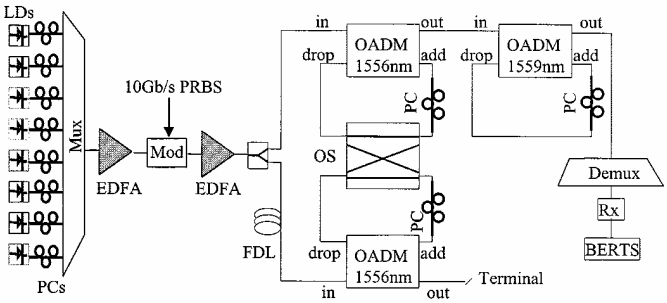

Fig. 3. Experimental setup of a 2 × 2 multiwavelength OXC. PC: polarization controller. Mux: Multiplexer. Mod: Lithium Niobate external modulator. FDL: Fiber delay line. OS: Mechanical optical switch. Demux: Demultiplexer. Rx: PIN receiver. BERTS: Bit-error-rate test set.

Penalty of each channel is defined as the difference between receiver sensitivities with and without the 2 × 2 OXC, and is shown in Fig. 4 as open squares together with the calculated value shown in solid line in the same figure. Maximum measured penalty is 0.7 dB. The calculated penalties agree well with the measured values for all channels. The crosstalk-induced penalty is calculated based on the measured transfer functions of the OADMs, on-off ratio of the optical switch and losses in the optical paths, using a Gaussian crosstalk model, described in [8]. Detailed analysis of crosstalk in the proposed OXC can be found in [6]. The transfer function of the 1559-nm OADM is shown in Fig. 5. The calculation also shows that the 1555.7 nm switching block gives little influence on the penalties of all channels because of the transfer functions of the OADMs and the high on–off ratio of the space switch. Penalties of all channels, except the one at 1559.0 nm, are mainly due to the poor extinction ratio E in the 1559-nm OADM; the low penalty in 1559.0 nm channel benefits from the high drop band rejection ratio R in the same OADM.

IV. Integration

Since the MZI-OADMs and optical switches can be fabricated as planar lightwave circuits (PLCs) [9], [10], the 2 × 2 wavelength-switching block can be integrated on a PLC. Fig. 6 shows a schematic diagram of the 2 × 2 wavelength switching block. The basic structure is 8 Mach–Zehnder interferometers (MZIs). Gratings, with the central wavelength of the switching channel, are written in the arms of a cascaded MZI to form two-stage MZI-OADMs, in order to obtain a high rejection ratio of the drop channels [11]. Thermal films are put on top of the MZI to realize the thermo-optic (TO) switches, and switching is performed by changing the electrical current through the thermal films. A double-gate TO switch is employed in the block to provide a high on–off ratio [10]. Integration of the 2 × 2 wavelength-switching blocks will make the proposed 2 × 2 multiwavelength OXC, promising for mass production at low cost.

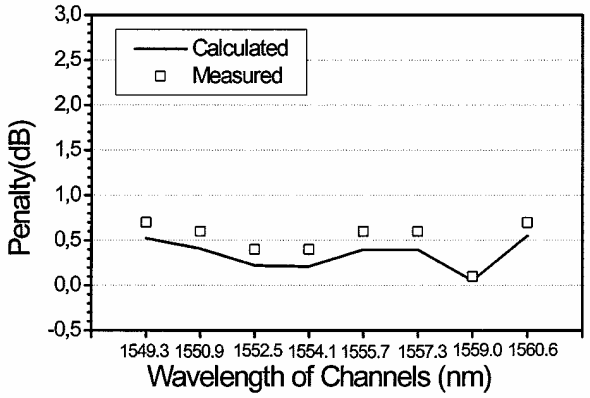

Fig. 4. Penalty of each channel after the 2 × 2 OXC.

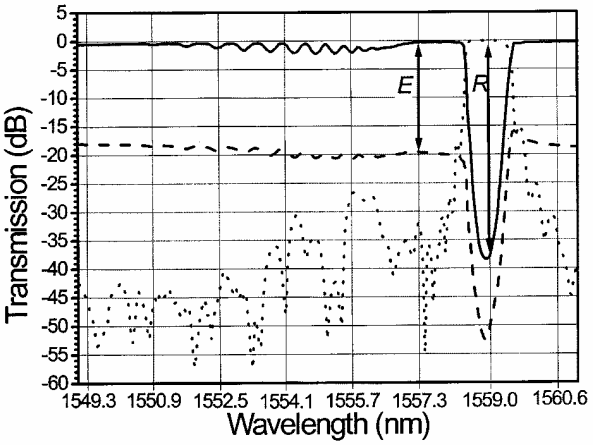

Fig. 5. Transfer functions of the OADM with drop wavelength at 1559.0 nm. ——— IN to OUT; . . . IN to DROP; ——— IN to ADD.

V. Conclusion

A new architecture of a 2 × 2 multiwavelength OXC has been presented. The proposed OXC is strictly nonblocking, has high degree of modularity, and can be constructed with low-loss differences between channels and low crosstalk. The transmission performance of the 2 × 2 multiwavelength OXC is experimentally demonstrated. A possible integration scheme of the 2 × 2 wavelength switching block is proposed, that enables low-cost mass production.

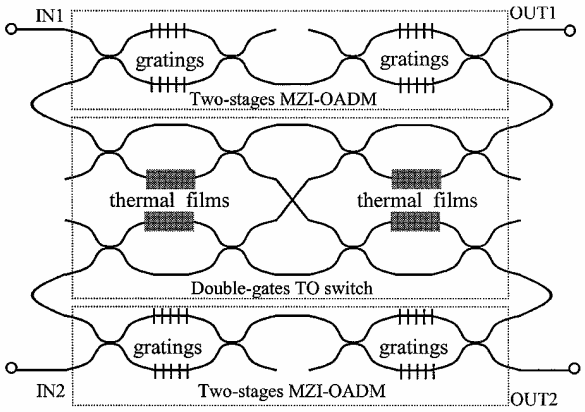

Fig. 6. Integration scheme of the 2 × 2 wavelength switching block using MZI-OADM's and TO switch.

References

[1] C. A. Brackett, "Dense wavelength division multiplexing networks: Principles and applications," *IEEE J. Select Areas Commun.*, vol. 8, pp. 948–964, 1990.

[2] E. Iannone and R. Sabella, "Optical path technologies: A comparison among different cross-connect architectures," *J. Lightwave Technol.*, vol. 14, no. June, pp. 2184–2196, 1996.

[3] Y. K. Chen and C. C. Lee, "Fiber Bragg grating-based large nonblocking multiwavelength cross-connects," *J. Lightwave Technol.*, vol. 16, no. October, pp. 1746–1756, 1998.

[4] K. I. Sato, *Advances in Transport Networks Technologies: Photonic Networks, ATM, and SDH.* Boston, MA: Artech House, 1996, pp. 175–199.

[5] L. Eldada, R. Blomquist, M. Maxfield, D. Pant, G. Boudoughian, C. Poga, and R. A. Norwood, "Thermally tunable polymer Bragg grating OADM's," in *Proc. OFC'99*, pp. 99–100.

[6] F. Liu, R. J. S. Pedersen, and P. Jeppesen, "Performance analysis of a novel multiwavelength cross-connect based on optical add/drop multiplexers," in *Proc. ECOC'99*, Nice, France, Sept. 1999, pp. 422–423.

[7] C. S. Wu, G.-K. Ma, and B. P. Lin, "Extend baseline architechture for nonblocking photonic switching," *J. Lightwave Technol.*, vol. 15, no. May, pp. 771–778, 1997.

[8] F. Liu, C. J. Rasmussen, and R. J. S. Pedersen, "Experimental verification of a new model describing the influence of incomplete signal extinction ratio on the sensitivity degradation due to multiple interferometric crosstalk," *IEEE Photon. Technol. Lett.*, vol. 11, no. Jan., pp. 137–139, 1999.

[9] J. M. Jouanno, D. Zauner, and M. Kristensen, "Low crosstalk planar optical add-drop multiplexer fabricated with UV-induced Bragg gratings," *Electron. Lett.*, vol. 33, pp. 2120–2121, 1997.

[10] K. Okamoto, M. Okuno, and Y. Ohmori, "16-chanel optical add/drop multiplexer consisting of arrayed-waveguide gratings and double-gate switches," *Electron. Lett.*, vol. 32, no. 16, pp. 1471–1472, 1996.

[11] T. Mizuochi, T. Kitayama, K. Shimizu, and K. Ito, "Interferometric crosstalk free optical add/drop multiplexer using Mach–Zehnder-based fiber gratings," *J. Lightwave Technol.*, vol. 16, pp. 265–276, 1998.

Optical Fiber Communication Conference, 2001, OFC'2001

TuW1

Fully reconfigurable 2×2 optical cross-connect using tunable wavelength switching modules

Fenghai Liu, Xueyan Zheng, Rune J.S. Pedersen* and Palle Jeppesen

Research Center COM, Technical University of Denmark, Building 349, Lyngby, DK-2800, Denmark
Phone: +45-45253845, Fax: +45-45936581, Email: LF@COM.DTU.DK
** Now with Tellabs Denmark A/S*

Abstract: A modular tunable wavelength switching module is proposed and used to construct 2×2 fully reconfigurable optical cross-connects. Large size optical switch is avoided in the OXC and it is easy to upgrade to more wavelength channels.

Introduction:

Wavelength division multiplexing (WDM) not only increases fiber transmission capacity but also simplifies network operation by introducing the optical path layer concept [1]. Multi-wavelength optical cross-connects (OXC) are key elements in reconfigurable WDM networks.

A conventional way of building an optical cross-connect is shown in Fig. 1. M wavelength channels packed in each of two input fibers are separated by demultiplexers, and put into a 2M×2M optical space switch. All channels are cross-connected by the switch and combined in two multiplexers after conversion to the proper wavelengths. As more and more wavelengths are packed into fibers (some transmission systems with more than 150 channels have been reported [2,3]), the conventional construction scheme is hard to implement due to the large dimension (e.g., 300×300) space switch that is required in the structure. The OXC constructed in the conventional way also has a low degree of modularity and it is hard to upgrade smoothly to more wavelengths once it has been installed.

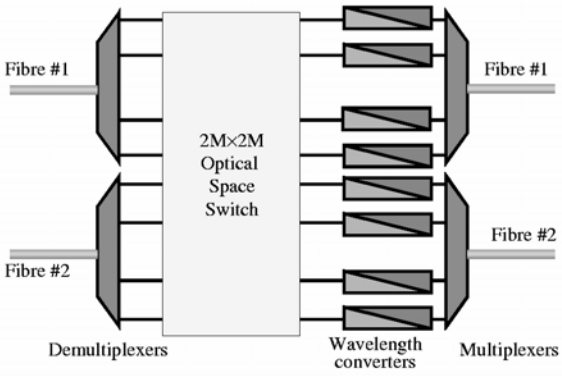

Fig.1. Schematic diagram of a conventional 2×2 fully reconfigurable OXC.

In this paper, a tunable wavelength switching block is proposed based on tunable optical add/drop multiplexers, a 2×2 space switch and tunable wavelength converters. Each block can cross-connect two channels between two fibers, and a fully reconfigurable 2×2 OXC can be built by cascading M such modules. Only 2×2 space switches are used, so that the structure of the OXC is simplified by avoiding use of a large dimension optical space switch. In nodes where the full reconfiguration is not needed, a smaller number of the modules can be chosen. Upgrade to more wavelengths can be easily done by adding more modules.

Structure of the proposed 2×2 OXC

The basic unit in the proposed 2×2 OXC is a tunable wavelength switching module, as shown in Fig. 2(a). This unit consists of two tunable optical add/drop multiplexers (OADMs), two tunable wavelength converters and a 2×2 optical space switch. Any two channels to be cross-connected between two fibers can be dropped by the two tunable OADMs tuned to the wavelengths of the corresponding channels. The two dropped channels are switched in the 2×2 space switch operated in "cross" state, and then they each proceed to its tunable wavelength converter. Each wavelength converter tunes its output to the same wavelength as the add/drop wavelength of the OADM connected, and converts any input to this wavelength. The converted channels are added to the respective output fibers through the add ports of the OADMs. When the space switch is set to "bar" state, no channels will be cross-connected.

When each fiber hosts M wavelength channels, a fully reconfigurable 2×2 OXC without wavelength swapping in the same fiber can be constructed by using a cascade of M such tunable wavelength switching modules. A schematic diagram of the 2×2 OXC is shown in Fig. 2(b). Tunable OADMs can be

realized in different ways, e.g., acous-optic filters [4] or tunable polymer Bragg gratings [5]; Many types of wavelength converters reported can be made tunable by using tunable optical probe sources [6, 7]; 2×2 space switches are commercially available, e.g., mechanical optic switches or thermo-optic switches. In case full reconfiguration is not necessary in one OXC node, less than M modules are needed, and the node can always be upgraded smoothly when the need for cross-connection increases. The 2×2 OXC is re-arrangeably non-blocking.

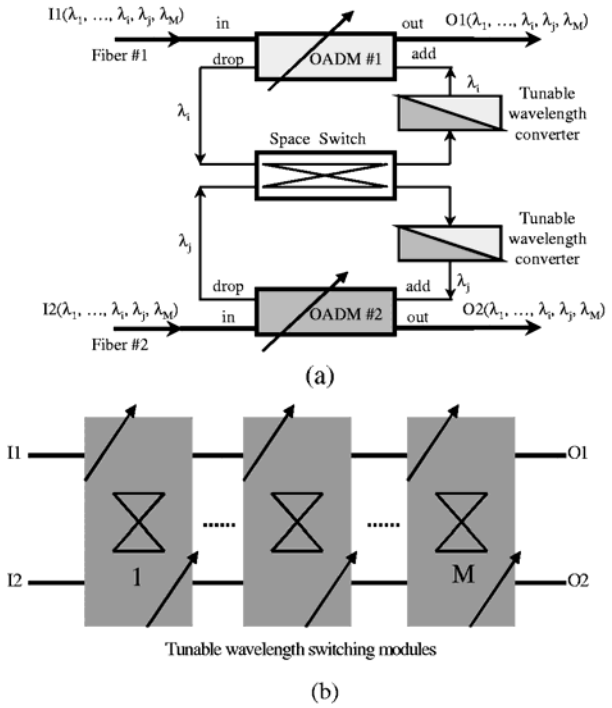

Fig.2. Schematic diagrams of the proposed tunable wavelength switching module (a) and a 2×2 fully reconfigurable OXC based on the modules (b)

Experiment:

In order to demonstrate the basic concept of the proposed 2×2 OXC, a wavelength switching module is constructed, as shown in Fig. 3. Two fiber Bragg grating based Mach-Zehnder interferometric OADMs with fixed instead of tunable add/drop wavelengths are used, since no tunable OADM is available for the experiment yet.

Tunable wavelength converters based on cross-gain modulation in semiconductor optical amplifiers (SOAs) are built. Each input optical signal from the space switch is coupled into an SOA via an optical circulator, and it subsequently modulates the gain of the SOA. CW light from a tunable external cavity laser tuned to the same wavelength as the add/drop channel of the OADM connected, is fed into the SOA. When the CW light counter-propagates with the input signal in the SOA, it is subjected to the modulated gain, and hence becomes intensity modulated. The modulated signal is guided out through the circulator and put into the add port of the connected OADM. Each wavelength converter is capable of converting any input to the particular wavelength that is needed in the wavelength switching module. In our experiment the optical space switch is simply replaced by manual connections since the crosstalk from a mechanical optical switch is very low (<-70dB) and switching speed is not the issue studied here.

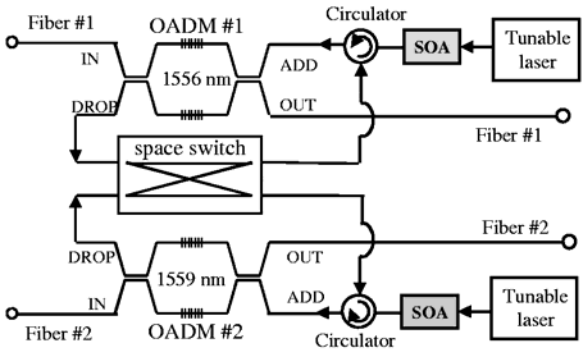

Fig.3. Experimental construction of the wavelength switching module.

8×10Gb/s WDM channels separated by 200GHz are hosted in each fiber. Fiber #1 is connected to OADM #1 with center wavelength 1556 nm, and the output of the wavelength converter connected to OADM #1 is tuned to 1556 nm. Fiber #2 is connected to OADM #2 with center wavelength 1559 nm and the output of the wavelength converter associated with OADM #2 is tuned to 1559 nm accordingly. The experiment focuses on the wavelength conversion part. With reference to Fig. 4, BER curves have been measured for channels at 1556 nm and 1559 nm after demultiplexing and detection by a PIN receiver. The following four situations are considered.

1. Channel at 1556 nm dropped from Fiber #1 is converted to 1559 nm and added to Fiber #2, referred to as 1556->1559.
2. Channel at 1559 nm dropped from Fiber #2 is converted to 1556 nm and added to Fiber #1, referred to as 1559->1556.
3. Channel at 1556 nm dropped from Fiber #1 is converted to the same wavelength and added back to Fiber #1, referred to as 1556->1556.
4. Channel at 1559 nm dropped from Fiber #2 is converted to the same wavelength and added back to Fiber #2, referred to as 1559->1559.

Among these four situations, the 1st and 2nd involves the optical switch in "cross" state, and the 3rd and 4th

Optical Fiber Communication Conference, 2001, OFC'2001

in "bar" state. For comparison, a base-line BER curve is also measured for the receiver, which is referred to as Back-Back. From Fig.4 we can see the power penalty for the four cases varies from 1dB to 2.3dB, which mainly stems from the wavelength converters used in the block. Wavelength conversion from long to short wavelength (1559->1556) exhibits the smallest penalty while conversion from short to long wavelength (1556->1559) shows the highest penalty. That is because the gain peak of the SOA shifts to longer wavelength for higher input power, which leads to a poor signal extinction ratio for conversion from short to long wavelength [7]. The wavelength conversion scheme used in the present experiment is very simple and we should emphasize that wavelength conversion does not always introduce power penalty. On the contrary a wavelength converter can also provide power equalization between the cross-connected channels and the bypassing channels and some wavelength conversion schemes can even provide a regenerative function [8, 9].

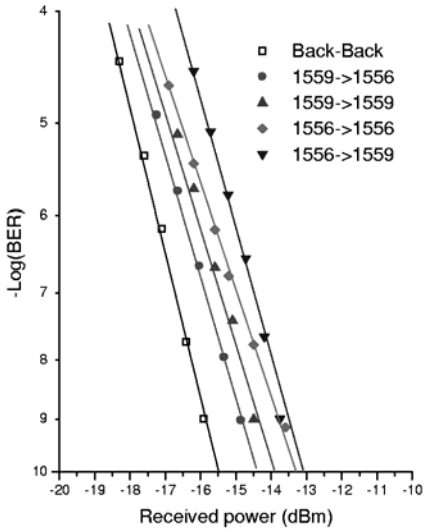

Fig.4 Bit-Error-Rate curves of back to back and after the wavelength switching module.

Conclusion:

We have proposed a new 2×2 fully reconfigurable OXC based on tunable wavelength switching modules. A large dimension of the optical space switch is avoided in the structure, and it has a high degree of modularity that enables smooth upgrade to more wavelength channels. Our experiments have demonstrated the feasibility of the wavelength switching module. Tuning speed and cascadability of the modules need to be further studied.

References:

[1] K.-I. Sato, S. Okamoto, H. Hadama: "Network performance and integrity enhancement with optical path layer technologies". IEEE Journal on Selected Areas in Communications, Vol.12, 1994, pp.: 159-170

[2] T. Ito, K. Fukuchi, K. Sekiya, D. Ogasahara, R. Ohhira, T.Ono: "6.4 Tb/s (160x40Gb/s) WDM transmission experiment with 0.8 bit/Hz spectral efficiency", ECOC'2000, PD 1.1.

[3] A. Farbert, G. Mohs, S. Spalter, J.-P. Elbers, C. Furst, A. Schopflin, E. Gottwald, C. Scheerer, C. Glingener, "7Tb/s (176x40 Gb/s) bi-directional interleaved transmission with 50 GHz channel spacing", ECOC'2000, PD1.3.

[4] D.A. Smith, J.J. Johnson, J.E. Baran, K.W. Cheung, S.C. Liew: "Integrated acoustically tunable optical filters: devices and applications", OFC'91, pp.142.

[5] L. Eldada, R. Blomquist, M. Maxfield, D. Pant, G. Boudoughian, C. Poga and R.A. Norwood: "Thermooptic planar polymer Bragg grating OADM's with broad tuning range", Photonics Technology Letters, 11, (4), 1999, pp.448-450.

[6] L.K. Oxenloewe, A.T. Clausen, H.N. Poulsen, "Wavelength conversion in an electroabsorption modulator", ECOC'2000, Vol.3, pp.303-304.

[7] T. Durhuus, B. Mikkelsen, C. Joergensen, S.L. Danielsen, K.E. Stubkjaer: "All optical wavelength conversion by semiconductor optical amplifiers", J. of Lightwave Technology, 14, (6), 1996, pp. 942-954.

[8] M.F.C. Stephens, R.V. Penty, I.H. White: "All-optical regeneration and wavelength conversion in an integrated semiconductor optical amplifier/distributed-feedback Laser". Photonics Technology Letters, 11, (8), 1999, pp.979-981.

[9] P.S. Cho, D. Mahgerefteh, J. Goldhar: "All-optical 2R regeneration and wavelength conversion at 20Gb/s using an electroabsorption modulator", Photonics Technology Letters, 11, (12), 1999, pp.1662-1664.

Cost-effective wavelength selectable light source using DFB fibre laser array

F. Liu, X. Zheng, R.J.S. Pedersen, P. Varming,
A. Buxens, Y. Qian and P. Jeppesen

A cost-effective wavelength selectable light source comprising a distributed feedback (DFB) fibre laser array is proposed. A large number of wavelengths can be selected via optical space switches using only one shared pump laser. The structure is a good candidate for use as a wavelength selectable backup transmitter for wavelength division multiplexed (WDM) systems.

Introduction: The distributed feedback (DFB) fibre laser is a strong candidate for use as a high quality light source in high bit rate optical systems due to its very high signal to noise ratio, singlemode operation without mode hoping, high output power and inherent fibre compatibility. It is even more attractive for use in dense wavelength division multiplexing (WDM) systems owing to its narrow linewidth, accurate wavelength setting and wavelength stability over a wide temperature range [1 – 3]. DFB fibre lasers with different wavelengths can be made for operation in both the C and L bands and have shown excellent performance in WDM transmission experiments [4 – 6]. However, the need for a pump source to obtain laser operation dramatically increases the cost of using DFB fibre lasers in transmission systems.

In this Letter, a wavelength selectable light source (WSLS) which uses a DFB fibre laser array and a single pump unit is proposed and results from an experiment are presented. Since only one shared pump laser is used to support many DFB fibre lasers with different wavelengths, it can be a cost-effective light source for use as a wavelength selectable backup transmitter in WDM systems.

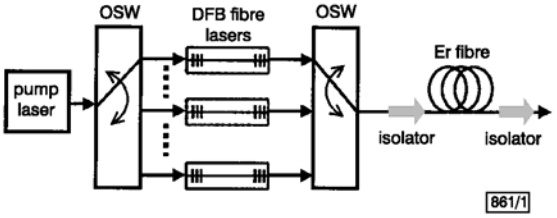

Fig. 1 *Schematic diagram of wavelength selectable light source using DFB fibre laser array*

OSW: optical space switch

Principle and experimental setup: A schematic diagram of the proposed WSLS is shown in Fig. 1. A set of DFB fibre lasers with different wavelengths is connected between two optical space switches. Pump power is guided into the desired DFB fibre laser via an optical space switch and the lasing signal is guided to the output of the DFB fibre laser array through another optical switch. The lasing signal from the DFB fibre laser is further amplified in the erbium-doped fibre by the residual pump power. By connecting the two optical switches to the different DFB fibre lasers, we can select the output wavelength from the array. Two isolators are placed before and after the erbium-doped fibre in order to obtain a stable output.

In our experimental setup, a 1480nm laser with 50mW output power was used as the pump source. Two 1×2 mechanical optic switches with an insertion loss of < 0.6dB at wavelengths between 1290 and 1570nm were used to select two DFB fibre lasers. The length of the erbium-doped fibre was 15m to provide extra amplification.

Results and discussions: Fig. 2 shows the spectrum of the output when the optical switches were connected to two different DFB fibre lasers with centre wavelengths of 1553.3 and 1559.6nm. The output powers are higher than 5dBm while maintaining a signal to ASE noise ratio of > 40dB in all cases. The response time of the WSLS is determined by the speed of the optical switches, the response time of the DFB fibre laser and the erbium-doped fibre amplifier. Time response measurements are shown in Fig. 3. A 7.6ms time delay from the mechanical optical switch alone can be found in Fig. 3*a* in relation to the control signal. Fig. 3*b* shows the time response after the DFB fibre laser; less than 0.5ms extra time delay from the DFB fibre laser can be found. Fig. 3*c* shows the time response after the erbium-doped fibre; the total time delay from the WSLS is 11ms, which is dominated by the delay from the optical switch.

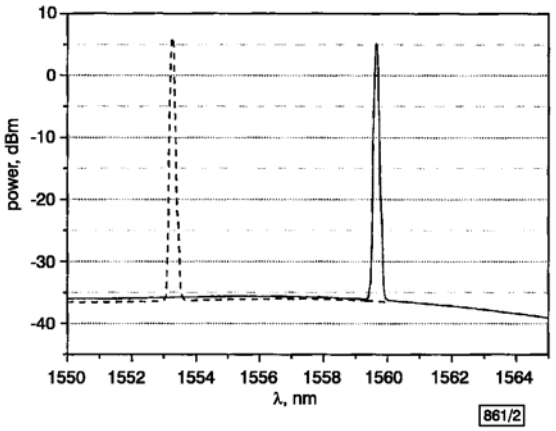

Fig. 2 *Spectrum of two DFB fibre lasers*

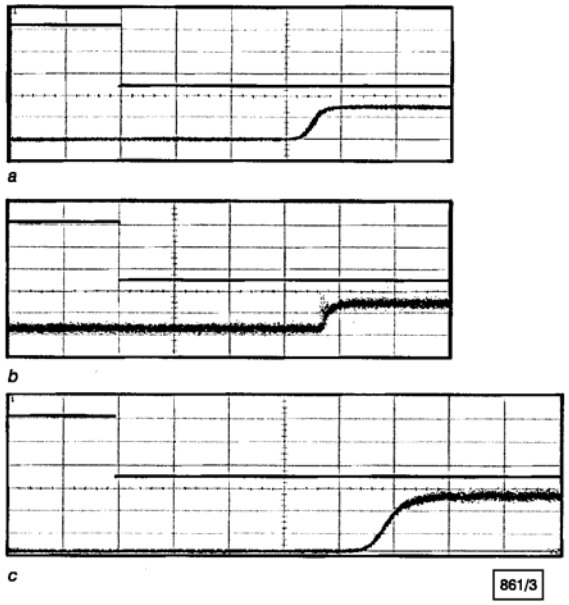

Fig. 3 *Time response after optical switch, DFB fibre laser, and erbium-doped fibre*

2ms/div
a Optical switch
b DFB fibre laser
c Erbium-doped fibre

Overshoot at the rising edge can be seen in Fig. 3*b*, which we believe is due to the relaxation oscillation of the DFB fibre laser. However, the overshoot is eliminated after the erbium-doped fibre.

A very low wavelength temperature coefficient of better than –2.8 $\times 10^{-4}$nm/°C has been reported for DFB fibre lasers using a temperature stabilised package developed in a special bimetal fixture [2]. If the DFB fibre lasers in the proposed DFB laser array are packaged in such a way, no complex wavelength lockers are necessary to monitor and stabilise the wavelength through active feedback control. Since optical space switches of size 1×50 are commercially available, the proposed structure could be made very cost-effectively for a large number of wavelengths using a single shared pump laser.

One of the most obvious applications of the proposed WSLS is as a wavelength selectable backup transmitter in WDM systems. The WSLS can be configured to the wavelength of a failing transmitter in a WDM system and thus provide transmitter failure protection.

Conclusions: A cost-effective wavelength selectable light source using a DFB fibre laser array has been proposed and demonstrated. A large number of wavelengths can be selected via optical space switches using only one shared pump laser. The structure is a good candidate for use as a wavelength selectable backup transmitter in WDM systems.

24 January 2000
Electronics Letters Online No: 20000492
DOI: 10.1049/el:20000492

F. Liu, X. Zheng, R.J.S. Pedersen, P. Varming, A. Buxens, Y. Qian and P. Jeppesen (*Research Center COM, Technical University of Denmark, Building 349, Lyngby, DK-2800, Denmark*)

E-mail: lf@com.dtu.dk

References

1 VARMING, P., HUBNER, J., and KRISTENSEN, M.: 'DFB fiber laser as source for optical communication systems'. Dig. Conf. Opt. Fiber Commun., 1997, p. 169

2 PAN, J.J., and SHI, Y.: '166-mW single-frequency output interactive fiber lasers with low noise', *IEEE Photonics Technol. Lett.,* 1999, **11**, pp. 36–38

3 IBSEN, M., ALAM, S., ZERVAS, M.N., GRUDININ, A.B., and PAYNE, D.N.: 'All fiber DFB laser WDM transmitters with integrated pump redundancy'. Proc. ECOC'99, Nice, France, 1999, pp. 74–75

4 HUBNER, J., VARMING, P., and KRISTENSEN, M.: 'Five wavelength DFB fibre laser source for WDM systems', *Electron. Lett.,* 1997, **33**, (2), pp. 139–140

5 IBSEN, M., FU, A., GEIGER, H., and LAMING, R.I.: 'Fiber DFB lasers in a 4 × 10Gb/s link with a single sinc-sampled fiber grating dispersion compensator'. Proc. ECOC'98, Madrid, Spain, 1998, Postdeadline Paper, pp. 107–111

6 POULSEN, H.N., VARMING, P., BUXENS, A., CLAUSEN, A.T., MUNOZ, I., JEPPESEN, P., POULDEN, C.V., PEDERSEN, J.E., and ESKILDSEN, L.: '1607 nm DFB fiber laser for optical communication in the L-band'. Proc. ECOC'99, Nice, France, 1999, Vol. 1, pp. 70–71

L-band transmission over 1000km using standard and dispersion-compensating fibres in pre-compensation scheme optimised at 1550nm

C. Peucheret, I. Muñoz, A. Buxens, F. Liu and S.N. Knudsen

Transmission over 1000km of a 10Gbit/s signal at 1597nm is demonstrated in a recirculating loop using standard fibre and wideband dispersion-compensating fibre in the pre-compensation configuration. It is shown that dispersion maps optimised for 1550nm can be successfully used in the L-band, removing the need for separate band dispersion compensation.

Introduction: One possible way to meet the ever increasing demand for capacity in dense wavelength division multiplexing (DWDM) optical communication systems is to extend the conventional C-band transmission window (1530 to 1565nm) into the L-band (1570 to 1610nm). The successful development of gain-shifted erbium doped fibre amplifiers (EDFA) has made this approach extremely promising [1]. Terabit WDM transmission using both C- and L-bands has been demonstrated [2] and continuing progress in the design of L-band EDFAs with low noise figure and better gain flatness should lead to increased transmission distances [3]. However, over such wide bandwidths the issue of dispersion management becomes even more critical. Most system experiments reported so far have been conducted with dispersion-shifted fibres (DSF) the small residual dispersion of which in the long wavelength region is used to counteract four wave mixing [4]. An alternative is to use fibres with a higher local dispersion over the entire bandwidth such as standard singlemode fibre (SMF) in conjunction with dispersion-compensating fibre (DCF). However, wideband dispersion slope compensation is required if the same piece of DCF is to be used for both the C- and L-bands.

In this Letter we report 10Gbit/s single-channel transmission at 1597nm over distances > 1000km using a recirculating loop setup. In particular, we demonstrate that dispersion maps designed for 1550nm and utilising SMF and wideband DCF [5] can be used successfully without any modification to the L-band, opening the way for wideband long-distance transmission over standard fibres.

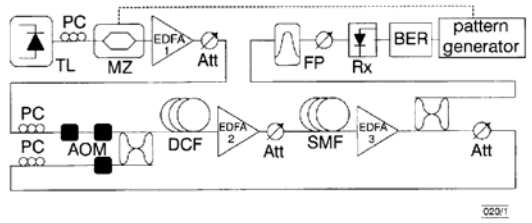

Fig. 1 *Experimental recirculating loop setup (pre-compensation)*

TL: tunable laser; PC: polarisation controller; MZ: Mach-Zehnder modulator; Att: variable attenuator; AOM: acousto-optic modulator; FP: Fabry-Perot filter; RX: receiver; BER: bit-error-rate test-set

Experimental setup: The recirculating loop setup is shown in Fig. 1. Light from an external cavity laser tuned to 1597nm was externally modulated at 10Gbit/s with a nonreturn-to-zero (NRZ) pseudorandom bit sequence (PRBS) in a chirpless Mach-Zehnder modulator. It was then amplified before being fed into a loop switch made of three acousto-optic modulators and a 3dB coupler. The transmission span consisted of two L-band EDFAs, one spool of SMF (50.850 or 80km) and a matching spool of wideband DCF. The DCF was placed either before (pre-compensation) or after (post-compensation) the SMF. The wideband DCF used in these experiments exhibited a dispersion of −100ps/(nm.km) and a dispersion slope of −0.37ps/(nm^2.km) at 1550nm. The DCF was cut at lengths corresponding to full compensation at 1550nm. The wavelength dependence of the total residual dispersion for the 50km SMF span is shown in Fig. 2. A small residual dispersion of +2.7ps/nm (corresponding to 99.7% compensation) was measured at 1550nm for this span. The measured values of the residual dispersion at 1597nm were −21.3ps/nm and −13.4ps/nm for the 50 and 80km spans respectively. The optimum performance for the three L-band EDFAs used in this experiment were reached at ~1597nm. Gains of between 18.5 and 22dB and noise figures of 5dB were measured for an input power of −10dBm at this wavelength. Variable attenuators were placed after each EDFA in order to optimise the power levels in the loop. The signal was tapped from the loop with a 13dB coupler placed after the last amplifier in the span and was fed via a 40GHz Fabry-Perot filter to a receiver consisting of a lightwave converter and a clock recovery circuit.

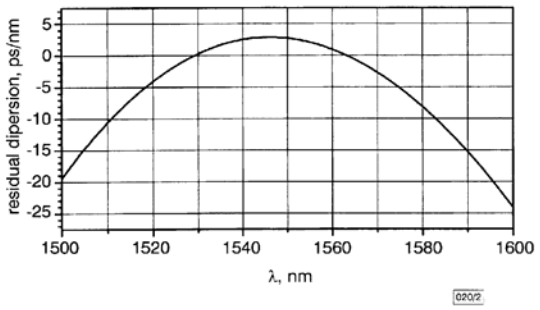

Fig. 2 *Total residual dispersion for 50km SMF span*

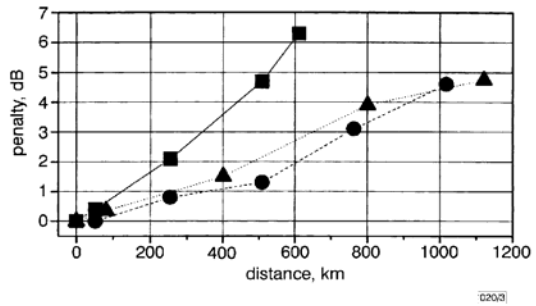

Fig. 3 *Power penalty ($BER = 10^{-9}$) against transmission distance*

▲ pre-compensation, 80km SMF spans
● pre-compensation, 50km SMF spans
■ post-compensation, 50km SMF spans

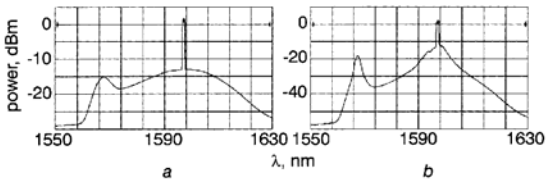

Fig. 4 *Spectra (in 1nm resolution bandwidth) after 1 and 20 recirculations for pre-compensation, 50km SMF spans*

a 1 recirculation
b 20 recirculations

Results and discussion: BER curves were measured at 1597nm for both pre- and post-compensation schemes with 50km SMF in the loop and for pre-compensation only with the 80km SMF span. The resulting penalties against distance are shown in Fig. 3. Only the SMF length is taken into account in the calculation of the transmitted distance in this graph. Using the 50km SMF span a power penalty of 4.6dB was measured in the pre-compensation case for 20 recirculations corresponding to 1017km. Penalties were significantly higher for post-compensation. In our experiment, the powers at the SMF and DCF inputs were set to values which maximised the transmission distance. The powers at the SMF and DCF inputs were 2.6dBm and −2.7dBm, respectively, for pre-compensation (50km SMF span). However, power budget limitations in the loop setup due to the 6.5dB attenuation of the loop switch and the limited gain of the amplifiers restricted the power at the input of the SMF in the post-compensation case. As self-phase modulation in the anomalous dispersion regime is known to lead to pulse compression [6], a higher power into the SMF would be desirable in the post-compensation case. The power levels are consequently not fully optimised in this case, which explains the significant difference in penalty compared to pre-compensation. Using 80km SMF spans and pre-compensa-

tion, a penalty of 4.7dB was measured for 14 recirculations corresponding to 1120km.

Fig. 4 shows the spectra recorded for 1 and 20 recirculations in the pre-compensation case for 50km SMF spans. In the experiment, no in-line filtering was used, causing a significant build-up of amplified spontaneous emission noise. With a total residual dispersion of −426ps/nm, noise accumulation becomes the limiting factor for such a system.

Conclusion: We have successfully transmitted a 10Gbit/s signal at 1597nm over distances > 1000km using 50 and 80km spans of SMF and DCF in the pre-compensation configuration. We have demonstrated experimentally that long-distance L-band transmission is feasible using wideband dispersion-compensating fibre lengths tailored for dispersion compensation in the C-band. Long-distance dual L- and C-band WDM transmission using a parallel amplifier configuration should therefore be practicable without the need for separate band dispersion compensation.

25 August 1999
Electronics Letters Online No: 19991213
DOI: 10.1049/el:19991213

C. Peucheret, I. Muñoz, A. Buxens and F. Liu (*Research Center COM, Technical University of Denmark, DK-2800 Lyngby, Denmark*)

E-mail: cp@com.dtu.dk

S.N. Knudsen (*Lucent Technologies Denmark A/S, Priorparken 680, DK-2605 Brøndby, Denmark*)

References

1 MASSICOTT, J.F., WYATT, R., and AINSLIE, B.J.: 'Low noise operation of Er^{3+} doped silica fibre amplifier around 1.6μm', *Electron. Lett.*, 1992, **28**, (20), pp. 1924–1925

2 AISAWA, S., SAKAMOTO, T., FUKUI, M., KANI, J., JINNO, M., and OGUCHI, K.: 'Ultra-wideband, long distance WDM demonstration of 1Tbit/s (50×20Gbit/s), 600km transmission using 1550 and 1580nm wavelength bands', *Electron. Lett.*, 1998, **34**, (11), pp. 1127–1129

3 CHUNG, H.S., LEE, M.S., LEE, D., PARK, N., and DIGIOVANNI, D.J.: 'Low noise, high efficiency L-band EDFA with 980nm pumping', *Electron. Lett.*, 1999, **35**, (13), pp. 1099–1100

4 SRIVASTAVA, A.K., SULHOFF, J.W., ZHANG, L., WOLF, C., SUN, Y., ABRAMOV, A.A., STRASSER, T.A., PEDRAZZANI, J.R., EPINDOLA, R.P., and VENGSARKAR, A.M.: 'L-band 64×10Gb/s DWDM transmission over 500km DSF with 50GHz channel spacing'. Proc. ECOC'98, Madrid, Spain, 1998, pp. 73–74

5 GRÜNER-NIELSEN, L., KNUDSEN, S.N., VENG, T., EDVOLD, B., and LARSEN, C.C.: 'Design and manufacture of dispersion compensating fibre for simultaneous compensation of dispersion and dispersion slope'. Tech. Dig. OFC'99, San Diego, USA, 1999, Paper WM13, pp. 232–234

6 AGRAWAL, G.P.: 'Nonlinear fiber optics' (Academic Press, San Diego, 1995), 2nd edn.

European Conference on Optical Communication, 2000, ECOC'2000

A NOVEL CHIRPED RETURN-TO-ZERO TRANSMITTER AND TRANSMISSION EXPERIMENTS

Fenghai Liu, Christophe Peucheret, Xueyan Zheng, Rune J.S. Pedersen and Palle Jeppesen

Research Center COM, Technical University of Denmark, Building 349, DK-2800 Lyngby, Denmark
Phone: +45-45253845, Fax: +45-45936581, Email: lf@com.dtu.dk

Abstract: A new 10 Gb/s chirped return-to-zero transmitter using CW light modulated by only one external modulator is proposed. Transmission over 3600 km of standard single mode fibre is performed in a re-circulating loop set-up with 80 km amplifier span.

Introduction

As the requirement for transmission of large capacity over long distance increases, different technologies to fulfill this purpose have been investigated. Among them, the return-to-zero (RZ) modulation format has become of great importance at high bit-rate, because of its robustness to fibre non-linearity and dispersion. Many of the transmission experiments achieving the longest distances with large capacity have used RZ format/1-3/.

There are many different ways to obtain an optical RZ format, and in most cases data is converted into RZ format in the optical domain by externally modulating the signal onto an optical short pulse train with a fixed repetition rate. Such an optical short pulse train can be generated by sources like mode-locked lasers/4/ or gain-switched DFB lasers/5/. A commonly used method referred to as chirped return-to-zero (CRZ) is obtained by modulating CW light in a chain of external modulators: first the amplitude of the light is modulated using the NRZ signal; second the amplitude is modulated again using a bit-synchronized clock to get the RZ pulse shape; last the phase is modulated using a bit-synchronized clock to add a chirp on the pulse. The signal generated in this way has shown very good performance in transmission over long distances/1,2/.

In this paper, we propose a new and simplified way to generate the CRZ pulses using only one external modulator and a CW light source. Using such a CRZ transmitter, 10 Gb/s transmission over 3600 km of standard single mode fibre has been obtained in a re-circulating loop set-up with 80 km amplifier span. Power penalty at BER of 10^{-9} is less than 6 dB after the transmission.

Structure of the CRZ transmitter

The schematic diagram of the CRZ transmitter is shown in Fig.1. An electrical 2:1 selector is used to generate 10 Gb/s RZ electrical pulses. A 10Gb/s NRZ signal (pattern = 2^{31}-1) is put into Data1 input of the selector while Data2 input is connected to a constant "space" which is the ground in this case. The Select-control is connected to a 10 GHz clock to select Data1 input at the rising edge of the clock and Data2 input at the falling edge. As a result, a 10 Gb/s RZ signal is obtained at Output of the selector. The eye-diagram of the electrical RZ pulses is shown in Fig.2 (a). In principle, AND logic operation between a 10 Gb/s NRZ signal and a synchronized 10 GHz clock in an electrical gate can also generate 10 Gb/s RZ signal.

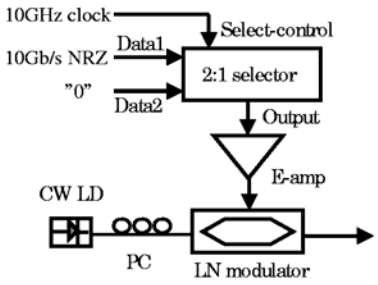

Figure 1: Schematic diagram of the CRZ transmitter

CW light from a DFB semiconductor laser is coupled into a Lithium Niobate (LN) Mach-Zehnder modulator via a polarization controller (PC). When the RZ signal generated from the 2:1 selector is amplified by an electrical amplifier (E-amp), and applied to one electrode of the LN modulator with a proper DC bias, a 10 Gb/s RZ optical signal is generated as shown in Fig.2 (b). Since only one electrode of the LN modulator is used, a bit-synchronized chirp is automatically added to the RZ pulse. To show this, the electric field E after the modulator can be written as:

$$E = E_0 \cos(\frac{\varphi(t)+\varphi_0}{2})\cos(\omega t + \frac{\varphi(t)+\varphi_0}{2} + \phi) \qquad (1)$$

where ω represents the angular frequency of the optical carrier, $\varphi(t)$ and φ_0 represent the optical phase change in the arm of the M-Z modulator stemming from the modulation and DC bias respectively, ϕ is the optical phase delay from the device and E_0 is amplitude of the input field. The first cosine function in equation (1) describes the intensity variation according to the modulation and the second cosine the phase variation under modulation.

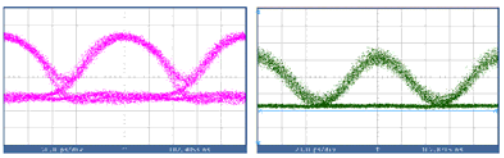

(a) (b)

Figure 2: Eye-diagram of electrical (a) and optical (b) RZ signal. 20ps/div.

A maximum phase shift of π/2 can be added to the optical signal in this scheme, depending on the modulation voltage of the signal and the switching voltage of the modulator V_π. The sign of the chirp can be adjusted by the DC bias. We use an absolute value of phase modulation index of 0.3π in our experiment.

Transmission experiments

In order to investigate the transmission performance of the CRZ pulse, a fibre re-circulating set-up is used as shown in Fig.3.

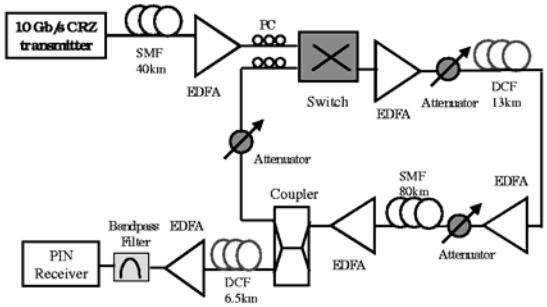

Figure 3: Fibre re-circulating set-up for transmission

The loop contains an 80 km span of SMF and a 13 km dispersion compensating fibre (DCF) providing 100% dispersion compensation. Three commercial EDFAs are used to compensate loss from the SMF, the DCF and the loop switch. Three optical attenuators are used to adjust the power accordingly. The powers into SMF and DCF are optimised at the 45th roundtrip. A 40 km SMF and a corresponding 6.5 km DCF are put after the transmitter and before the receiver, respectively, to reduce the maximum accumulated dispersion in the transmission. A PIN receiver is used and a 1.2 nm optical band pass filter is put before the receiver to reduce the out-of-band ASE noise. BER curves for different transmission distances are shown in Fig.4, from which a 6 dB power penalty at BER=10^{-9} can be found after 3600 km transmission.

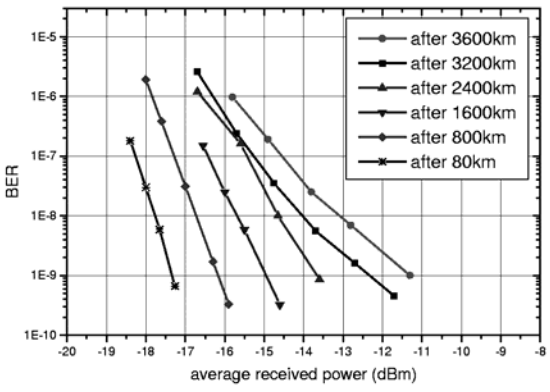

Figure 4: BER curves after transmission

Discussion

Using the new CRZ transmitter, transmission over 3600 km standard single mode fibre has been achieved. The transmission distance is limited by accumulated ASE noise. The ASE noise accumulation is shown in Fig. 5, where ASE level is measured after 80 km and 3200km respectively. This high ASE floor after 3200 km is due to: 1) a long amplifier span of 80 km SMF is used; 2) short loop configuration with only one span of transmission fibre, where one of the 3 EDFAs is used to compensate the loss from the loop switch instead of transmission loss; 3) commercial EDFAs are used in the loop without optimal noise figure.

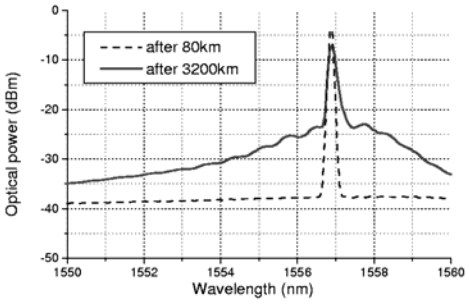

Figure 5: Spectra after 80 km and 3200 km

Conclusions

A new and simple CRZ transmitter has been proposed and demonstrated using a CW light source and only one external modulator. Transmission over 3600 km SMF has been obtained in a re-circulating loop set-up with 80km SMF span and full dispersion compensating fibre.

The work is partly supported by the ACTS project DEMON. Authors would like to thank Lucent Technologies Denmark for providing the SMF and DCF fibres.

Reference

/1/ E.A. Golovchenko, N.S. Bergano, C.A. Davidson and A.N. Pilipestskii, *Tech. Dig. OFC'1999*, pp246-248.

/2/ C.R. Davidson, C.J. Chen, M. Nissov, A. Pilipetskii N. Ramanujam, H.D. Kidorf, B. Pedersen, M.A. Mills, C. Lin, M.I. Hayee, J.X. Cai, A.B. Puc, P.C. Corbett, R. Menges, H. Li, A. Elyamani, C. Rivers and N.S. Bergano, *Tech. Dig. of OFC'2000*, PD25.

/3/ T. Ito, K. Fukuchi, Y. Inada, T. Tsuzaki, M. Harumoto and M. Kakui, *Tech. Dig. of OFC'2000*, PD24.

/4/ C. Caspar, H.-M. Foisel, A. Gladisch, N. Hanik, F. Kuppers, R. Ludwig, A. Mattheus, W. Pieper, B. Strebel and H.G. Weber, *IEEE Photon. Technol. Lett.*, 11 (4), 1999, pp481-483.

/5/ O. Leclerc, P. Brindel, D. Rouvillain, B. Dany, E. Pincemin, E. Desurvire, C. Duchet, A. Shen, F. Blache, F. Devaux, A. Coquelin, M. Goix, S. Bouchoule and P.Nouchi, *Electron. Lett.*, 36(4), 2000, pp337-338.

Chirped return-to-zero source used in 8 × 10Gbit/s transmission over 2000km of standard singlemode fibre

F. Liu, X. Zheng, C. Peucheret, S.N. Knudsen, R.J.S. Pedersen and P. Jeppesen

A new and simple chirped return-to-zero transmitter is proposed and successfully used in 8 × 10Gbit/s transmission over 2000km of standard singlemode fibre with 80km amplifier span.

Introduction: As the demand for communication capacity over long distances increases, different modulation formats such as duo-binary, dispersion-managed soliton and chirped return-to-zero (CRZ) have been studied [1 – 3]. Many DWDM systems are using CRZ format in long-distance transmission because of its simple implementation and robustness to fibre nonlinearity and dispersion [3]. Record transmission distance and capacity production has been achieved using this format [4].

To generate CRZ pulses, a chain of three external modulators is usually required [3]. One modulator is used to modulate the amplitude of CW light with an NRZ (non return-to-zero) signal; another modulator is used to modulate the amplitude again with a bit-synchronised clock to obtain the RZ shape; the third modulator is used to modulate the optical phase with a bit-synchronised clock to add a proper chirp on the RZ pulses.

In this Letter, we propose a new method of generating CRZ pulses using an electrical gate and only one external modulator. Using this scheme in DWDM systems, the total number of external modulators as well as electrical amplifiers driving the modulators is significantly reduced. Using such CRZ transmitters, we have transmitted 8 × 10Gbit/s WDM signals over 2000km of standard singlemode fibre in a re-circulating loop setup with 80km amplifier span.

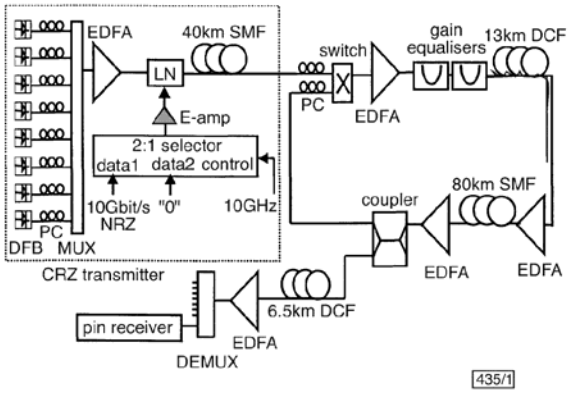

Fig. 1 *Schematic diagram of CRZ transmitters and transmission experiment setup*

CRZ transmitters shown in dashed frame

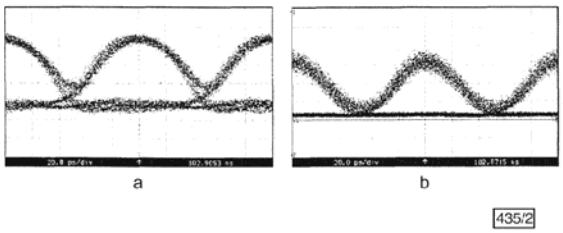

Fig.2 *Eye diagrams of electrical RZ signal and optical CRZ signal*

a Electrical RZ signal
b Optical CRZ signal
Time scale is 20ps/div

Principle and experiments: A schematic diagram of the transmission setup using the new CRZ transmitter is shown in Fig. 1, and the CRZ transmitters are highlighted in a dashed frame. To generate the CRZ pulse, an electrical 2:1 selector is used to generate 10Gbit/s RZ electrical pulses. A 10Gbit/s NRZ signal (pattern length = 2^{31}–1) is fed into the data1 input of the selector, and the data2 input is connected to a constant '0' that is the ground in this case. The select-control is connected to a synchronised 10GHz clock to select data1 input at the rising edge of the clock and data2 input at the falling edge. As a result, a 10Gbit/s RZ signal is obtained at the output of the selector. In principle, creating AND logic between a 10Gbit/s NRZ signal and a synchronised 10GHz clock in an electrical gate can also generate the 10Gbit/s RZ signal. The RZ signal generated from the 2:1 selector is amplified by an electrical amplifier (E-amp), and used to modulate one arm of a lithium niobate (LN) Mach-Zehnder (M-Z) modulator. A proper DC bias is applied to the other arm of the M-Z modulator. When CW light is coupled into the M-Z modulator with a perfect split-combining ratio in two arms, the electric field E of the optical signal after the modulator can be written as follows:

$$E = A\cos\left(\frac{\varphi_1(t)-\varphi_2}{2}\right)\cos\left(\omega t+\frac{\varphi_1(t)+\varphi_2}{2}\right) \quad (1)$$

where A represents a constant amplitude and ω the angular frequency of the optical carrier; $\varphi_1(t)$ the optical phase change in the arm of the M-Z modulator induced by the modulation signal; and φ_2 represents the optical phase change in the other arm of the M-Z modulator induced by the DC bias. The first cosine function of eqn. 1 describes the intensity variation according to the modulation, and the term $(\varphi_1(t)+\varphi_2)/2$ in the second cosine describes the phase modulation. From eqn. 1, we find that a maximum bit-synchronised phase modulation of 0.5π can be applied to the optical signal in this scheme without destroying the amplitude modulation. If the two arms of the M-Z modulator are modulated by the same signal but with different amplitudes, any value of phase modulation can be applied to the optical signal, which is determined by the common mode of the modulation signal $(\varphi_1(t)+\varphi_2(t))/2$, while the amplitude modulation is determined by the differential mode $(\varphi_1(t)-\varphi_2(t))/2$. In practice, the actual phase modulation applied to the signal depends on the modulation voltage of the electrical signal and the switching voltage of the modulator V_π. In our experiment, we modulated one arm of the M-Z modulator with a 4.8V peak-peak RZ signal and obtained 0.3π of bit-synchronised phase modulation. Fig. 2 shows the eye diagrams of the electrical RZ signal (*a*) and optical CRZ signal (*b*) at 10Gbit/s.

To construct 8 × 10Gbit/s CRZ transmitters, eight DFB semiconductor lasers working in CW operation with 200GHz frequency spacing on the ITU-T grid were coupled into the M-Z modulator via an arrayed-waveguide grating (AWG) multiplexer and polarisation controllers (PCs). A fibre re-circulating loop setup was used to investigate the transmission performance.

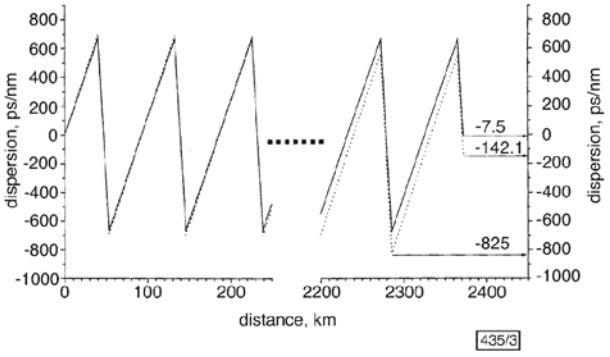

Fig.3 *Dispersion map used in 8 × 10Gbit/s transmission over 2000km of SMF*

——— channel 1
····· channel 8

The loop contained a span made of 80km of SMF and 13km dispersion-compensating fibre (DCF), to provide 100% dispersion compensation. A 40km SMF was placed after the modulator and a 6.5km DCF fibre placed before the demultiplexer, so that the maximum accumulated dispersion during transmission was reduced by half. A new type of DCF [5] was used not only for dispersion compensation but also for dispersion slope compensation in order to avoid channel-by-channel dispersion compensation at the receiver end. From the dispersion map shown in Fig. 3 it can be seen that the maximum accumulated dispersion during transmission is –825ps/nm. After 25 rounds corresponding to 2000km transmission of SMF, the maximum residual dispersion

was –142.1ps/nm for channel 8 at 1560.6nm, and the smallest was only –7.5ps/nm for channel 1 at 1549.3nm.

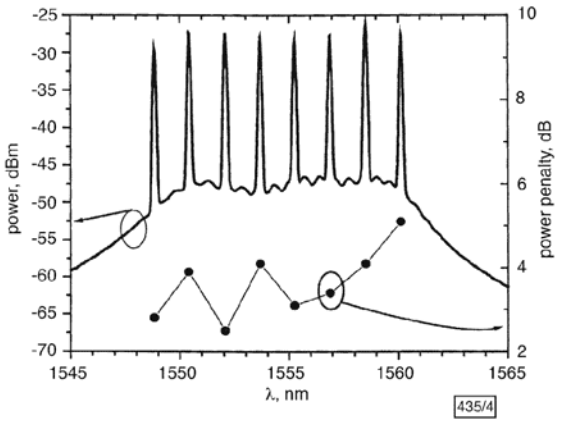

Fig.4 *Spectrum and power penalty of eight channels after transmission over 2000km SMF*

Resolution bandwidth is 0.1nm

Two gain equalisers were used before the DCF in order to obtain uniform input power from the eight channels. From the spectrum after 25 round-trips shown in Fig. 4, it can be seen that the power variation between channels is kept within 5dB.

A fraction of the signal was coupled out of the loop via a 10:1 coupler, and launched into a *pin* receiver after being demultiplexed by an AWG demultiplexer. The power penalty for different channels after transmission over 2000km of SMF is shown in solid circles in Fig. 4. Fig. 4 shows that the maximum penalty is ~5dB.

Conclusions: A new CRZ transmitter using only one external modulator has been proposed and 8 × 10Gbit/s CRZ transmission over 2000km SMF with 80km span has been demonstrated. The transmitter uses an electrical gate to generate the RZ format, so that the total number of optical modulators and electrical amplifiers in a DWDM system is significantly reduced. This makes the CRZ transmitter simpler, less expensive and very promising for use in future long-haul DWDM systems.

12 June 2000
Electronics Letters Online No: 20000982
DOI: 10.1049/el:20000982

F. Liu, X. Zheng, C. Peucheret, S.N. Knudsen, R.J.S. Pedersen and P. Jeppesen (*Research Center COM, Technical University of Denmark, Building 349, DK-2800 Lyngby, Denmark*)

E-mail: lf@com.dtu.dk

S.N. Knudsen: Also with Lucent Technologies Denmark, Priorparken 680, DK-2605 Brøndby, Denmark

References

1 YANO, Y., ONO, T., FUKUCHI, K., ITO, T., YAMAZAKI, H., YAMAGUCHI, M., and EMURA, K.: '2.6Terabit/s WDM transmission experiment using optical duobinary coding'. Proc. ECOC '96, 1996, Vol. 5, pp. 3–6

2 FUKUCHI, K., MAKUI, M., SASAKI, A., ITO, T., INADA, Y., TSUZAKI, T., SHITOMO, T., FUJII, K., SHIKII, S., SUGAHARA, H., and HASEGAWA, A.: '1.1Tb/s (55 × 20Gb/s) dense WDM soliton transmission over 3020-km widely-dispersion-managed transmission line employing 1.55/1.58-μm hybrid repeaters'. Proc. ECOC'99, 1999, Paper PD2–10

3 TSURITANI, T., TAKEDA, N., IMAI, K., TANAKA, K., AGATA, A., MORITA, E., YAMAUCHI, H., EDAGAWA, N., and SUZUKI, M.: '1Tbit/s (100 × 10.7Gbit/s) transoceanic transmission using 30nm wide broadband optical repeaters with A_{eff}-enlarged positive dispersion fibre and slope-compensating DCF', *Electron. Lett.*, 1999, **35**, (24), pp. 2126–2128

4 DAVIDSON, C.R., CHEN, C.J., NISSOV, M., PILIPETSKII, A., RAMANUJAM, N., KIDORF, H.D., PEDERSEN, B., MILLS, M.A., LIN, C., HAYEE, M.I., CAI, J.X., PUC, A.B., CORBETT, P.C., MENGES, R., LI, H., ELYAMANI, A., RIVERS, C., and BERGANO, N.S.: '1800Gb/s transmission of one hundred and eighty 10Gb/s WDM channels over 7000km using the full EDFA C-band'. Dig. Conf. Opt. Fiber Commun., 2000, Paper PD25

5 GRUNER-NIELSEN, L., KNUDSEN, S.N., VENG, T., EDVOLD, B., and LARSEN, C.C.: 'Design and manufacture of dispersion compensating fibre for simultaneous compensation of dispersion and dispersion slope'. Dig. Conf. Opt. Fiber Commun., 1999, Vol. 2, pp. 232–234

Measurement of small dispersion values in optical components

C. Peucheret, F. Liu and R.J.S. Pedersen

It is reported that small dispersion values in optical components can be measured using the RF modulation method originally restricted to large dispersions. Using a constant dispersion offset, arbitrarily small dispersion values can be measured with a resolution as good as 1.2ps/nm.

Introduction: In dense wavelength division multiplexing (DWDM) networks, the cascading of narrowband devices such as filters and (de-)multiplexers might result in phase induced degradation of the optical signal, especially at high bit rates [1]. Therefore, a precise method for measuring the dispersion characteristics of individual optical components is necessary. The phase-shift technique has been previously used to measure the group delay of optical devices [1]. Curve fitting and numerical differentiation are required to obtain the dispersion from the measured group delay, resulting in additional inaccuracy. Here we extend the RF modulation method originally used for optical fibres [2, 3] by adding a constant dispersion offset which enables a determination of small dispersion values in optical components.

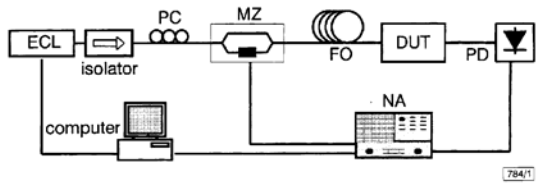

Fig. 1 *Experimental setup*

ECL: external cavity laser; PC: polarisation controller; MZ: Mach-Zehnder modulator; FO: fibre offset; DUT: device under test; NA: network analyser; PD: photodiode

Description of method: The experimental setup for the RF modulation method is depicted in Fig. 1. Light from a tunable external cavity laser is intensity modulated with a small modulation index by an $LiNbO_3$ Mach-Zehnder modulator before being coupled into a fibre offset followed by the device under test. A photodiode is used to detect the light at the output. As the modulation frequency is continuously swept from 130MHz to 20GHz, the small signal frequency response is measured by a network analyser. The method relies on the fact that, owing to the dispersive nature of optical components, the propagation constants of the two sidebands of the amplitude modulated signal are different [2]. For a given dispersion value, modulation frequencies can be found where the components of the beat signal between the carrier and the sidebands are in counterphase, resulting in cancellations of the photocurrent, seen as dips in the small signal frequency response. The total dispersion D can be calculated from these frequencies according to [2]

$$D = \frac{\left(n - \frac{1}{2}\right) c}{\lambda^2 \cdot f_n^2} \qquad (1)$$

where f_N is the centre frequency of the nth dip in the small signal frequency response, and c and λ are the speed of light and the wavelength, respectively. From eqn. 1 we can see that the minimum dispersion which can be measured by this method depends on the maximum frequency at which the Mach-Zehnder modulator can be driven. This limitation arises from the fact that, for a given amount of dispersion, the phase mismatch between the sidebands required for cancellation of the photocurrent is only achieved when the sideband separation is large enough. By inserting a constant dispersion offset (in our case 50km of standard singlemode fibre) in the setup, we have been able to measure small values of both positive and negative dispersions. Such an offset will increase the total amount of dispersion to a value large enough to be measured by our setup. The dispersion of the device under test is equal to the change in total dispersion after it has been inserted.

When characterising components such as filters, the two sidebands of the amplitude modulated signal can experience different levels of attenuation. If a and b are the relative amplitude attenuations experienced by the upper and lower sidebands, respectively, then the electric field of the modulated optical signal can be expressed as

$$\vec{E}(z,t) = \vec{E}_0\left[\cos(\omega_0 t - \beta_{\omega_0} z) + \frac{m}{2} a \cos((\omega_0 + \omega_m)t - \beta_{\omega_0+\omega_m} z) + \frac{m}{2} b \cos((\omega_0 - \omega_m)t - \beta_{\omega_0-\omega_m} z)\right] \qquad (2)$$

where ω_0 and ω_M are the optical carrier and modulation angular frequencies, respectively, and m is the modulation index. We can use a second order expansion of the propagation constant around the optical carrier frequency

$$\beta_\omega = \beta_{\omega_0} + \beta_1(\omega - \omega_0) + \frac{1}{2}\beta_2(\omega - \omega_0)^2 \qquad (3)$$

where the parameter β_2 is related to the total dispersion D by

$$D = -\frac{2\pi c}{\lambda^2}\beta_2 L \qquad (4)$$

The detected RF current component at the modulation frequency becomes

$$i_{\omega_m}(t) = i_0 \frac{m}{2}\sqrt{a^2 + b^2 + 2ab\cos(\beta_2 \omega_m^2 L)}\cos(\omega_m t - \beta_1 \omega_m L - \varphi) \qquad (5)$$

where L can be considered as an effective propagation length through both the fibre offset and the device under test. A modulation frequency dependent phase φ has been introduced.

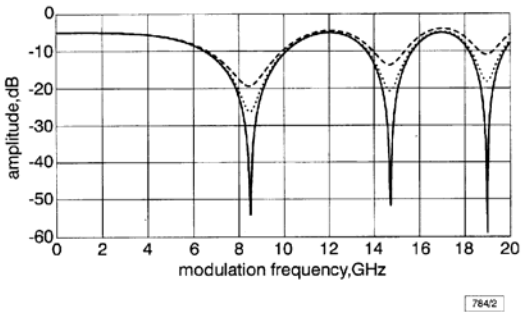

Fig. 2 *Calculated frequency responses for D = 860ps/nm with power transfer function slopes of 0, 15 and 30dB/nm*

——— 0dB/nm
····· 15dB/nm
- - - - 30dB/nm

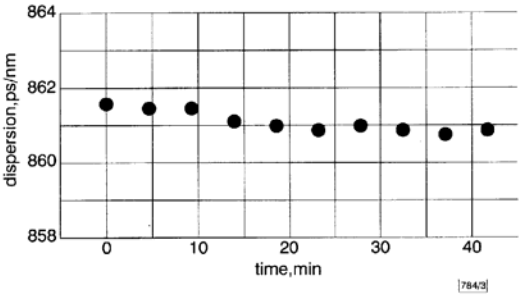

Fig. 3 *Stability of dispersion offset*

In this case, imperfect cancellation of the sidebands occurs, resulting in shallower dips in the measured small signal frequency response. However, our calculation shows that the frequencies of the dips are the same as in the ideal case when $a = b$ and therefore eqn. 1 can still be used to evaluate the dispersion. This point is illustrated in Fig. 2 where the small signal frequency response of a device with a dispersion value of 860ps/nm has been calculated for power transfer function slopes of 0, 15 and 30dB/nm. Therefore, this technique does not require the amplitude transfer function of the device to be flat.

Since the method relies on a constant dispersion offset, its stability with time is an important issue. We have investigated the stability

of our dispersion offset made of 50km of standard singlemode fibre which had been previously packaged ito reduce thermal fluctuations. Over a 40min period, the frequency of the second dip remained within a 10MHz frame, which translates into a 1.2ps/nm uncertainty for a total dispersion of 861ps/nm at the measurement wavelength of 1557.65nm.

Fig. 3 shows the measured dispersion of the fibre offset as a function of time. This 40min duration is far longer than the time required for performing the two modulation frequency sweeps necessary for evaluating the dispersion of a device at a single wavelength and enables wavelength dependent characterisations.

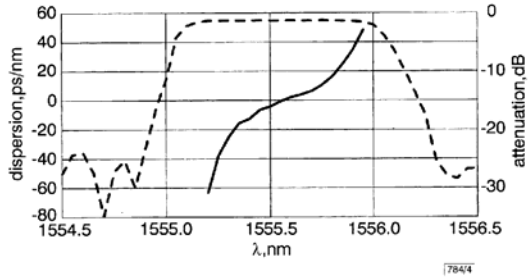

Fig. 4 *Dispersion of fibre grating Mach-Zehnder OADM*

– – – – attenuation
——— dispersion

Results: A computer program is used to synchronise the instruments and to record the small signal frequency response traces from the network analyser. All measurements were performed on the second dip of the transfer function as it allows the determination of a wide range of both positive and negative dispersion values. The technique has been used for determining the dispersion of a fibre grating Mach-Zehnder optical add-drop multiplexer (OADM) [4]. The dispersion curve measured from the 'in' to the 'drop' ports is shown in Fig. 4 together with the power transfer function of the device. Values in excess of ± 40ps/nm have been measured in the considered wavelength range. When reaching the edges of the passband of the filter, the dips in the small signal frequency response become shallower and the determination of their centre frequencies becomes more difficult until they totally vanish in the noise.

Conclusion: We have measured small dispersion values in optical components with an RF modulation technique. A length of 50km of standard singlemode fibre has been shown to constitute a dispersion offset stable enough for measuring small dispersion values with a resolution as good as 1.2ps/nm. The technique can directly measure the dispersion of optical components in cases where the numerical differentiation of noisy phase-shift measurement data would only be applicable with difficulty. Its resolution is limited by the accuracy in the determination of the dip frequency influenced by noise and by the short term stability of the dispersion offset. The dispersion of a fibre grating Mach-Zehnder optical add-drop multiplexer has been characterised successfully using this technique.

26 January 1999
Electronics Letters Online No: 19990256
DOI: 10.1049/el:19990256

C. Peucheret, F. Liu and R.J.S. Pedersen (*COM, Center for Communications, Optics and Materials, Technical University of Denmark, DK-2800 Lyngby, Denmark*)

E-mail: cp@com.dtu.dk

References

1 CASPAR, C., FOISEL, H.-M., V. HELMOLT, C., STREBEL, B., and SUGAYA, Y.: 'Comparison of cascadability performance of different types of commercially available wavelength (de)multiplexers', *Electron. Lett.*, 1997, **33**, (19), pp. 1624–1626

2 CHRISTENSEN, B., MARK, J., JACOBSEN, G., and BØDTKER, E.: 'Simple dispersion measurement technique with high resolution', *Electron. Lett.*, 1993, **29**, (1), pp. 132–134

3 DEVAUX, F., SOREL, Y., and KERDILES, J.F.: 'Simple measurement of fiber dispersion and of chirp parameter of intensity modulated light emitter', *J. Lightwave Technol.*, 1993, **LT-11**, (12), pp. 1937–1940

4 JOHNSON, D.C., HILL, K.O., BILODEAU, F., and FAUCHER, S.: 'New design concept for a narrowband wavelength-selective optical tap and combiner', *Electron. Lett.*, 1987, **23**, (13), pp. 668–669

Appendix I

Improved Gaussian crosstalk model

1. Introduction

The influence of interferometric crosstalk in optical transmission systems and optical networks has attracted a lot of attention [1]-[8]. This kind of crosstalk which originates from signals with a frequency difference less than the receiver bandwidth has stronger influence on system performance than the so-called power-addition crosstalk from neighboring channels.

When considering the choice of statistics for the interferometric crosstalk, two limiting cases are common in the literature: Arc-sine statistics for a single crosstalk contribution [1, 2, 6] and Gaussian statistics for multiple crosstalk contributions [4-6]. In optical networks, several independent crosstalk contributions with approximately equal power normally exist, and according to [5] and our numerical calculations in paper [II] only a few crosstalk contributions are necessary before the Gaussian statistics is a good approximation. Based on the Gaussian crosstalk model described in [5], an improved crosstalk model is proposed for calculating interferometric crosstalk induced penalty for both PIN receivers and optically pre-amplified (OPA) receivers, taking into account the imperfect signal extinction ratio which has a significant influence. The improved model will be described in this appendix.

2. Signal crosstalk beat noise

The crosstalk model is illustrated in Figure 1. Signal field E_s and N terms of crosstalk field E_x are combined via a lossless coupler and detected by a photo detector.

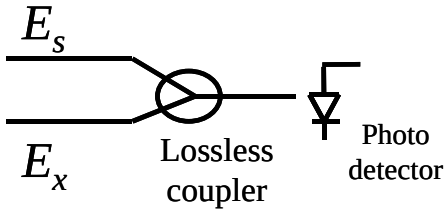

Figure 1. Illustration of interferometric crosstalk

Following assumptions are made throughout the discussion:

1) The signal and crosstalk terms have the same polarization state in order to maximize the beat noise which corresponds to the worst case.
2) The frequency difference between signal and crosstalk carriers is less than the receiver bandwidth, so that all beat noise falls within the receiver bandwidth.
3) The total crosstalk power is contributed by multiple independent terms, so signal crosstalk beat noise follows a Gaussian probability density distribution.

Firstly, we only consider the case that a CW signal and CW crosstalk light are combined at the photo detector, and we define the fields of the CW signal and crosstalk light as:

$$E_s(t) = \sqrt{2}E_s \sin(2\pi f_0 t + \phi_s(t)) \quad (1)$$

$$E_1(t) = \sqrt{2}E_1 \sin(2\pi f_0 t + \phi_1(t)) \quad (2)$$

Here f_0 is the laser oscillation frequency, $\phi_s(t)$ and $\phi_1(t)$ express the phase noise of the lasers. After the signal and crosstalk light are received by the PIN receiver, the output photo current is given by:

$$i_p(t) = \frac{e\eta}{h\nu} S \sqrt{\frac{\varepsilon}{\mu}} (E_s(t) + E_1(t))^2 = A(E_s(t) + E_1(t))^2 \quad (3)$$

A is the conversion coefficient and is assumed to be unity hereafter for simplicity. By inserting (1) and (2) into (3), we can get:

$$\begin{aligned} i_p(t) &= (\sqrt{2}E_s \sin(2\pi f_0 t + \phi_s(t)) + \sqrt{2}E_1 \sin(2\pi f_0 t + \phi_1(t)))^2 \quad (4) \\ &= 2E_s^2 \sin^2(2\pi f_0 t + \phi_s(t)) + 4E_s E_1 \sin(2\pi f_0 t + \phi_s(t)) \sin(2\pi f_0 t + \phi_1(t)) + 2E_1^2 \sin^2(2\pi f_0 t + \phi_1(t)) \end{aligned}$$

Using the relations of tri-angular functions:

$\sin^2\alpha = (1 - \cos 2\alpha)/2$ and $\sin\alpha \sin\beta = (\cos(\alpha+\beta) - \cos(\alpha-\beta))/2$

the photo current can be further written as:

$$\begin{aligned} i_p(t) &= E_s^2(1 - \underline{\cos(4\pi f_0 t + 2\phi_s(t))}) + 2E_s E_1(\cos(\phi_s(t) - \phi_1(t)) - \underline{\cos(4\pi f_0 t + \phi_s(t) + \phi_1(t))}) \quad (5) \\ &+ E_1^2(1 - \underline{\cos(4\pi f_0 t + 2\phi_1(t))}) \end{aligned}$$

The underlined terms in the above expression are very high frequency components which are out of the receiver bandwidth. After removal of these terms, the photo current in (5) can be written as:

$$i_p(t) = E_s^2 + 2E_s E_1 \cos(\phi_s(t) - \phi_1(t)) + E_1^2 \quad (6)$$

When more crosstalk terms are added to the signal, the electrical field of the crosstalk is:

$$E_x(t) = \sum_{i=1}^{N} \sqrt{2}E_i \sin(2\pi f_0 t + \phi_i(t)) \quad (7)$$

Following the same procedure as from (3) to (6), the output photo current is given by:

$$i_p(t) = E_s^2 + \sum_{i=1}^{N} 2E_s E_i \cos(\phi_s(t) - \phi_i(t)) + \sum_{i,j=1(i>j)}^{N} 2E_i E_j \cos(\phi_i(t) - \phi_j(t)) + \sum_{i=1}^{N} E_i^2 \quad (8)$$

The first and last terms are the optical power of the signal and crosstalk, respectively. The second term is called signal-crosstalk beat noise, which is of our interest. The third term is crosstalk-crosstalk beat noise and is negligible compared to the signal-crosstalk beat noise, so (8) can be re-written as:

$$i_p(t) = E_s^2 + \sum_{i=1}^{N} 2E_s E_i \cos(\phi_s(t) - \phi_i(t)) + \sum_{i=1}^{N} E_i^2 \quad (9)$$

From (9) it can be seen that the photo current varies with time due to the presence of crosstalk; When the receiver bandwidth is broader than the spectral width of the light, the signal-crosstalk beat noise power totally falls into the receiver, the average value $< i_p >$ and variance $< i_p^2 >$ of the photo current are given by:

$$< i_p >= \frac{1}{T}\int_0^T i_p(t)dt = E_s^2 + \sum_{i=1}^{N} E_i^2 \tag{10}$$

$$< i_p^2 >= \frac{1}{T}\int_0^T (i_p(t) - < i_p >)^2 dt = 2E_s^2 \sum_{i=1}^{N} E_i^2 \tag{11}$$

Equation (11) shows that the electrical power of signal crosstalk beat noise is two times the product of optical signal power and the crosstalk power, or two times the product of signal induced photo current and crosstalk induced photo current, that is:

$$\sigma^2_{signal-xtalk} =< i_p^2 >= 2i_s i_x \tag{12}$$

i_s and i_x stand the photo current induced by the signal and crosstalk, respectively.

When the signal and crosstalk are intensity modulated light instead of CW light, we define the signal extinction ratio *r*, average power $\overline{P}_s$ of the signal without crosstalk:

$$r = \frac{P_0}{P_1} \qquad \overline{P_s} = (\frac{1+r}{2})P_1 \tag{13}$$

Here the P_0 and P_1 are the optical power in the "space" and "mark", respectively. We assume equal power in all "marks" and equal power in all "spaces", and no waveform distortion and timing jitter is taken into account. The mark density is 0.5. We also define the relative crosstalk power ε as:

$$\varepsilon = \overline{P}_{xtalk} \Big/ \overline{P}_s \tag{14}$$

Here $\overline{p}_{xtalk}$ is the total average crosstalk power. Inserting (13) and (14) into (12) and giving the i_1 as the photo current when the signal bit is "mark" without crosstalk, the variance of the signal crosstalk beat noise in the "mark" and "space" levels respectively can be written as:

"mark": $\varepsilon(1+r)i_1^2$ (15)

"space": $r\varepsilon(1+r)i_1^2$ (16)

3. PIN receiver

3.1. Error probability in absence of crosstalk

The PIN receiver here converts the optical signal into photo current. Only thermal noise with variance of σ_{th}^2 is considered when the crosstalk is absent, so the error probability is given by:

$$P_e = \frac{1}{4}erfc(\frac{1}{\sqrt{2}}\frac{i_1 - i_d}{\sqrt{\sigma_{th}^2}}) + \frac{1}{4}erfc(\frac{1}{\sqrt{2}}\frac{i_d - ri_1}{\sqrt{\sigma_{th}^2}}) \tag{17}$$

where i_d is the decision threshold and *erfc* is the complementary error function. The first and second terms are the error probability when the signals are "mark" and "space", respectively. When the thermal noise is the dominant in the receiver, they are the same on the "mark" and

"space". The optimum decision threshold is equal to the average threshold: $i_d = (1+r)i_1/2$. When the optimum decision threshold is used, the total error probability can be written as:

$$P_e = \frac{1}{2} erfc(\frac{1}{\sqrt{2}} \frac{(1-r)i_1}{2\sqrt{\sigma_{th}^2}}) \tag{18}$$

In order to get error probability of 10^{-9}, the following equation need to be satisfied:

$$\frac{(1-r)i_1}{2\sqrt{\sigma_{th}^2}} = Q = 6 \tag{19}$$

That is:

$$i_1 = \frac{2Q\sqrt{\sigma_{th}^2}}{1-r} \tag{20}$$

3.2. Crosstalk induced power penalty using average power decision threshold

We have assumed that the signal crosstalk noise has an approximately Gaussian probability density distribution, therefore, the total noise power in the presence of the crosstalk is simply given by the sum of the beat noise and receiver noise. When thermal noise and signal crosstalk beat noise are considered, under the Gaussian assumption, the error probability is given by:

$$P_e = \frac{1}{4} erfc(\frac{1}{\sqrt{2}} \frac{i_1 - i_d}{\sqrt{\sigma_{th}^2 + \varepsilon(1+r)i_1^2}}) + \frac{1}{4} erfc(\frac{1}{\sqrt{2}} \frac{i_d - ri_1}{\sqrt{\sigma_{th}^2 + \varepsilon r(1+r)i_1^2}}) \tag{21}$$

The first and second terms are the error probability when the signals are "mark" and "space", respectively. When average power decision threshold is used, $i_d = (1+r)i_1/2$, the errors from the "mark" level dominate the error probability, and the error probability can be written as:

$$P_e = \frac{1}{4} erfc(\frac{1}{\sqrt{2}} \frac{(1-r)i_1}{2\sqrt{\sigma_{th}^2 + \varepsilon(1+r)i_1^2}}) \tag{22}$$

In order to get the error probability of 10^{-9}, the following equation need to be satisfied:

$$\frac{(1-r)i_1}{2\sqrt{\sigma_{th}^2 + \varepsilon(1+r)i_1^2}} = Q' = 5.9 \tag{23}$$

that is:

$$i_1' = \frac{2Q'\sqrt{\sigma_{th}^2}}{\sqrt{(1-r)^2 - 4Q'^2\varepsilon(1+r)}} \tag{24}$$

Please notice that the photo current of "mark" is re-written as i_1' in order to distinguish it from the "mark" current in absence of the crosstalk. The power penalty at $P_e = 10^{-9}$ is defined as:

$$Penalty(dB) = 10\log(\frac{i_1'}{i_1}) \tag{25}$$

where *log* is the base 10 logarithm. By Inserting (20) and (24) into (25), the power penalty can be written as:

$$Penalty(dB) = 10\log(\frac{Q^{'}}{Q}) - 5\log(1 - 4\varepsilon Q^{'2}\frac{1+r}{(1-r)^2}) \approx -5\log(1 - 4\varepsilon Q^{'2}\frac{1+r}{(1-r)^2}) \tag{26}$$

When $r = 0$, equation (26) takes the form of the widely quoted power penalty equation [3-5].

3.3. Crosstalk induced power penalty using optimum decision threshold

A variable decision threshold can be used to minimize the total error probability. In order to derive the optimum decision threshold, a more general expression of the error probability is used:

$$P_e = \frac{1}{4}erfc(\frac{1}{\sqrt{2}}\frac{i_1 - i_d}{\sqrt{\sigma_1^2}}) + \frac{1}{4}erfc(\frac{1}{\sqrt{2}}\frac{i_d - i_0}{\sqrt{\sigma_0^2}}) \tag{27}$$

Where σ_1^2 denotes the noise power on "mark" level, σ_0^2 denotes the noise power on "space" level and i_0 is the average phone current of "space". The *erfc* function and its first order differentiation is given as:

$$erfc(x) = \frac{2}{\sqrt{\pi}}\int_x^{\infty} e^{-y^2}dy \tag{28}$$

$$\frac{derfc(x)}{dx} = -\frac{2}{\sqrt{\pi}}e^{-x^2} \tag{29}$$

The optimum decision threshold can be found when the differentiation of error probability over decision current is set to zero, that is:

$$\frac{dP_e}{di_d} = \frac{1}{4}\left[-\frac{2}{\sqrt{\pi}}e^{-\left(\frac{i_1-i_d}{\sqrt{2}\sigma_1}\right)^2}\left(-\frac{1}{\sqrt{2}\sigma_1}\right) - \frac{2}{\sqrt{\pi}}e^{-\left(\frac{i_d-i_0}{\sqrt{2}\sigma_0}\right)^2}\left(\frac{1}{\sqrt{2}\sigma_0}\right)\right] = 0 \tag{30}$$

that is:

$$\frac{1}{\sigma_0\sqrt{2\pi}}e^{-\left(\frac{i_d-i_0}{\sqrt{2}\sigma_0}\right)^2} = \frac{1}{\sigma_1\sqrt{2\pi}}e^{-\left(\frac{i_1-i_d}{\sqrt{2}\sigma_1}\right)^2} \tag{31}$$

From equation (31), it can be found that the optimum decision threshold is at the crossing point of probability density functions (PDFs) between "space" and "mark". Making logarithm of the two sides in equation (31), the following equation can be obtained:

$$\frac{(i_d - i_0)^2}{\sigma_0^2} = \frac{(i_1 - i_d)^2}{\sigma_1^2} + 2\ln\frac{\sigma_1}{\sigma_0} \approx \frac{(i_1 - i_d)^2}{\sigma_1^2} \tag{32}$$

The approximation is easy to fulfill when signal to noise ratio (Q factor) is high, where the error contributions from "space" and "mark" are very close, that is:

$$\frac{(i_d - i_0)}{\sigma_0} = \frac{(i_1 - i_d)}{\sigma_1} = Q >> 0 \tag{33}$$

By solving equation (32), the optimum decision threshold i_{opt} is given by:

$$i_{opt} = \frac{\sigma_0 i_1 + \sigma_1 i_0}{\sigma_0 + \sigma_1} \tag{34}$$

The optimum decision threshold is slightly smaller than that of the average power decision threshold. By setting $i_d = i_{opt}$, the error probability (21) can be written as:

$$P_e = \frac{1}{2} erfc\left(\frac{1}{\sqrt{2}} \frac{(1-r)i_1}{\sqrt{\sigma_{th}^2 + r\varepsilon(1+r)i_1^2} + \sqrt{\sigma_{th}^2 + \varepsilon(1+r)i_1^2}} \right) \tag{35}$$

In order to get $P_e = \frac{1}{2} erfc(\frac{1}{\sqrt{2}} Q) = 10^{-9}$, Q=6, the following equation need to be fulfilled:

$$\frac{(1-r)i_1}{\sqrt{\sigma_{th}^2 + r\varepsilon(1+r)i_1^2} + \sqrt{\sigma_{th}^2 + \varepsilon(1+r)i_1^2}} = Q \tag{36}$$

Following steps until (37) are used to solve equation (36):

$$(1-r)i_1 = Q(\sqrt{\sigma_{th}^2 + r\varepsilon(1+r)i_1^2} + \sqrt{\sigma_{th}^2 + \varepsilon(1+r)i_1^2})$$

$$(1-r)i_1 - Q\sqrt{\sigma_{th}^2 + \varepsilon(1+r)i_1^2} = Q\sqrt{\sigma_{th}^2 + r\varepsilon(1+r)i_1^2}$$

Square the two sides of the above equation:

$$(1-r)^2 i_1^2 - 2(1-r)i_1 Q\sqrt{\sigma_{th}^2 + \varepsilon(1+r)i_1^2} + Q^2(\sigma_{th}^2 + \varepsilon(1+r)i_1^2) = Q^2(\sigma_{th}^2 + r\varepsilon(1+r)i_1^2)$$

$$2Q\sqrt{\sigma_{th}^2 + \varepsilon(1+r)i_1^2} = ((1-r) + Q^2\varepsilon(1+r))i_1$$

Square the two sides again:

$$4Q^2(\sigma_{th}^2 + \varepsilon(1+r)i_1^2) = ((1-r)^2 + 2(1-r)Q^2\varepsilon(1+r) + Q^4\varepsilon^2(1+r)^2)i_1^2$$

$$i_1^2((1-r)^2 - 2Q^2\varepsilon(1+r)^2 + Q^4\varepsilon^2(1+r)^2) = 4Q^2\sigma_{th}^2$$

Finally, we can obtain:

$$i_1^{'} = \frac{2Q\sqrt{\sigma_{th}^2}}{\sqrt{(1-r)^2 - 2\varepsilon Q^2(1+r)^2 + \varepsilon^2 Q^4(1+r)^2}} \tag{37}$$

where the i_1' is the "mark" current to get error probability of 10^{-9} when crosstalk is present. Inserting (20) and (37) into (25), the power penalty at $P_e = 10^{-9}$ is given by:

$$Penalty(dB) = -5\log(1 - 2\varepsilon Q^2(\frac{1+r}{1-r})^2 + \varepsilon^2 Q^4(\frac{1+r}{1-r})^2) \tag{38}$$

3.4. Short summery for the case using a PIN receiver

In a short summary, the crosstalk induced penalty in a PIN receiver can be calculated using the following formulas which appeared in paper [I] as equation (2) and (4):

$Penalty(dB) = -5\log(1 - 4\varepsilon Q'^2 \frac{1+r}{(1-r)^2})$	for average decision threshold;
$Penalty(dB) = -5\log(1 - 2\varepsilon Q^2(\frac{1+r}{1-r})^2 + \varepsilon^2 Q^4(\frac{1+r}{1-r})^2)$	for optimum decision threshold.

The crosstalk induced penalty as a function of total crosstalk power with signal extinction ratio as a parameter is plotted in Figure 2.

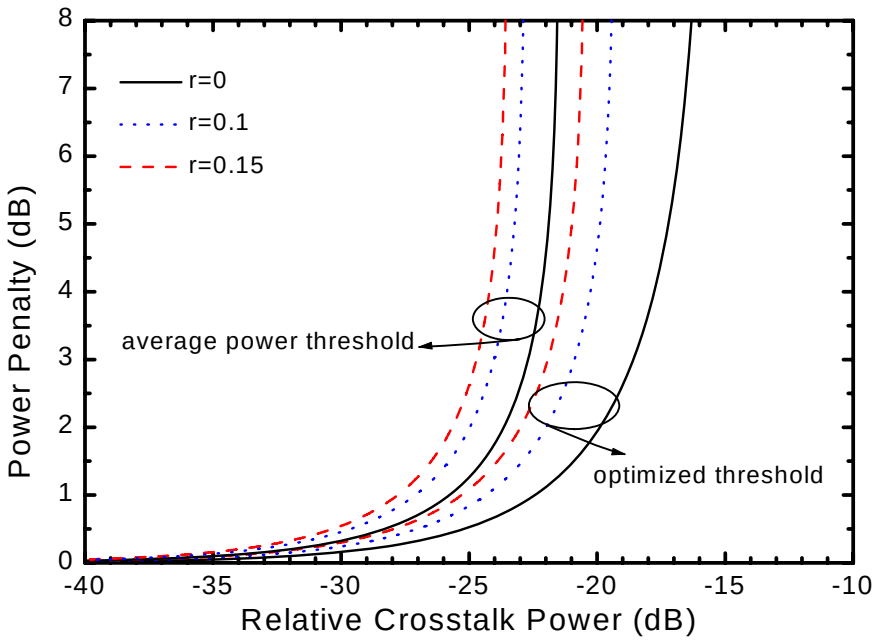

Figure 2. Crosstalk induced power penalty versus relative crosstalk power for PIN receivers with signal extinction ratio as parameter.

Figure 2 shows that a degradation of the signal extinction ratio means that less crosstalk power can be tolerated for a given power penalty. At 1 dB power penalty, an extinction ratio deterioration from $r = 0$ to $r = 0.15$ (ITU-T requirement for STM16 [10]) results in a 2.0 dB

reduction of tolerable crosstalk power in the case of average power decision threshold, and 2.8 dB in the case of optimized decision threshold.

4. Optically Pre-amplified (OPA) Receiver

4.1 Error Probability in absence of crosstalk

For a well-designed OPA receiver, the main noise contribution is the signal spontaneous emission beat noise, which is given in Ref. [11]:

$$\delta_{s-sp}^2 = 2i_s i_{sp} B_e / B_o \tag{39}$$

Where i_s is the received signal photo current, (i_1 stands for "mark" and ri_1 stands for "space", r is the extinction ratio as defined in (13)); B_e is the receiver electrical bandwidth, B_o is the optical bandwidth of the ASE incident on the photo detector. i_{sp} is the spontaneous noise photo current, which is further given by:

$$i_{sp} = 2n_{sp}(G-1)h\nu B_o LR \tag{40}$$

where $2n_{sp}(G-1)h\nu B_o$ is the ASE power from the amplifier, n_{sp} is the amplifier spontaneous emission factor, G is the amplifier gain, L is the total loss from the amplifier output to the photo detector, $R = e\eta / h\nu$ is the photo current conversion factor. The error probability of the received signal without crosstalk can be written as:

$$P_e = \frac{1}{4} erfc\left(\frac{1}{\sqrt{2}} \frac{i_1 - i_d}{\sqrt{2i_1 i_{sp} B_e / B_o}}\right) + \frac{1}{4} erfc\left(\frac{1}{\sqrt{2}} \frac{i_d - ri_1}{\sqrt{2ri_1 i_{sp} B_e / B_o}}\right) \tag{41}$$

When average power decision threshold is used, $i_d = (1+r)i_1/2$, the errors from the "mark" level dominate the error probability, and the error probability can be written as:

$$P_e = \frac{1}{4} erfc\left(\frac{1}{\sqrt{2}} \frac{(1-r)i_1}{2\sqrt{2i_1 i_{sp} B_e / B_o}}\right) \tag{42}$$

In order to get the error probability of 10^{-9}, i.e., $P_e = \frac{1}{4} erfc\left(\frac{1}{\sqrt{2}} Q'\right) = 10^{-9}$, $Q'=5.9$, the following equation need to be satisfied:

$$\frac{(1-r)i_1}{2\sqrt{2i_1 i_{sp} B_e / B_o}} = Q' \tag{43}$$

that is:

$$i_1 = \frac{8Q'^2 i_{sp} B_e / B_o}{(1-r)^2} \tag{44}$$

The optimum decision threshold is determined using the same procedure as before, that is:

$$\frac{i_1 - i_d}{\sqrt{2i_1 i_{sp} B_e / B_o}} = \frac{i_d - ri_1}{\sqrt{2ri_1 i_{sp} B_e / B_o}} \tag{45}$$

By solving equation (45), the optimum decision threshold i_{opt} can be found:

$$i_{opt} = \sqrt{r} i_1 \tag{46}$$

Setting $i_d = i_{opt}$, the error probability (41) can be written as:

$$P_e = \frac{1}{2} erfc\left(\frac{1}{\sqrt{2}} \frac{(1-\sqrt{r})i_1}{\sqrt{2 i_1 i_{sp} B_e / B_o}}\right) \tag{47}$$

In order to get $P_e = \frac{1}{2} erfc\left(\frac{1}{\sqrt{2}} Q\right) = 10^{-9}$, Q=6, the following equation need to be fulfilled:

$$\frac{(1-\sqrt{r})i_1}{\sqrt{2 i_1 i_{sp} B_e / B_o}} = Q$$

that is:

$$i_1 = \frac{2Q^2 i_{sp} B_e / B_o}{(1-\sqrt{r})^2} \tag{48}$$

4.2. Crosstalk induced power penalty using average power decision threshold

When crosstalk is added to the signal, the noise contributions are signal spontaneous emission beat noise and the signal crosstalk beat noise. The error probability is then given by:

$$P_e = \frac{1}{4} erfc\left(\frac{1}{\sqrt{2}} \frac{i_1 - i_d}{\sqrt{\varepsilon(1+r) i_1^2 + 2\frac{B_e}{B_o} i_{sp} i_1}}\right) + \frac{1}{4} erfc\left(\frac{1}{\sqrt{2}} \frac{i_d - r i_1}{\sqrt{r\varepsilon(1+r) i_1^2 + 2r\frac{B_e}{B_o} i_{sp} i_1}}\right) \tag{49}$$

When average power decision threshold is used, $i_d = (1+r)i_1/2$, the errors from the "mark" level dominate the error probability, and the error probability (49) can be written as:

$$P_e = \frac{1}{4} erfc\left(\frac{1}{\sqrt{2}} \frac{(1-r)i_1}{2\sqrt{2 i_1 i_{sp} B_e / B_o + \varepsilon(1+r) i_1^2}}\right) \tag{50}$$

In order to get the error probability of 10^{-9}, i.e., $P_e = \frac{1}{4} erfc\left(\frac{1}{\sqrt{2}} Q'\right) = 10^{-9}$, Q'=5.9, the following equation need to be satisfied:

$$\frac{(1-r)i_1}{2\sqrt{2 i_1 i_{sp} B_e / B_o + \varepsilon(1+r) i_1^2}} = Q' \tag{51}$$

that is:

$$i_1' = \frac{8Q'^2 i_{sp} B_e / B_o}{(1-r)^2 - 4Q'^2 \varepsilon(1+r)} \tag{52}$$

Inserting (44) and (52) into (25), crosstalk induced penalty can be found:

$$Penalty(dB) = -10\log\left(1 - 4Q'^2 \varepsilon \frac{1+r}{(1-r)^2}\right) \tag{53}$$

4.3. Crosstalk induced power penalty using optimum decision threshold

The optimum decision threshold is found using equation (34):

$$\frac{i_1 - i_d}{\sqrt{2i_1 i_{sp} B_e / B_o + \varepsilon(1+r)i_1^2}} = \frac{i_d - r i_1}{\sqrt{2r i_1 i_{sp} B_e / B_o + r\varepsilon(1+r)i_1^2}} \tag{54}$$

By solving equation (54), the optimum decision threshold i_{opt} can be found:

$$i_{opt} = \sqrt{r} i_1 \tag{55}$$

Setting $i_d = i_{opt}$, the error probability (44) can be written as:

$$P_e = \frac{1}{2} erfc\left(\frac{1}{\sqrt{2}} \frac{(1-\sqrt{r})i_1}{\sqrt{2i_1 i_{sp} B_e / B_o + \varepsilon(1+r)i_1^2}}\right) \tag{56}$$

In order to get $P_e = \frac{1}{2} erfc\left(\frac{1}{\sqrt{2}} Q\right) = 10^{-9}$ Q=6, the following equation need to be fulfilled:

$$i_1' = \frac{2Q^2 i_{sp} B_e / B_o}{(1-\sqrt{r})^2 - Q^2 \varepsilon(1+r)} \tag{57}$$

Inserting (48) and (57) into (25), the crosstalk induced penalty can be obtained:

$$Penalty(dB) = -10\log\left(1 - \varepsilon Q^2 \frac{1+r}{(1-\sqrt{r})^2}\right) \tag{53}$$

4.4 Short summary for OPA receiver

In a short summary, the crosstalk induced penalty in an OPA receiver can be calculated using the following formulas which are appeared in paper [I] as equation (6) and (7):

$Penalty(dB) = -10\log\left(1 - 4Q'^2 \varepsilon \frac{1+r}{(1-r)^2}\right)$	for average decision threshold;
$Penalty(dB) = -10\log\left(1 - \varepsilon Q^2 \frac{1+r}{(1-\sqrt{r})^2}\right)$	for optimum decision threshold.

The crosstalk induced penalty as a function of total crosstalk power with signal extinction ratio as a parameter is plotted in Figure 3. The crosstalk induced power penalty curves in Figure 3 show a similar tendency as in the PIN receiver case when the signal extinction ratio is degrading. For OPA receivers at 1 dB power penalty, an extinction ratio deterioration from $r = 0$ to $r = 0.15$ results in a reduction of tolerable crosstalk power of 2.0 dB for average power decision threshold, and 4.8 dB for optimized decision threshold.

5. Conclusion

We have investigated the performance degradation caused by multiple interferometric crosstalk in 4 cases: PIN receiver with average power and optimized decision threshold as well OPA receiver with average power and optimized decision threshold. Imperfect signal extinction ratio is found to have strong influence on the crosstalk induced power penalty.

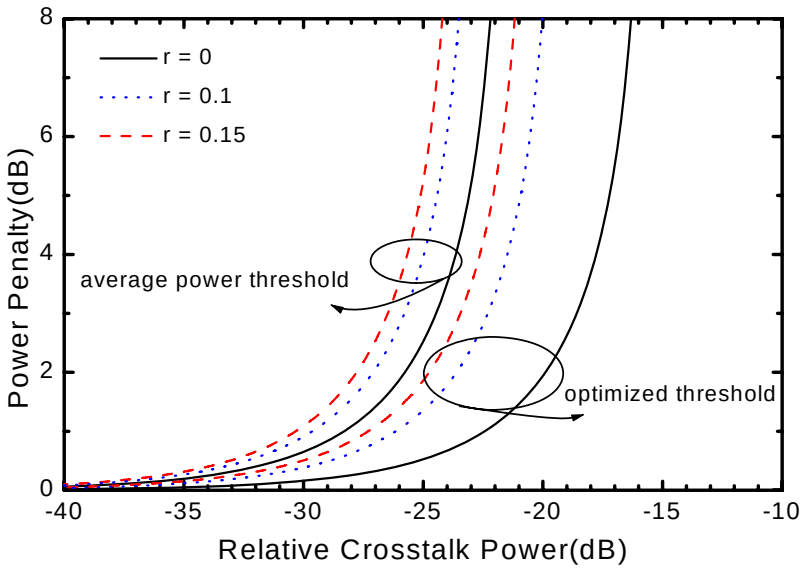

Figure 3. Crosstalk induced power penalty versus relative crosstalk power for optically pre-amplified receivers with signal extinction ratio as parameter.

References:

[1] M. Tur and Evan L. Goldstein, "Probability distribution of phase-induced intensity noise generated by distributed-feedback lasers", *Opt. Lett.*, vol.15, No.1, pp.1-3, 1990.

[2] L. Eskildsen and P. B. Hansen "Interferometric noise in lightwave systems with optical preamplifier", *IEEE Photo. Technol. Lett.*, vol. 9, pp.1538-1540, 1997.

[3] E. L. Goldstein, L. Eskildsen, and A. F. Elrefaie, "Performance implications of component crosstalk in transparent lightwave networks" , *IEEE Photon. Technol. Lett.*, vol. 6, pp.657-660, 1994.

[4] E. L. Goldstein and L. Eskildsen, "Scaling limitations in transparent optical networks due to low-level crosstalk", *IEEE Photo. Technol. Lett.*, vol. 7, pp.93-94, 1995.

[5] Hiroshi Takahashi, Kazuhiro Oda and Hiromu Toba, "Impact of crosstalk in an arrayed-waveguide multiplexer on N×N optical interconnection", *IEEE J. Lightwave Technol.*, vol.14, pp.1097-1105, 1996.

[6] P.J. Legg, M. Tur, and I. Andonovic, "Solution paths to limit interferometric noise induced performance degradation in ASK/direct detection lightwave networks", *IEEE J. Lightwave Technol.*, vol.14, pp1943-1954, 1996.

[7] M. Gustavsson, L. Gillner, C.P. Larsen, “Statistical analysis of interferometric crosstalk: theory and optical network examples”, *IEEE J. Lightwave Technol*., vol.15, pp2006-2019, 1997.

[8] Keang-Po Ho “Analysis of co-channel crosstalk interference in optical networks”, *Electron. Lett*., vol. 19, pp.383-384, 1998.

[9] T. Okoshi and K. Kikuchi, *Coherent optical fiber communications.* Netherland: Kluwer Academic, 1988.

[10] ITU-T Recommendation G.957(07/95), STM-16 Optical Interface Specification, Application code L-16.2 and L16.3.

[11] Y.K. Park and S.W. Granlund: “Optical preamplifier receivers: application to long-haul digital transmission”, *Optical fiber technology*, Vol.1 (1), pp.59-71, 1994.

Appendix II

Dispersion measurement in WDM components

1. Introduction

The RF modulation method originally used to measure dispersion in optical fibers [1, 2] is extended to measure small dispersion in optical components. The measurement setup is shown in Figure 1.

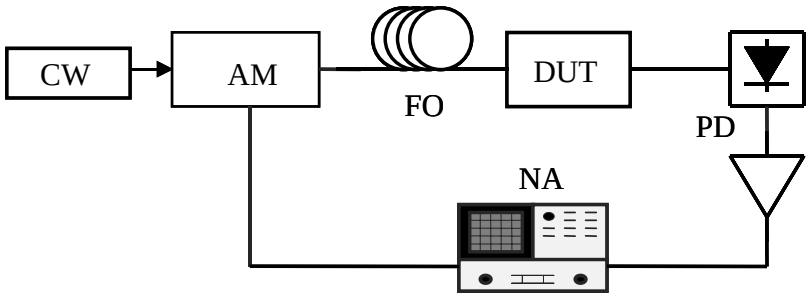

Figure. 1 Measurement set-up. CW: continuous wave laser, AM: amplitude modulator, FO: fiber offset, DUT: device under test, NA: network analyzer, PD: photodiode.

CW light from a laser is amplitude modulated with a small modulation index by the network analyzer, and the modulation frequency can be continuously swept from 130 MHz to 20 GHz. The modulated light is coupled into a 50 km standard single mode fiber as a dispersion offset followed by the device under test. A photodiode is used to detect the light at the output. The electrical signal at the modulation frequency only is measured by a network analyzer. The method relies on the fact that, due to the dispersive nature of optical components (the fiber offset and optical device under test in this setup), the propagation constants of the two sidebands of the amplitude modulated signal are different [1]. For a given dispersion value, modulation frequencies can be found where the components of the beat signal between the carrier and the sidebands are in counter-phase, resulting in cancellations of the photocurrent seen as dips in the small signal frequency response. The total dispersion *D* can be calculated from these frequencies according to [1]

$$D = \frac{\left(n - \frac{1}{2}\right)c}{\lambda^2 . f_n^2} \tag{1}$$

where f_n is the center frequency of the *n*th dip in the small signal frequency response, *c* and λ are the speed of light and the wavelength, respectively. From (1) we can see that the minimum dispersion which can be measured by this method depends on the maximum frequency at which the AM modulator can be driven. This limitation arises from the fact that for a given amount of dispersion the phase mismatch between the sidebands required for cancellation of the photocurrent is only achieved when the sideband separation is large enough. By inserting a constant dispersion offset (in our case 50 km of standard single mode fiber) in the set-up, we have been able to measure small values of both positive and negative dispersions. Such an offset will increase the total amount of dispersion to a value large

enough to be measured by our set-up. The dispersion of the device under test is equal to the change in total dispersion after it has been inserted.

2. Influence from the amplitude transfer function of optical components

When characterizing components such as filters, the two sidebands of the amplitude modulated signal can experience different levels of attenuation. Hereafter, expression of dispersion will be derived for the optical components with different loss on the two sidebands.

If *a* and *b* are the relative amplitude attenuation experienced by the upper and lower sidebands, respectively, then the electric field of the modulated optical signal after the optical component can be expressed as:

$$\vec{E}(z,t)=\vec{E}_0\left[\cos(\omega_0 t-\beta_0 z)+\frac{m}{2}a\cos((\omega_0+\omega_m)t-\beta_+ z)+\frac{m}{2}b\cos((\omega_0-\omega_m)t-\beta_- z)\right] \tag{2}$$

where ω_0 and ω_m are the optical carrier and modulation angular frequencies, respectively, and *m* is the modulation index. β_0, β_+ and β_- are the propagation constant of the optical carrier, the upper sideband and the lower sideband, respectively. The photo current is proportional to the received optical power, that is:

$$i \propto \left|\vec{E}(z,t)\right|^2 \tag{3}$$

The optical instant power into the photodiode can be further written as:

$$\left|\vec{E}(t,z)\right|^2 = \vec{E}_0{}^2\left\{\cos(\omega_0 t-\beta_0 L)+\frac{m}{2}a\cos\left[(\omega_0+\omega_m)t-\beta_+ L\right]+\frac{m}{2}b\cos\left[(\omega_0-\omega_m)t-\beta_- L\right]\right\}^2$$

The right side of the equation can be expressed as:

$$\left|\vec{E}(t,z)\right|^2 =$$

$$\vec{E}_0{}^2\left\{\begin{array}{l}\cos^2(\omega_0 t-\beta_0 L)+\frac{m^2}{4}a^2\cos^2\left[(\omega_0+\omega_m)t-\beta_+ L\right]+\frac{m^2}{4}b^2\cos^2\left[(\omega_0-\omega_m)t-\beta_- L\right]\\ +ma\cos\left[(\omega_0+\omega_m)t-\beta_+ L\right]\cos(\omega_0 t-\beta_0 L)+mb\cos\left[(\omega_0-\omega_m)t-\beta_- L\right]\cos(\omega_0 t-\beta_0 L)\\ +\frac{m^2}{2}ab\cos\left[(\omega_0+\omega_m)t-\beta_+ L\right]\cos\left[(\omega_0-\omega_m)t-\beta_- L\right]\end{array}\right\}$$

(4)

Using the relations of tri-angular functions, equation (4) can be further expressed as:

$$\left|\vec{E}(t,z)\right|^2 = \vec{E}_0{}^2 \left\{ \begin{array}{l} \frac{1}{2}(1+\cos 2(\omega_0 t-\beta_0 L)) \\ +\frac{m^2}{8}a^2(1+\cos 2\left[(\omega_0+\omega_m)t-\beta_+ L\right] \\ +\frac{m^2}{8}b^2(1+\cos 2\left[(\omega_0-\omega_m)t-\beta_- L\right] \\ +\frac{ma}{2}\left[\cos\left[(2\omega_0+\omega_m)t-(\beta_++\beta_0)L\right]+\underline{\cos(\omega_m t-(\beta_+-\beta_0)L)}\right] \\ +\frac{mb}{2}\left[\cos\left[(2\omega_0-\omega_m)t-(\beta_-+\beta_0)L\right]+\underline{\cos(\omega_m t-(\beta_--\beta_0)L)}\right] \\ +\frac{m^2}{4}ab\left[\cos(2\omega_0 t-(\beta_++\beta_-)L)+\cos(2\omega_m t-(\beta_+-\beta_-)L)\right] \end{array} \right\} \quad (5)$$

Since the network analyzer only detects the signal with the same frequency as the modulation, which is the underlined terms in (3), the detected photo current is given by:

$$i_{w_m}(t) = i_0\left(\frac{ma}{2}\cos(\omega_m t-(\beta_+-\beta_0)L)+\frac{mb}{2}\cos(\omega_m t-(\beta_--\beta_0)L)\right) \quad (6)$$

We can use a second order expansion of the propagation constant around the optical carrier frequency:

$$\beta_\omega = \beta_{\omega_0}+\beta_1(\omega-\omega_0)+\frac{1}{2}\beta_2(\omega-\omega_0)^2 \quad (7)$$

where the parameter β_1 is related to group velocity $v_g = \beta_1$ and parameter β_2 is related to the total dispersion D through:

$$D = -\frac{2\pi c}{\lambda^2}\beta_2 L \quad (8)$$

The propagation constants of the upper and lower sideband can be written as:

$$\beta_+ = \beta_0+\beta_1\omega_m+\tfrac{1}{2}\beta_2\omega_m^2 \quad (9)$$

$$\beta_- = \beta_0-\beta_1\omega_m+\tfrac{1}{2}\beta_2\omega_m^2 \quad (10)$$

Inserting (9) and (10) into (6), the photo current at modulation frequency can be written as:

$$i_{\omega_m}(t) = i_0\frac{m}{2}\left\{a\cos\left[\omega_m t-\beta_1\omega_m L-\tfrac{1}{2}\beta_2\omega_m^2 L\right]+b\cos\left[\omega_m t-\beta_1\omega_m L+\tfrac{1}{2}\beta_2\omega_m^2 L\right]\right\} \quad (11)$$

$$= i_0\frac{m}{2}\left\{(a+b)\cos(\tfrac{1}{2}\beta_2\omega_m^2 L)\cos(\omega_m t-\beta_1\omega_m L)+(a-b)\sin(\tfrac{1}{2}\beta_2\omega_m^2 L)\sin(\omega_m t-\beta_1\omega_m L)\right\}$$

The right side can be re-written as:

$$i_{\omega_m}(t) = i_0 \frac{m}{2}\sqrt{a^2+b^2+2ab\cos(\beta_2\omega_m^2 L)}\left\{\begin{array}{l}\dfrac{(a+b)\cos(\frac{1}{2}\beta_2\omega_m^2 L)}{\sqrt{a^2+b^2+2ab\cos(\beta_2\omega_m^2 L)}}\cos(\omega_m t-\beta_1\omega_m L)\\ +\dfrac{(a-b)\sin(\frac{1}{2}\beta_2\omega_m^2 L)}{\sqrt{a^2+b^2+2ab\cos(\beta_2\omega_m^2 L)}}\sin(\omega_m t-\beta_1\omega_m L)\end{array}\right\} \quad (12)$$

Introducing: $$\cos\varphi = \frac{(a+b)\cos(\frac{1}{2}\beta_2\omega_m^2 L)}{\sqrt{a^2+b^2+2ab\cos(\beta_2\omega_m^2 L)}} \quad (13)$$

The detected current at modulation frequency is:

$$i_{\omega_m}(t) = i_0 \frac{m}{2}\sqrt{a^2+b^2+2ab\cos(\beta_2\omega_m^2 L)}\cos(\omega_m t-\beta_1\omega_m L-\varphi) \quad (14)$$

The dips occur in the frequency response curve when the following equation is fulfilled:

$$\beta_2(2\pi f_N)^2 L = (2N-1)\pi \quad (15)$$

Inserting the (15) into (8), the relation between dispersion and the frequency of the dips is:

$$D = \frac{\left(n-\frac{1}{2}\right)c}{\lambda^2 . f_n^2} \quad (16)$$

It is the same expression as for the optical components with uniform amplitude transfer function.

Inserting (15) into (14), the photo current at the dips can be written:

$$i_{dip} = i_0 \frac{m}{2}|a-b| \quad (17)$$

The dips become shallower when a loss difference between the two sidebands increases as seen in equation (17), due to incomplete cancellation of the two sidebands. However, when a = b, which corresponds to no loss difference between the two sidebands, the equation (14) takes the form used in Ref. [1]

Reference:

[1] B. Christensen, J. Mark, G. Jacobsen and E. Bødtker, 'Simple dispersion measurement technique with high resolution', Electronics Letters, 1993, Vol. 29, No. 1, pp. 132-134.

[2] F. Devaux, Y. Sorel and J. F. Kerdiles, 'Simple measurement of fiber dispersion and of chirp parameter of intensity modulated light emitter', Journal of Lightwave Technology, 1993, Vol. 11, No. 12, pp. 1937-1940.